The Pennsylvania State University

The Graduate School

College of Earth and Mineral Sciences

ANNUAL VARIATIONS IN GROUND-WATER TEMPERATURE AS A TRACER OF RIVER-AQUIFER INTERACTIONS

A Thesis in

Geosciences

by

Geoff J.M. Moret

Submitted in Partial Fulfillment
of the Requirements
for the Degree of

Doctor of Philosophy

December 2007

The thesis of Geoff J.M. Moret was reviewed and approved* by the following:

Richard R. Parizek
Professor of Geology and Geo-Environmental Engineering
Thesis Adviser
Chair of Committee

Charles Ammon
Associate Professor of Geosciences

Derek Elsworth
Professor of Energy and Geo-Environmental Engineering

Demian Saffer
Associate Professor of Geosciences

Kamini Singha
Assistant Professor of Geosciences

Katherine H. Freeman
Professor of Geosciences
Head of the Department of Geosciences Graduate Program

*Signatures are on file in the Graduate School.

ABSTRACT

In recent years, annual and diurnal variations in aquifer temperature have increasingly been used to investigate surface-water-ground-water interactions. This thesis represents three separate but related investigations into the value of annual temperature in characterizing and quantifying infiltration from surface-water bodies.

Currently, there is a great deal of interest in the exchange between the Rio Grande and the underlying aquifer in Albuquerque, New Mexico so that surface stream depletion can be properly estimated. The USGS has collected temperature time series in a series of piezometers along a profile perpendicular to the river to characterize horizontal flow. The current method for interpreting these data is to calibrate a 2-D numerical model of the aquifer, a process that can be time-consuming. We propose that a simple 1-D analytical solution can be used to estimate horizontal flux through an aquifer based on temperature variations. This analytical model does not fully represent all of the factors that contribute to aquifer temperature signals, but in many cases it may represent the system sufficiently well to produce a useful estimate of ground-water flux.

At the Mohawk River site near Schenectady, NY, a large number of wells drilled to characterize induced infiltration have permitted spatially extensive measurements of the annual variation in aquifer temperature. These data show a zone of high temperature variation caused by a plume of infiltrated river water pulled towards municipal supply wells. The aquifer at the site is highly transmissive, so we developed a method-of-characteristics, particle-tracking code to model the advection-dominated thermal transport. Our model of the site shows that the plume of high temperature variation is caused by aquifer thickening over a known bedrock depression. The annual temperature

variation data were also sensitive to the magnitude and spatial variation of the riverbed conductance. The results of this study suggest that numerical modeling is required to fully understand temperature data collected in aquifers with complex geometries.

If the spatial distribution of temperature measurements is sufficiently dense, then high transmissivity zones acting as preferential flow paths for infiltrated surface-water can be identified. A limitation of this method is that ground-water temperature can be measured only in wells or in natural discharge points. For some shallow aquifers, however, this temperature reversal can be seen in temperature measurements taken in shallow soil borings. By collecting temperature data in a large number of shallow soil borings, preferential flow paths in shallow soil borings can be mapped. In this paper we model soil temperature variations, investigate the range of conditions under which aquifer temperature variations can be detected, and demonstrate the technique with a data set from a site along the Mohawk River near Schenectady, New York.

TABLE OF CONTENTS

LIST OF TABLES

LIST OF FIGURES

ACKNOWLEDGEMENTS

First, I would like to thank my advisor, Richard Parizek, together with Chuck Ammon, Derek Elsworth, Andy Nyblade, Demian Saffer and Kamini Singha for all that I have learned from him about hydrogeology and geology throughout the course of my Ph.D. I would like to thank Dave Janesko for assistance in the field, and Burt Thomas and Henry Gong for sample analysis, and James Bartolino of the USGS for providing unpublished data. I would like to acknowledge financial support from the Krynine fund. Finally, I would like to thank all my friends and family, particularly my wife, Libby Hausrath, for support throughout my Ph.D program.

Chapter 1

Annual Variations in Ground-water Temperature as a Tracer of River-Aquifer Interactions

1.1 Introduction

Ground-water-surface-water interactions are an important topic in hydrogeology research. Many areas rely on shallow aquifers as a source of water. Interactions with surface-water bodies can both recharge these aquifers and potentially degrade their water quality. Similarly, infiltration induced by ground-water withdrawal can lower water levels in wetlands and reduce the discharge of streams and rivers.

The flux of water in and out of surface streams can be estimated with point measurements using seepage meters, mini-piezometers, or streambed temperature sensors, but seepage is often heterogeneous on a scale of meters (e.g., Conant, 2004). An integrated measurement of loss or gain over a reach can be made by gauging the flow up and downstream, but, unless the flux represents a significant portion of the stream flow, these measurements may not be accurate. A typical method of estimating the infiltration rate from surface-water bodies is to use an aquifer model to determine what range of values is consistent with available head and flow data. In many cases, however, the total flux through the aquifer is unknown, making it difficult to resolve the infiltration flux.

Aquifer temperature measurements are also used to investigate surface-water infiltration. In one dimension, the partial differential equation describing advective and conductive heat transfer in an aquifer is:

$$k\frac{\partial^2 T}{\partial x^2} + \rho_w c_w q \frac{\partial T}{\partial x} = \rho c \frac{\partial T}{\partial t} \qquad (1.1),$$

where T is temperature, k is the thermal conductivity of the saturated aquifer in W m^{-1} $°C^{-1}$, ρc and $\rho_w c_w$ are the heat capacities of the saturated aquifer material and water, respectively, in J $°C^{-1}$ m^{-3}, and q is the Darcy flux of water through the aquifer, in m s^{-1}. The presence of q in Equation 1.1 indicates that aquifer temperature measurements contain information regarding the magnitude of flux through the aquifer.

1.2 Previous Work

It has long been recognized that ground-water temperature measurements provided information relevant to hydrogeologists (For a complete review see Anderson, 2005). Much of the early work in the field involved analytical solutions to mathematically-tractable situations such as steady state temperature profiles (e.g., Bredehoeft and Papadopulos, 1965) or sinusoidally-varying temperature signals (e.g., Suzuki, 1960; Stallman, 1965). A few studies investigated ground-water temperatures in more complex environments (e.g., Schneider, 1962; Winslow et al. 1965; O'Brien, 1970), but they lacked the computational tools to analyze their data quantitatively.

The use of ground-water temperature signals in hydrogeology greatly increased with the development of small, self-contained, data-logging temperature sensors (for discussions

of the currently available technology, see Stonestrom and Blasch, 2003 and Johnson et al. 2005). For the first time, these sensors allowed temperature time series to be collected with a high sampling frequency. Much of the work using these temperature time series was inspired by Lapham (1989), who used annual and diurnal temperature oscillations beneath streams to estimate the magnitude of surface-water infiltration. Since the publication of Lapham (1989), there have been many papers (e.g. Silliman and Booth, 1993; Constantz et al. 1994; Silliman et al. 1995; Ronan et al. 1998; Bartolino and Niswonger, 1999; Fryar et al. 2000; Constantz et al. 2003; Niswonger and Prudic, 2003; Becker et al. 2004; Su et al. 2004; Hatch et al. 2006) that have used temperature oscillations to estimate flux either directly beneath or within a few meters of surface-water bodies.

There have been only two studies that have used temperature oscillations to characterize infiltration fluxes at the aquifer scale. Bravo et al. (2001) used annual temperature variations due to seepage from wetlands ponds to calibrate a numerical ground-water flow model on the sclae of tens to hundreds of meters. Burow et al. (2005) also used temperature variations to calibrate a model of wetlands-aquifer interaction, this time on the scale of tens of meters.

1.3 Contributions of this Dissertation

The purpose of this thesis is to demonstrate that annual temperature variations can be used to characterize surface-water-ground-water interactions at scales that are directly relevant to ground-water modelers (e.g., hundreds to thousands of meters).

Chapter 2 uses annual temperature variations to quantify horizontal flow due to river recharge at the aquifer scale near the Rio Grande in Albuquerque, New Mexico.. Chapter 3 uses spatially-variable temperature patterns in an aquifer to constrain the magnitude and location of flux from the Mohawk River near Schenectady, New York. Chapter 4 uses temperatures measured in a network of soil borings to detect a shallow preferential pathway for river infiltration at the Mohawk River site.

While this work contributes valuable information regarding surface-water ground-water interchange at these sites, there are also broader contributions:

- Chapters 2 and 3 double the number of sites, from two to four, at which annual temperature variations have been used to constrain aquifer-scale ground-water models.
- Chapter 2 presents the first application of the Suzuki-Stallman equation to horizontal, aquifer-scale flux estimation.
- Chapter 3 solves the problem of modeling thermal-transport in high Peclet number regimes using a method-of-characteristics, particle-tracking approach.
- Chapter 4 investigates the range of conditions under which aquifer temperature variations will be detectable in shallow soil borings, and uses soil temperature variations to detect a preferential flow-path.

Taken together, these chapters represent an advance in the interpretation of annual variations in temperature at the aquifer scale.

Chapter 2

Estimating Horizontal Ground-water Flux from the Rio Grande Using Temperature Records: an Analytical Approach

Abstract

Currently, there is a great deal of interest in the exchange between the Rio Grande and the underlying aquifer in Albuquerque, New Mexico so that surface stream depletion can be properly estimated. The USGS has collected temperature time series in a network of piezometers along a profile perpendicular to the river to characterize horizontal flow. The current method for interpreting these data is to calibrate a 2-D numerical model of the aquifer, a process that can be time-consuming. We propose that a simple 1-D analytical solution can be used to estimate horizontal flux through an aquifer based on temperature variations. This analytical model does not fully represent all of the factors that contribute to aquifer temperature signals, but in many cases it may represent the system sufficiently well to produce a useful estimate of ground-water flux.

2.1 Introduction

The infiltration of surface-water into aquifers is important to the management of water resources. Accurate estimates of the flux from surface-water bodies are important in preventing ground-water contamination, estimating sustainable yield, and predicting the impact of climate or pumping related changes in surface-water on the aquifer. Standard methods for measuring surface-water-ground-water exchange include seepage meters, stream-bed piezometers, and flow-gauging. Annual and diurnal oscillations in ground-water temperature are a useful tracer of surface-water- ground-water interaction (for a review, see Anderson, 2005). In many studies, temperatures have been recorded in and

below surface-water bodies to estimate the vertical seepage (e.g., Suzuki, 1960; Stallman, 1965; Lapham, 1989; Silliman and Booth, 1993; Silliman et al. 1995; Bartolino and Niswonger, 1999; Fryar et al. 2000; Becker et al. 2004; Hatch et al. 2006). These methods provide point measurements of seepage, but seepage can vary greatly over scales as small as a single stream reach (e.g., Conant, 2004).

In a smaller number of studies, temperature time series recorded in wells some distance from streams or rivers with an oscillating temperature have been used to characterize lateral flow in an aquifer. Winslow et al. (1965) measured temperatures in 51 wells near the Mohawk River near Schenectady, New York, and used the magnitude of observed temperature variations to delineate a zone of high transmissivity within glacial outwash deposits. Ronan et al. (1998) used temperature measurements collected both beneath a streambed and beneath its banks to calibrate a 2-D numerical model of unsaturated flow within a few meters of an ephemeral stream. Bravo et al. (2001) measured soil and ground-water temperatures beneath riverside wetlands, and used them in a parameter estimation routine to estimate the hydraulic conductivity of the underlying aquifer. Bartolino (2003) used temperature variations in a chain of piezometers between the Rio Grande and a riverside drain more than 100 m away to confirm that the drain was intercepting river water. Su et al. (2004) manually calibrated six 2-D models to fit temperature data collected in the Russian River and six nearby wells to determine both the hydraulic conductivity of the aquifer and its anisotropy. Burow et al. (2005) used temperatures in their calibration of a 2-D model of the flow system beneath wetland ponds to obtain estimates of the hydraulic conductivity of a layered aquifer. We note that the data analysis in these studies has either been strictly qualitative (Winslow et al. 1965;

Bartolino, 1999) or has involved the calibration of numerical models (Bravo et al. 2001; Su et al. 2004; Burow et al. 2005).

In this study, we use the temperature and head data collected by Bartolino (2003) to estimate the total flux from the Rio Grande through the Upper Santa Fe Group aquifer. Using the analytical model developed by Suzuki (1960) and Stallman (1965), we estimate that the total flux is 1.2-1.6 m^3 per day per meter of riverbank. Because the data are collected along a 234 m profile away from the river, it represents a truly aquifer-scale flux estimate.

2.2 Study Area

2.2.1 Middle Rio Grande Basin

Albuquerque, New Mexico, lies in the Middle Rio Grande Basin. The basin, which was formed by rift faulting, is filled by hundreds to thousands of meters of sediments known as the Santa Fe Group. These sediments are typically alluvial, although there are some aeolian deposits. The spatial distribution of sedimentary facies in the rift basin tends to be complex and three-dimensional rather than a simple, layered system (Bartolino and Cole, 2002). The Santa Fe Group and the younger alluvial sediments that overly them are known as the Santa Fe Group aquifer. The hydrology, hydrogeology, and geology of this aquifer and its importance to the region are described in detail in Bartolino and Cole (2002).

New Mexico regulations require major ground-water users to obtain surface-water rights for any surface stream depletion they cause. As ground-water withdrawals in the Albuquerque area have drawn down the water-table more than 50 m from pre-settlement levels (Bartolino, 2003), there is a great deal of interest in quantifying the river-aquifer

interaction in the Middle Rio Grande basin. Previous studies, summarized by Bartolino (2002) have used streambed permeameters (Gould, 1994), the transient response of the aquifer to a flood pulse (Pruitt and Bower, 1994; Roark, 1998), vertical profiles of temperature measurements (Bartolino and Niswonger, 1999), and calibrated numerical models (e.g., Kernodle et al. 1995; Tiedeman et al. 1998) to estimate the flux between the Rio Grande and the Santa Fe Group aquifer. Currently, a basin scale ground-water model is used in the official assessment of surface stream depletion (Baroll, 2001).

2.2.2 Paseo Del Norte Site

This study focuses on data collected in the area where the Paseo Del Norte crosses the Rio Grande (Figure 2.1). The sediments at the site consist of heterogeneous alluvial deposits of silt, sand, and gravel. Bartolino and Niswonger (1999) collected temperature profiles in a piezometer on the riverbank. They modeled these data, and determined that the aquifer beneath the river consisted of two layers- a shallow layer between 3.1 and 8.8 m depth with a vertical hydraulic conductivity between 6.8×10^{-6} m $s^{-1}$and 6.0×10^{-5} m $s^{-1}$and a deeper layer 8.8 m-14.7 m below the surface with a hydraulic conductivity of 2.0×10^{-6} m $s^{-1}$and 1.4×10^{-5} m s^{-1}. The estimated monthly flux through the riverbed at the site, which seemed to correlate with river stage, ranged from 9.0×10^{-8} m s^{-1} in September 1996 to 9.6×10^{-7} m s^{-1} in December 1996, with an annual average flux of $4.22 \pm 3.57 \times 10^{-7}$ m s^{-1}.

As the second stage of the temperature study, USGS researchers installed eight piezometer nests on both banks of the Rio Grande along Paseo Del Norte (Figure 2.1). Bartolino (2003) collected daily temperature readings between March 1999 and July 2000 in these piezometers. Data used in this study were collected in pieozometers 6, 7,

and 8, which were installed on the east bank between the Rio Grande and a riverside drain 234 m away (Figure 2.1). The purpose of the riverside drain is to dewater the land near the river, so it generally acts as a hydraulic sink, with a head varying with its water level. Piezometer P06 is on the riverbank, piezometer P07 is 125 m from the river, and piezometer P08 is near the drain 235 m from the river. Daily temperature readings were recorded between March 1999 and July 2000. Temperatures were collected at 2 or 3, 4 or 4.5, 6, 8, and 10 m depth in each piezometer, but we will focus on the temperatures at 4 and 4.5 m (Figure 2.2a) and 8 m (Figure 2.2b) as they appear to be representative of the two layers of different transmissivities identified by Bartolino and Niswonger (1999).

2.3 Methods

2.3.1 Suzuki-Stallman Equation

The 1-D partial differential equation describing advective and conductive heat transfer in an aquifer is:

$$k\frac{\partial^2 T}{\partial x^2} + \rho_w c_w q \frac{\partial T}{\partial x} = \rho c \frac{\partial T}{\partial t} \qquad (2.1)$$

where T is temperature, k is the thermal conductivity of the saturated aquifer in W m^{-1} °C^{-1}, ρc and $\rho_w c_w$ are the heat capacities of the saturated aquifer material and water, respectively, in J °C^{-1} m^{-3}, and q is the Darcy flux of water through the aquifer, in m s^{-1}. Consider an aquifer, bounded at $x = 0$ by fully penetrating river, where all flow is uniform and horizontal in the positive x direction. The temperature of the river, T_{river}, varies sinusoidally with a period of one year:

$$T_{river} = T_{avg} + T_0 \sin\left(\frac{2\pi}{\tau} t + \phi\right) \qquad (2.2)$$

where T_{avg} is the average river temperature, T_0 is the magnitude of the river's temperature oscillation, τ is the period of the oscillation (one year), ϕ is the phase lag in the river's temperature signal, and t is time. If the aquifer extends far enough in the x direction that the variation in the river temperature does not affect the temperature at the far boundary, then the aquifer temperature is the sum of a steady state term, T_{ss}, that varies in space, and an oscillatory term, T_{osc}, that varies in time and space. T_{ss} depends on T_{avg} and the boundary conditions at the far boundary. This paper, however, deals only with T_{osc}.

If the temperature dependence of the viscosity of water is ignored, then the analytic solution for advective and conductive heat transport proposed by Suzuki (1960) and further developed by Stallman (1965) can be used to model T_{osc}:

$$T_{osc} = T_0 e^{-a x} \sin\left(\frac{2\pi}{\tau} t - bx + \phi\right) \qquad (2.3)$$

where

$$a = \left[\sqrt{K^2 + V^4/4} + V^2/2\right]^{\frac{1}{2}} - V \qquad (2.4)$$

$$b = \left[\sqrt{K^2 + V^4/4} - V^2/2\right]^{\frac{1}{2}} \qquad (2.5)$$

The parameter a, with units of m^{-1}, controls the attenuation of the temperature wave. The spatial frequency b, with units of radians per meter, controls the propagation of the wave through space. In Equations 2.4 and 2.5, K and V are given by:

$$K = \frac{\pi \rho c}{k \tau} \qquad (2.6)$$

$$V = \frac{\rho_w c_w q}{2k} \qquad (2.7)$$

Figure 2.3 shows how a and b vary as a function of flux through the aquifer. At low fluxes, signals attenuate quickly and propagate.

If a and b can be determined from the data, then the flux through the aquifer, q, can be estimated from type curves such as Figure 2.3. The parameters a and b can be found using temperature records measured in two wells at distances x_1 and x_2 from the river. The differences between the maximum and minimum temperatures in these records, ΔT_{x1} and ΔT_{x2}, can be used to estimate a:

$$a = \frac{-1}{x_2 - x_1} \log\left(\frac{\Delta T_{x1}}{\Delta T_{x2}}\right) \qquad (2.8)$$

The phase lag between the two temperature records, Δt, yields b:

$$b = \frac{2\pi\,\Delta t}{(x_2 - x_1)\tau} \qquad (2.9)$$

Suzuki (1960) presented an approximate solution for q:

$$q = \frac{2k}{\rho_w c_w}(b - a) \qquad (2.10)$$

As Figure 2.4 shows, the Suzuki approximation is valid for low values of q, but becomes increasingly inaccurate once q exceeds a threshold value (roughly 10^{-7} m s^{-1} for the parameters used in Figure 2.4).

Stallman (1965) derived the exact solution for q from Equations 2.4 and 2.5:

$$q = \frac{k}{\rho_w c_w} \cdot \frac{b^2 - a^2}{a} \qquad (2.11)$$

However, the q estimates obtained from this equation are particularly sensitive to error in b. We have found that the best way to estimate q is to plot the measured values of a and b on type curves such as Figure 2.3. With this method, the user can both determine

whether or not *a* and *b* are physically realistic and consistent with each other and assess the sensitivity of *q* to measurement error.

2.3.2 Limitations and Sensitivities

2.3.2.1 Range of Applicability

Figure 2.3 shows the values of *a* and *b* as a function of *q* calculated using typical values for the thermal properties of the aquifer. For low values of *q*, conduction is the dominant method of heat transfer, and *a* and *b* approach the square root of *K*. For high values of *q*, advection dominates, and *a* and *b* approach zero. The Suzuki-Stallman equation can only be used to estimate flux in regions of the curves where *a* and *b* vary as a function of *q*. The exact limits of detectability depend on the quality of the temperature data, the strength of the original temperature signal, and the distance between measuring points, but in general the fluxes between 10^{-8} and 10^{-5} m s^{-1} should be detectable.

2.3.2.2 Spatial Aliasing

The spatial wavelength, λ, of a temperature wave described by Equation 2.3 is given by

$$\lambda = \frac{2\pi}{b} \qquad (2.12)$$

Using the values of *b* from Figure 2.3, fluxes of 10^{-8} and 10^{-5} m s^{-1} result in wavelengths of 17 and 415 m, respectively. When the wells used to measure temperature are separated by more than one wavelength, the apparent lag between the temperature series will be incorrect, a phenomenon known as spatial aliasing. In this situation, *b* will be greatly underestimated. A measured value of *b* can be evaluated by plotting it along with the measured *a* value for the same time series pair on plot generated using Equation 2.5, such as Figure 2.3. If the *q* values that correspond to *a* and *b* do not agree reasonably

well, then one year increments can be added to the measured lag until they do. Estimates of b also can be evaluated by calculating q using Equation 2.10 and then solving equation 2.5 for K. This value can then be transformed to k using Equation 2.6 and a reasonable value of ρc. The lag can then be adjusted until the apparent k value is a reasonable value for the thermal conductivity of an aquifer (see section 2.3.2.5). This multi-step process is extremely susceptible to error, so the apparent k value for the correct lag may only be within an order of magnitude of the true value. However, the apparent k values for spatially-aliased lags can be several orders of magnitude from the correct value, so the technique can be used to diagnose a spatial aliasing problem.

2.3.2.3 Surface Temperature Variations

Shallow aquifer temperatures may be affected by the annual variation in the ground surface temperature. The surface temperature is generally an attenuated version of the atmospheric temperature signal (e.g., Smerdon et al. 2004). If the surface temperature is approximated as a sinusoid with a magnitude T_{surf} and a phase lag of ϕ_{surf}, and vertical seepage is small, then the analytical solution for the propagation of a conductive wave into a uniform half-space, $T_{correction}$, is (Carslaw and Jaeger, 1959):

$$T_{correction} = T_{surf} e^{-\sqrt{K}z} \sin\left(\frac{2\pi}{\tau}t - \sqrt{K}z + \varphi_{surf}\right) \quad , \qquad (2.13)$$

where K is defined in Equation 2.6. The solution for a two-layer earth (Larson and Hsui, 1992; Lunardini, 1992) may be useful for modeling a confined aquifer overlain by an aquitard or an unconfined aquifer overlain by an unsaturated zone. Because of the exponential decay of the signal, temperatures measured more than a few meters below the surface will not be affected. For shallow measurements, the surface signal and the aquifer signal will add constructively or destructively depending on the difference

between their phases, which depends on subsurface thermal properties. The best approach is to measure the temperature at several depths above the aquifer so that the surface-temperature effect can be accurately modeled (e.g., Smerdon et al. 2004). In the absence of shallow temperature data, q can be estimated with several different corrections to get a sense of the uncertainty associated with the effect of surface temperature.

At the Paseo Del Norte site, the temperatures recorded at 4.5 m can be slightly affected by annual variations in ground surface temperature. However, in piezometers P06 and P07 (Figure 2.5) there is no significant difference between the temperatures recorded at 2-3 m depth and the temperatures recorded at 4-4.5 m depth, suggesting that the effect of surface temperature is small. There is a 3.6 °C difference in the magnitudes of the temperature waves recorded at 2 and 4.5 m depth in piezometer P08 (Figure 2.5). However, as this difference is greater than what we would expect if it were due to the surface temperature effect, it seems likely that the sediments at 2 m depth in piezometer 8 have a lower hydraulic conductivity than the sediments in the aquifer below.

2.3.2.4 Temperature Dependence of Viscosity

The viscosity of water changes by a factor of two between 0 °C and 25 °C. Since hydraulic conductivity is inversely dependent on the viscosity of the fluid, surface-water recharge fluxes can vary significantly with the temperature of the water (e.g., Constantz, 1994). A fundamental limitation of the Suzuki-Stallman equation is that it does not consider the effect of temperature on hydraulic conductivity. We evaluated this limitation using a 2-D finite element model (Appendix A) that accounts for the effect of temperature-dependent hydraulic conductivity. A triangular grid was used with a

maximum triangle side length of 1 m. In the modeled system, the aquifer had a hydraulic conductivity of 5 x 10^{-5} m s^{-1}, a storativity of 5 x 10^{-4}, a thermal conductivity of 2.2 W m^{-1} °C^{-1} and a heat capacity of 3.2 x 10^{6} J °C^{-1} m^{-3}. The latter two values are typical of the thermal properties for saturated sediments (e.g., Lapham, 1989; Stonestrom and Blasch, 2003).

Constant head boundaries were imposed within the aquifer at the river boundary and at a position 50 m from the river, with the distant boundary's head fixed 0.3 m lower than the river boundary's. The resultant flux through the aquifer was 3 x 10^{-7} m s^{-1}, a value towards the lower end of the range of detectability determined in section 2.4.2.1. The river's temperature varied sinusoidally with an amplitude of 10 °C and a magnitude of 10 °C, while the far boundary was held at 10 °C. The top and bottom of the aquifer were modeled as zero flux boundaries for both heat and ground-water flow.

Figure 2.6 compares the temperature profile in the aquifer 3000 days from the start of the simulation as calculated using the finite element model to the profile calculated using Equation 2.3. The RMS difference between the two profiles is 0.1 °C, which is at least partly due to numerical error.

Figure 2.7 compares the numerical and analytical results for the same aquifer with the hydraulic conductivity raised to 5 x 10^{-4} m s^{-1}, resulting in a flux of 3 x 10^{-6} m s^{-1}, near the maximum level at which we expect the Suzuki-Stallman method to be applicable. For this simulation, a method-of-characteristics, particle-tracking model was used (Chapter 3). The two models do not agree particularly well. The sinusoidal waveform of the numerical model becomes increasingly distorted further from the river, with wider areas and narrower cool areas. The magnitude of both the temperature maxima and the

temperature minima decrease, and the two models become increasingly out of phase. This distortion, which only occurs at high flow rates, should be easily identifiable in field data. If temperature time series data appear to be sinusoidal, then the temperature dependence of viscosity does not limit the applicability of the Suzuki-Stallman model to them.

2.3.2.5 Uncertainty in Thermal Properties

The thermal properties of the aquifer, k and ρc, are generally not well known. The volumetric heat capacity of saturated sediments, ρc, is typically considered to be the volumetrically-weighted sum of the heat capacities of the matrix material and of water. Lapham (1989) presents calculated values of ρc ranging from 2.1-3.6 x 10^6 J °C^{-1} m^{-3}, but the upper and lower limits correspond to sediments with exceptionally low and high porosities. For aquifers consisting of unconsolidated sediments, the range of k values reported in the literature is not large. Niswonger and Prudic (2003) recommend using k values between 1.4 and 2.2 W m^{-1} °C^{-1}, with the lower values representing soils containing a significant fraction of silt and clay (Stonestrom and Blasch, 2003). For clean, saturated sands and gravels, published values of k range from 1.88 to 2.69 W m^{-1} °C^{-1} (Markle et al. 2006, and references therein). Thus, if site specific measurements are not readily available, a thermal conductivity chosen based solely on the aquifer's lithology will introduce an uncertainty into the estimate of q of a few tens of percent. In this study, we use the average of the four values obtained by Bartolino and Niswonger (1999) for the thermal conductivity (2.16 W m^{-1} °C^{-1}), and saturated heat capacity (3.2 x 10^6 J °C^{-1} m^{-3}) of the upper Santa Fe Group aquifer.

2.3.2.6 Data Error

Another possible limitation in the interpretation of temperature oscillations using the Suzuki-Stallman Equation is uncertainty in the estimation of best fit sinusoids for the observed data series, which would result in uncertainty in *a* and *b*. As Figure 2.2 shows, the diffusive attenuation of the higher frequency components of the original temperature signal, so errors in sinusoid fitting are likely to be greatest closer to the source of the surface-water recharge.

If it is assumed that there is no error in ΔT_{x2}, then the error in the value of *a* calculated using an incorrect value of ΔT_{x1} is given by:

$$a_\varepsilon - a = \frac{-1}{x_2 - x_1} \log\left(\frac{\Delta T_{x1} + \varepsilon_T}{\Delta T_{x1}}\right) \qquad (2.14),$$

where ε_T is the error in ΔT_{x1} and a_ε is the value of *a* calculated using the erroneous value. Errors in the phase propagate linearly into *b*:

$$b_\varepsilon - b = \frac{2\pi\varepsilon_t}{(x_2 - x_1)\tau} \qquad (2.15),$$

where ε_t is the error in the lag of the best fit sinusoid and b_ε is the value of *b* calculated with the incorrect lag.

2.3.2.7 Heterogeneity

The Suzuki-Stallman equation assumes a uniform flow field, a condition not met in a heterogeneous aquifer. If temperature signals measured at points with different flow rates are compared, then the estimated fluxes will be incorrect. It is advisable to measure the temperature at a number of depths in as many observation wells are available to limit the impact of time series recorded in non-representative locations.

2.3.2.8 Variable Recharge

Bartolino and Niswonger (1999) determined that the flux through the riverbed at the Paseo Del Norte site varied by roughly an order of magnitude over the course of the year (Figure 2.8a). We used their monthly recharge estimates as a variable forcing for a synthetic aquifer with a hydraulic conductivity of 1 x 10^{-4} m s^{-1}. Other aquifer properties were as described in 2.3.2.4. Figure 2.8b compares the resulting temperature signal with the analytic model corresponding to the mean annual flux (4.22 x 10^{-7} m s^{-1}). The two models agree reasonably well, with a maximum difference of 0.6 °C at the highest temperature point. The phase difference between the models is less than 1 m, the spatial discretization of the numerical model. It appears from this result that the Suzuki-Stallman equation represents aquifers with annual variations in river recharge reasonably well.

2.4 Results

All of the pairs of time series used in this study are spatially aliased. Figure 2.9 shows the trial values of *b* for the temperature signals in P07 and P08 at 4.5 m depth. We estimated the lag between these signals by taking the cross-covariance of the two time series and averaging the lags of the maximum and minimum values. The resulting value, 94 days, is similar to the lag of 13 weeks (91 days) directly estimated from the data by Bartolino (2003). As Figure 2.9 shows, a lag of 2 years and 94 days results in a *q* estimate (1.2 x 10^{-6} m s^{-1}) that agrees reasonably well with the *q* estimate derived from *a* (1.4 x 10^{-6} m s^{-1}). We evaluated the apparent lags between the other time series pairs in the same way.

Table 2.1 shows the *a* and *b* values for pairs of temperature time series measured in the Rio Grande and piezometers P06 to P08 at 4-4.5 m depth and 8 m depth. The *a* and *b* values at 4-4.5 m depth range from 3.58 x 10^{-3} to 4.68 x 10^{-3} m^{-1} and 0.11 to 0.13 rad m^{-1}, respectively. The *a* and *b* values at 8 m depth, which are slightly greater than the shallower values, range from 6.2 x 10^{-3} to 7.7 x 10^{-3} m^{-1} and 0.16 to 0.19 rad m^{-1}, respectively. The greater values of *a* and *b* in the lower layer are consistent with the finding of Bartolino and Niswonger (1999) that the lower layer had a lower hydraulic conductivity than the upper layer.

These values of *a* and *b* are transformed to values of *q* using type curves in Figure 2.10. The total range of *q* values is 1.2-1.5 x 10^{-6} m s^{-1} for the upper layer and 0.8-1.2 x 10^{-6} m s^{-1} for the lower layer. The small range in *q* values (~20% deviation from the mean) lends confidence in the results. Of some concern is the fact that the *q* estimates corresponding to *b* (q_b) are systematically lower than the *q* estimates corresponding to *a* (q_a). This may indicate that the phase of the signals is slightly distorted by the effects of the temperature dependence of viscosity (Section 2.4.2.4).

An important aspect of the results in Table 2.1 is that the estimates of *a*, *b*, and *q* obtained using the temperature signals measured in the river and a single piezometer are within the range of values obtained using two piezometers. Thus, the technique may be useful when temperature measurements are available for only one well and the surface-water body.

The magnitude of the uncertainty in the flux estimates in Table 1 is difficult to assess, as much of it is derived from aquifer heterogeneity, temporal variations in flow, 2-D or 3-D effects, and other factors not accounted for in the conceptual model. However, it is possible to estimate the uncertainty due to data errors and incorrect values of the aquifer

thermal properties. Data errors are unlikely to affect the uncertainty in the results of this experiment by more than a few percent. Aquifer temperature errors are a fraction of a degree, and it is the logarithm of the ratio of two temperature differences that appears in Equation 2.8. The uncertainty in lag estimates is several days, which, with the multi-year lags in this experiment, is less than 1% of the total. Errors in positioning, which may reach several percent of the total distance, affect *a* and *b* linearly. The effect of incorrect aquifer parameters can be examined by plotting the measured values of *a* and *b* on different type curves. Figure 2.11 shows the results of using two the highest and lowest published values for the thermal conductivity of saturated sediments. The *q* estimates obtained from these curves range from 1.2-1.6 x 10^{-6} m s^{-1} for the upper layer and 0.8-1.3 x 10^{-6} m s^{-1} for the lower layer, or not much greater than the scatter in the data points. Varying the heat capacity of the aquifer within the range of reasonable values produces even smaller variations in flux estimates.

The water levels recorded in piezometers P06, P07, and P08 (Bartolino, 2003) show that the head gradient in the aquifer was relatively steady over the study period, with a value of approximately 0.0085. Using Darcy's law, we can then transform our flux estimates to hydraulic conductivities. The means of the *q* estimates for the upper and lower layers correspond to hydraulic conductivities of 1.6 x 10^{-4} m $s^{-1}$and 1.1 x 10^{-4} m s^{-1}, respectively. Kernodle et al. (1995) assigned hydraulic conductivities between 3.5 x 10^{-5} m $s^{-1}$and 2.5 x 10^{-4} m s^{-1} to the upper Santa Fe group, a range that brackets the results of this study. Bartolino and Niswonger (1999) used temperature profiles to estimate vertical hydraulic conductivities between 4.3 x 10^{-6} m $s^{-1}$and 2.0 x 10^{-5} m s^{-1}. As it is common for horizontal hydraulic conductivities for unconsolidated deposits to be an order of

magnitude higher than vertical hydraulic conductivities, our results agree reasonably well with their values.

The differences between the flux estimates at 4-4.5 m depth and at 8 m depth could reflect layering or gradational changes in the subsurface. To obtain an approximate estimate of the total flux through the aquifer, we can assume that the aquifer consists of two layers, each 7.1 m thick. Using the maximum and minimum fluxes for each layer, the total flux through the aquifer can be estimated to be 1.2-1.8 m^3 per day per meter of riverbank. This estimate could be affected by lateral changes in aquifer geometry, spatial variations in aquifer properties, or a flow velocity field with components in the vertical direction or parallel to the river. For comparison, Bartolino and Niswonger (1999) estimated the mean annual flux through the riverbed at the Paseo Del Norte site was $4.22 \pm 3.57 \times 10^{-7}$ m s^{-1}. If we assume that this flux is evenly split between the two sides of the river, and that the river is roughly 100 m wide at the site, then each bank would receive a flux of $2.1 \pm 1.8 \times 10^{-5}$ m^2 s^{-1}, or 1.8 ± 1.5 m^3 per day per meter of riverbank. The overlapping ranges of the estimates increase our confidence in the validity of our estimate.

2.5 Conclusions

The application of our method to field data from the Paseo del Norte Site near the Rio Grande proved successful. While conceptual model errors are difficult to quantify, the scatter in the flux estimates was relatively minor, and the final hydraulic conductivities were consistent with previous studies. The overall flux estimate of 1.2-1.8 m^3 per day per meter of riverbank could be useful in developing a water budget for the Upper Santa Fe Group aquifer east of the Rio Grande in Albuquerque. It agrees well with previous work

by Bartolino and Niswonger (1999). It is important to note, however, that this flux estimate is derived from one piezometer profile- the flux from other reaches of the river may be different. Another limitation of the estimate is that it is averaged over the several years that it takes the temperature signal from the river to propagate to the drain. Thus, it is not possible to measure the impact of a single year of drought or flood on the flux using this method.

The Suzuki-Stallman method described in this paper should work for fluxes between 10^{-8} and 10^{-5} m s^{-1}, although at the higher end the waveform of the temperature signal may be too distorted for the method to be applied. Possible problems include contamination of the signal by surface temperature oscillations and underestimation of the lag between time series due to spatial aliasing. While the Suzuki-Stallman equation does not model temperature dependence of hydraulic conductivity, our numerical simulation suggested that if the effect is large enough to cause significant errors it should be visible in the raw data. An interesting result was that fluxes estimated using time series from a river and single piezometer fell within the range of estimates produced using two piezometers, indicating that the method can be applied when only one observation well is available.

The intent of this paper is not to suggest that calibrated numerical models of temperature signals are superfluous. Numerical models can incorporate 2-D and 3-D geometries, partially-penetrating surface-water bodies, heterogeneous hydraulic conductivities, non-steady and non-horizontal flow, and many other features. The analytic approach described here can be used much as simple analytic solutions are used in contaminant transport studies: to obtain an approximate flux estimate rapidly, to gain understanding of

how different parameters affect aquifer temperature signals, to choose monitoring well locations, and to provide starting parameters for the calibration of numerical models.

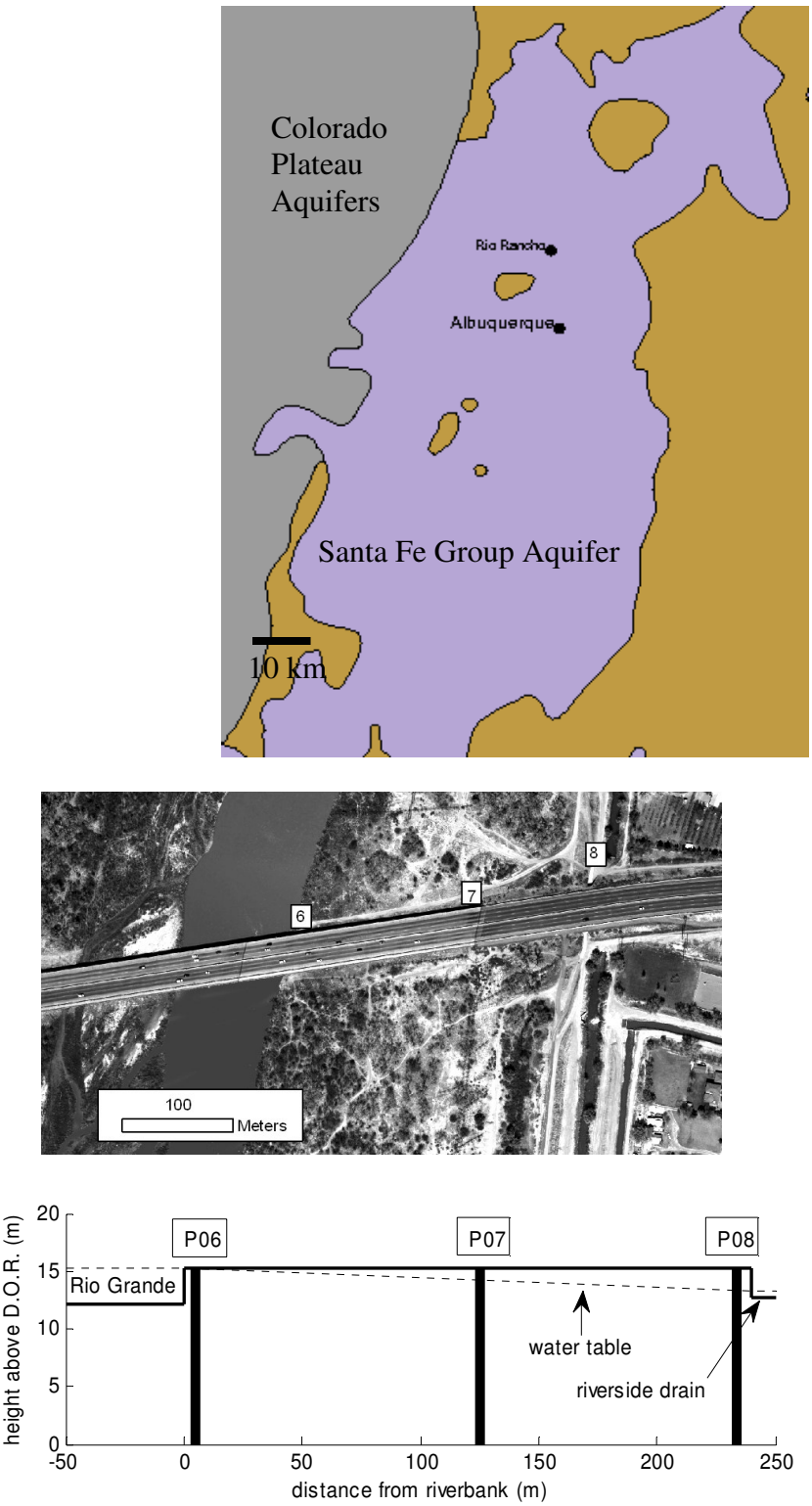

Figure 2.1. a) Map of the middle Rio Grande Basin. b) Aerial photograph of the Paseo Del Norte Site in Albuquerque with P06, P07, and P08 indicated. C) Vertically-exaggerated cross section of the piezometer transect. D.O.R. is depth of refusal.

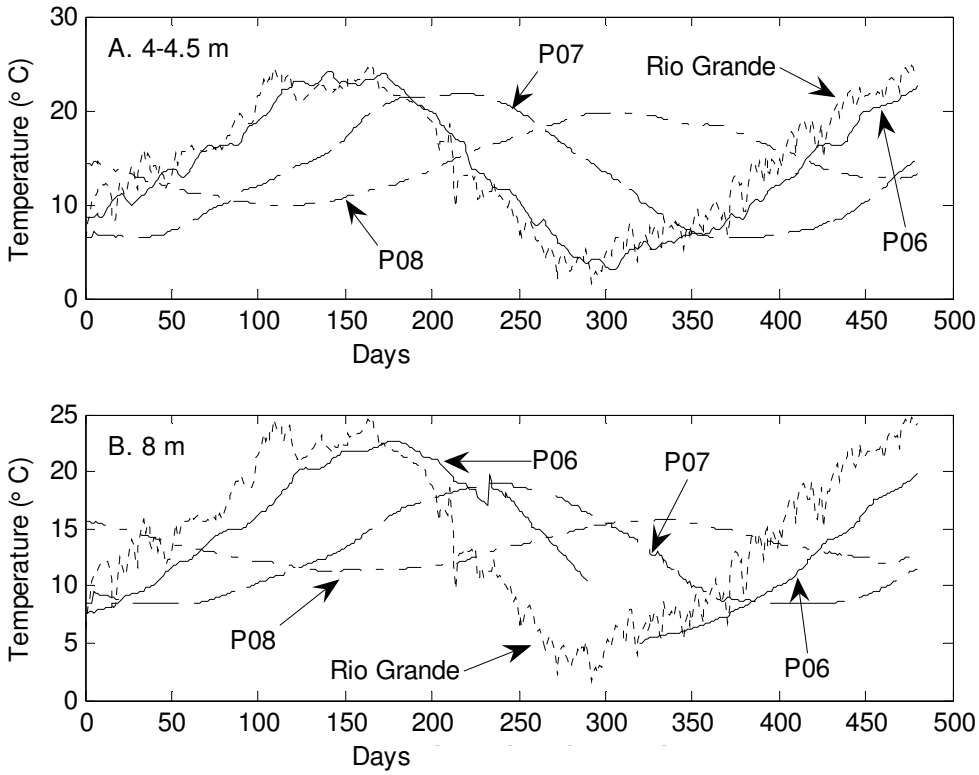

Figure 2.2. Temperature data collected in the Rio Grande and piezometers P06, P07, and P08 at (A) 4-4.5 m depth, and (B) 8 m depth. There are some data gaps in the 8 m temperature time series due to malfunctioning magnetic switches on the data loggers (J. Bartolino, personal communication, 2007).

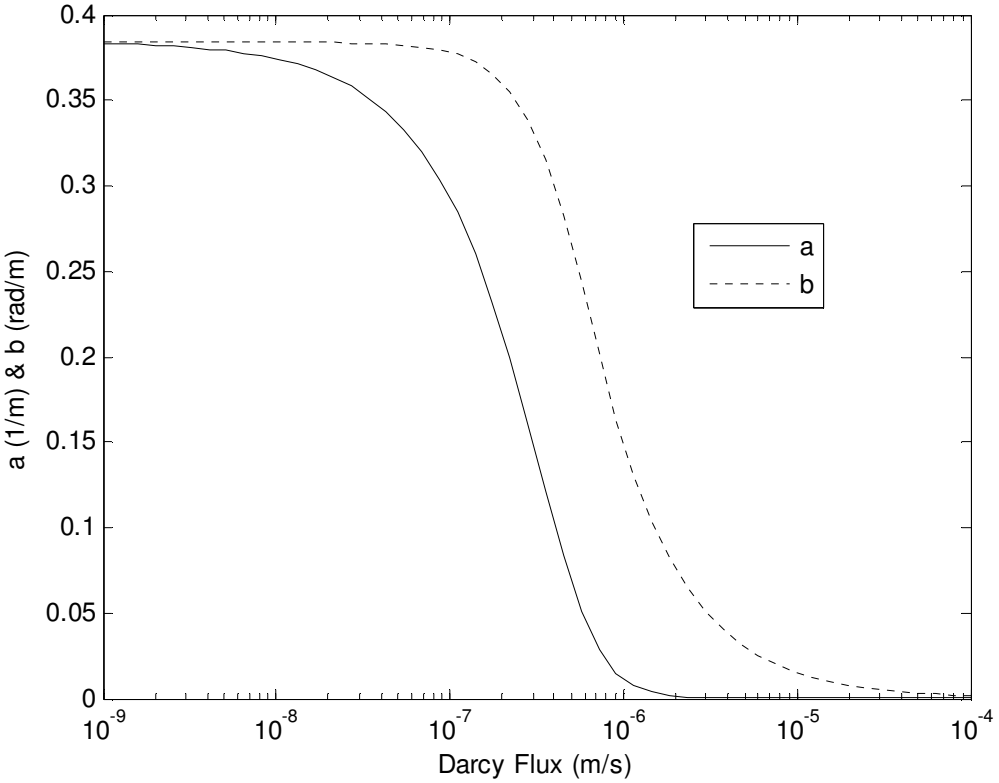

Figure 2.3. Values of the parameters *a* and *b*, as a function of flux, *q*. The curves shown here were calculated with a thermal conductivity of 2.16 W m^{-1} °C^{-1} and a heat capacity of 3.2 x 10^6 J °C^{-1} m^{-3}.

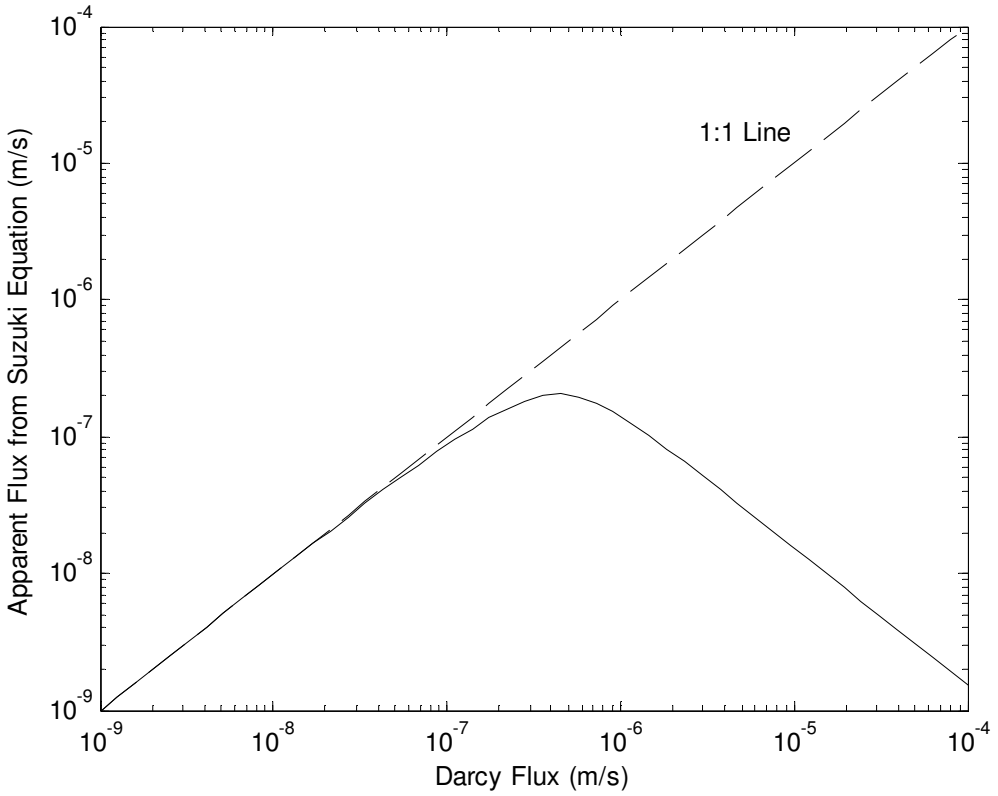

Figure 2.4. Apparent q as calculated using Equation 2.10, the approximation of Suzuki (1960). The values of a and b used in the calculation were taken from Figure 2.3. The approximation becomes increasingly inaccurate for fluxes greater than 10^{-7} m s^{-1}.

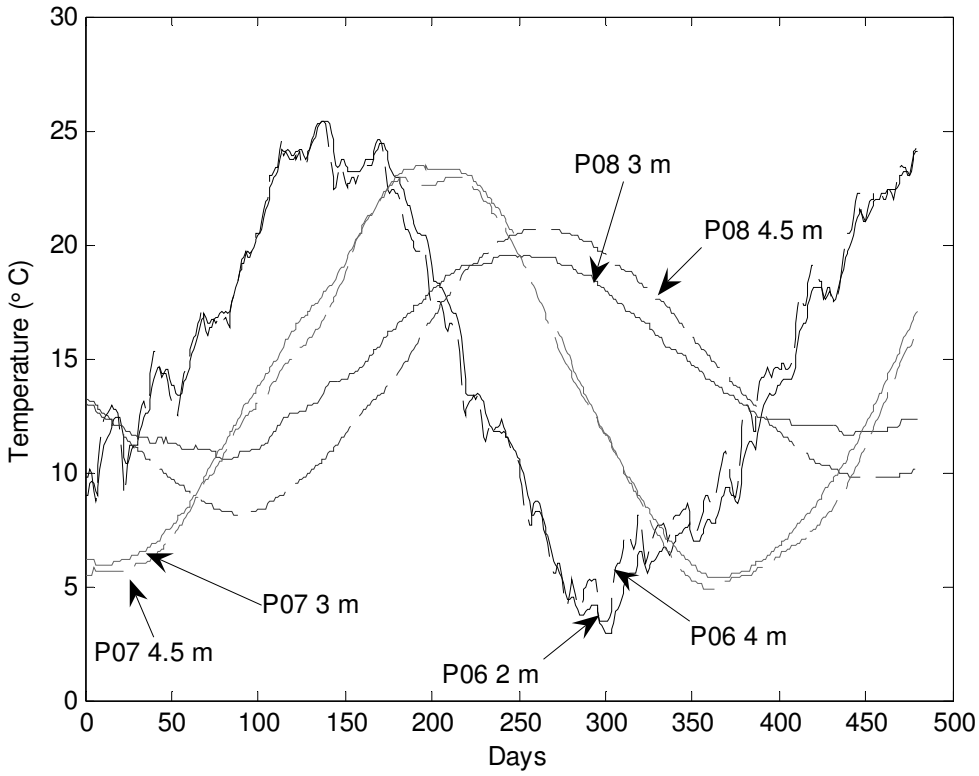

Figure 2.5. Comparison of the shallowest two temperature time series recorded in each of P06, P07, and P08.

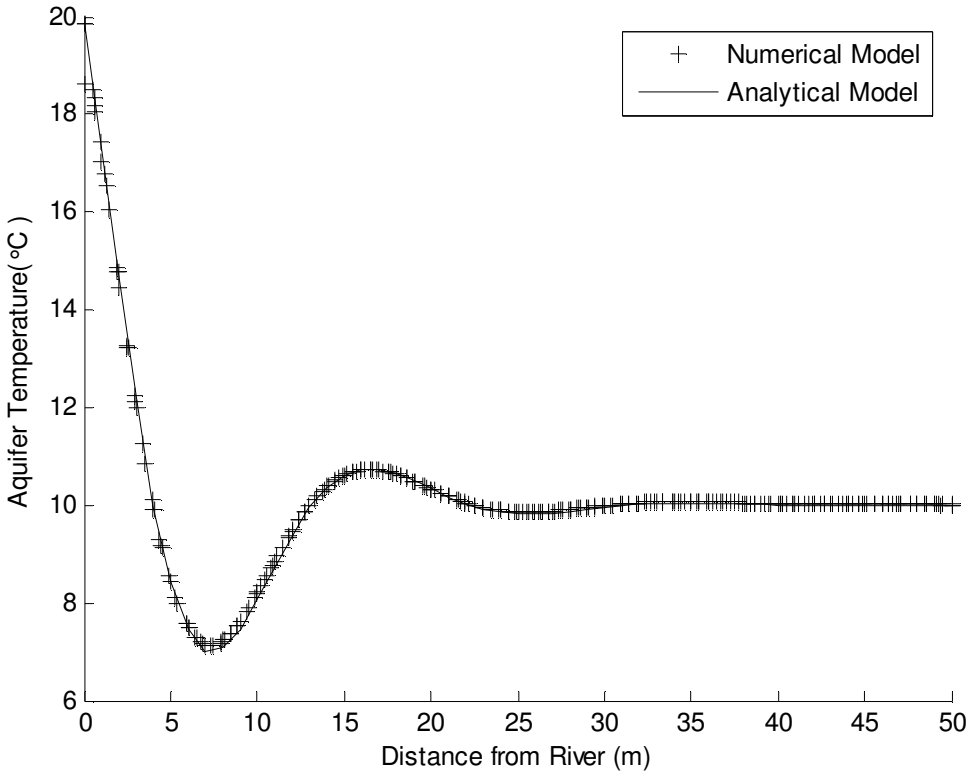

Figure 2.6. Comparison of the analytical and numerical solutions for the aquifer temperature as a function of distance from the source of surface-water recharge. The model was run with a q of 3 x 10^{-7} m s^{-1}, a thermal conductivity of 2.2 W m^{-1} °C^{-1}, and a heat capacity of 3.2 x 10^{6} J °C^{-1} m^{-3}.

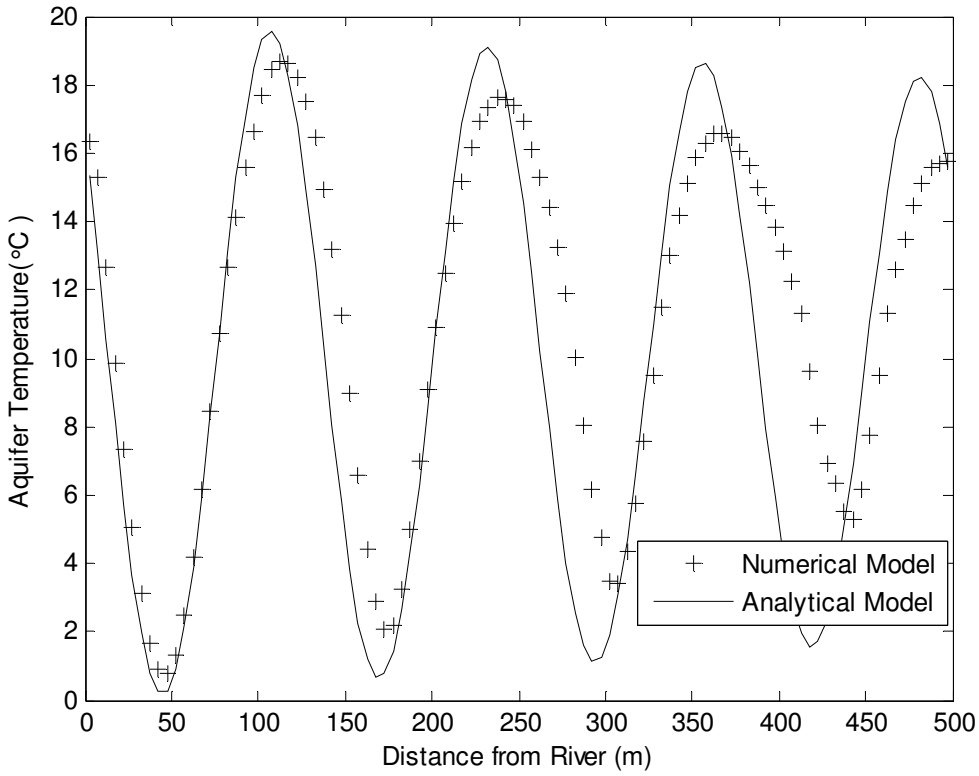

Figure 2.7. Comparison of the analytical and numerical solutions for the aquifer temperature as a function of distance from the source of surface water recharge. The model was run with a *q* of 3 x 10-6 m s^{-1}, a thermal conductivity of 2.2 W m^{-1} °C^{-1}, and a heat capacity of 3.2 x 10^6 J °C^{-1} m^{-3}.

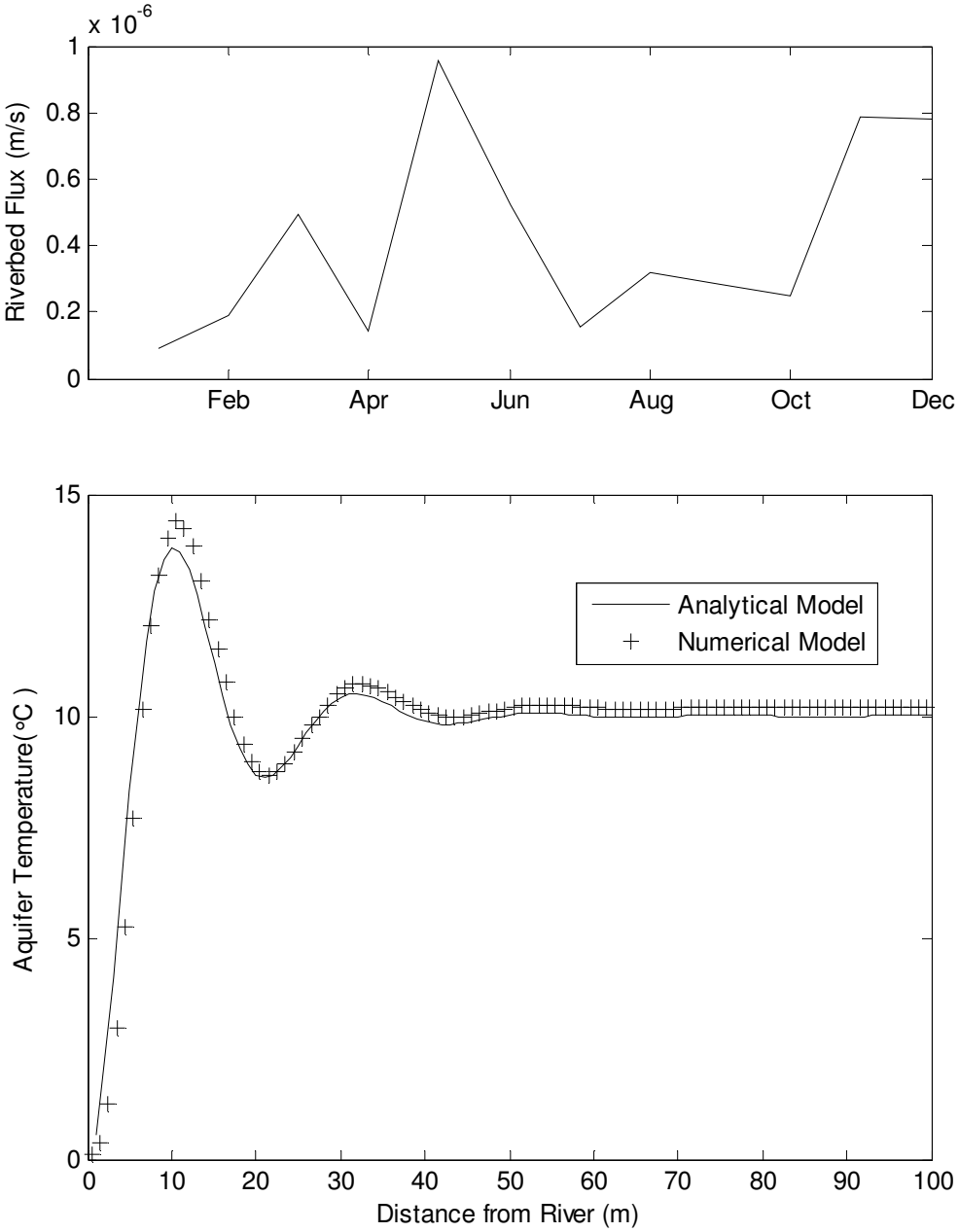

Figure 2.8. Effect of variable recharge on aquifer temperature signal. a) Monthly average fluxes as determined by Bartolino and Niswonger (1999). b) Comparison of the numerical model generated using the monthly fluxes shown in Figure 2.8a with the analytical model generated using a uniform flux of 4.22 x 10^{-7} m s^{-1}. The maximum temperature difference between the two signals is 0.6 °C, while the phase difference in less than 1 m.

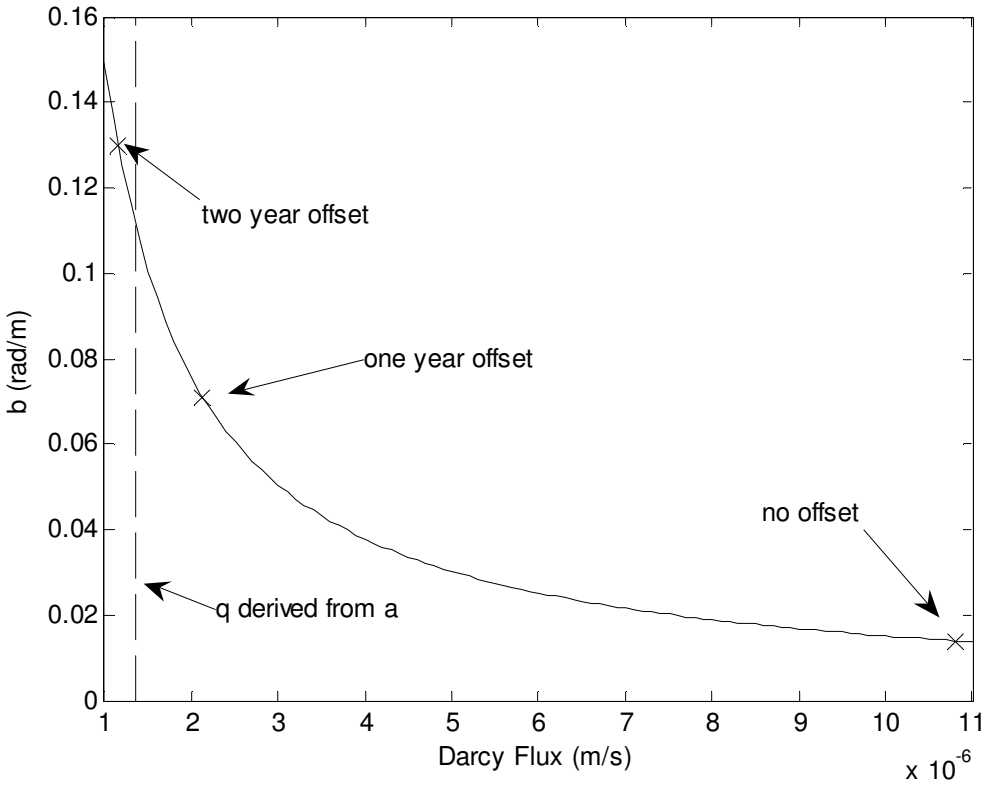

Figure 2.9. The *q* values corresponding to *b* values for P07 and P08 at 4.5 m depth calculated using different lags. The *b*-*q* curve was calculated using a thermal conductivity of 2.16 W m^{-1} $°C^{-1}$ and a heat capacity of 3.2 x 10^6 J $°C^{-1}$ m^{-3}. The *b* value for an offset of three years (not shown) was 0.70, which is outside the range of reasonable values (see Figure 2.3).

Table 2.1. Values of a, b, q_a, and q_b for different time series pairs and depths

Time Series	Depth	a (1/m)	q_a (m/s)	b (rad/m)	q_b (m/s)
P06-P07	4-4.5	3.6×10^{-3}	1.5×10^{-6}	0.11	1.4×10^{-6}
P06-P08	4-4.5	3.8×10^{-3}	1.5×10^{-6}	0.12	1.3×10^{-6}
P07-P08	4.5	4.7×10^{-3}	1.4×10^{-6}	0.13	1.3×10^{-6}
R.Grande-P07	4.5	3.7×10^{-3}	1.5×10^{-6}	0.11	1.4×10^{-6}
R.Grande-P08	4.5	3.8×10^{-3}	1.5×10^{-6}	0.12	1.3×10^{-6}
P06-P07	8	6.2×10^{-3}	1.2×10^{-6}	0.16	9.4×10^{-7}
P06-P08	8	6.9×10^{-3}	1.2×10^{-6}	0.17	8.7×10^{-7}
P07-P08	8	7.7×10^{-3}	1.1×10^{-6}	0.19	7.9×10^{-7}
R.Grande-P07	8	6.8×10^{-3}	1.2×10^{-6}	0.16	9.1×10^{-7}
R.Grande-P08	8	7.2×10^{-3}	1.2×10^{-6}	0.17	8.5×10^{-7}

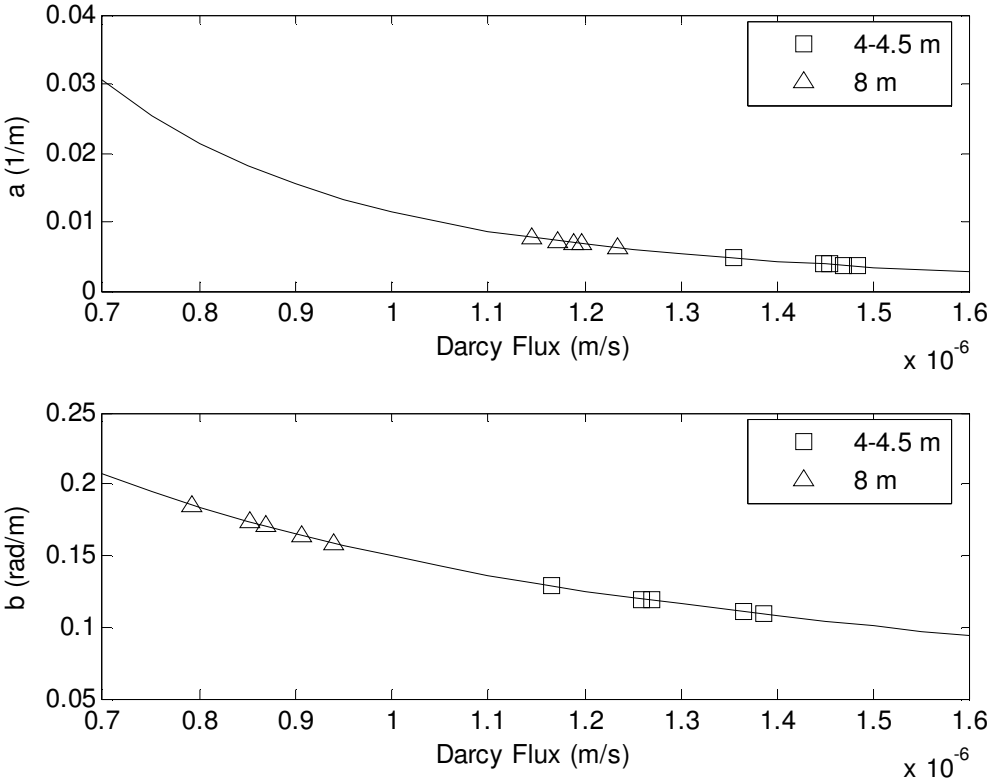

Figure 2.10. Measured values of *a* (above) and *b* (below) plotted on type curves. The curves in this figure are identical to those in Figure 2.3.

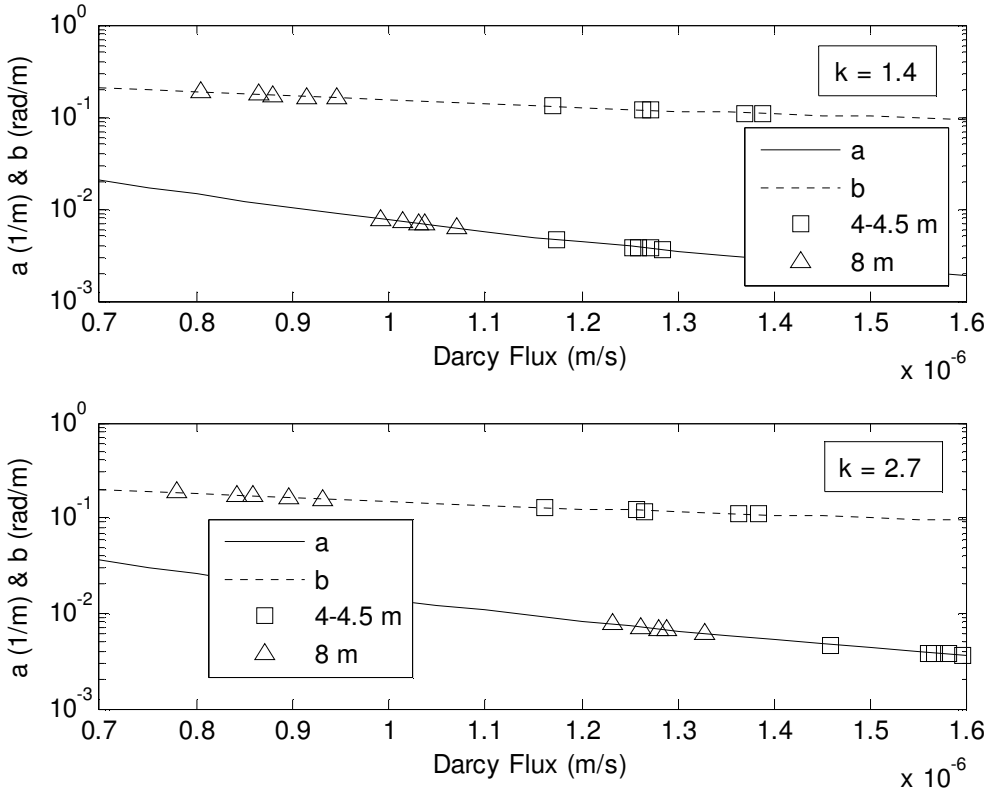

Figure 2.11. The effect of extreme thermal conductivities (1.4 W m^{-1} °C^{-1} for the upper plot, 2.7 W m^{-1} °C^{-1} for the lower plot) on the fluxes estimated from *a* and *b* for the Rio Grande site. Using these values of thermal conductivity changes the fluxes inferred from the type curves in Figure 2.11 by between 10 and 20% for q_a and slightly less for q_b.

Chapter 3

Using Annual Variations in Ground-water Temperature to Characterize Surface-Water-Ground-water Interactions in a Heterogeneous Aquifer near the Mohawk River, New York

Abstract

Annual variations in ground-water temperature can be a useful tracer of infiltrated surface-water. At the Mohawk River site near Schenectady, NY, a large number of wells drilled to characterize induced infiltration have permitted spatially extensive measurements of the annual variation in aquifer temperature. These data show a zone of high temperature variation caused by a plume of infiltrated river water pulled towards municipal supply wells. The aquifer at the site is highly transmissive, so we developed a method-of-characteristics, particle-tracking code to model the advection-dominated thermal transport. Our model of the site shows that the plume of high temperature variation is caused by aquifer thickening over a known bedrock depression. The annual temperature variation data were also sensitive to the magnitude and spatial variation of the riverbed conductance. The results of this study suggest that numerical modeling is required to fully understand temperature data collected in aquifers with complex geometries.

3.1 Introduction

Infiltration of surface-water provides a significant portion of the ground-water budget for many shallow aquifers. When ground-water is pumped from the aquifer, additional infiltration can be induced. The spatial and temporal patterns of induced infiltration can control both the water budget of the aquifer and the ground-water quality. Thus, these

patterns must be understood in order to determine well head protection zones and allowable yields for water supply wells.

Ground-water temperature can be used to delineate spatial and temporal patterns in induced infiltration (for a review, see Anderson, 2005). The temperature of many surface-water bodies varies over annual and diurnal time scales. These temperature changes are propagated into the aquifer by infiltrating surface-water. The advent of new technologies (e.g., Stonestrom and Blasch, 2003; Johnson et al. 2005) has led to an increase in the number of studies using temperature variations to study surface-water-ground-water interactions. Many workers (e.g., Suzuki, 1960; Stallman, 1965; Lapham, 1989; Silliman and Booth, 1993; Silliman et al. 1995; Bartolino and Niswonger, 1999; Fryar et al. 2000; Becker et al. 2004; Hatch et al. 2006) have calibrated analytical or numerical models to measured temperature variations beneath surface-water bodies to estimate the vertical infiltration rate. Ronan et al. (1998) and Su et al. (2004) calibrated numerical models to estimate the fluxes and hydraulic conductivities within a few meters of streams, and Bravo et al. (2002) and Burow et al. (2005) calibrated numerical models of wetlands-aquifer interactions, Bravo et al. (2003) on the scale of tens to hundreds of meters and Burow et al. (2005) on the scale of tens of meters. None of these studies considered the effect of heterogeneity in transmissivity on temperature patterns within an aquifer.

One site where spatially-extensive ground-water temperature data are available is the west bank of the Mohawk River just below Lock E-8 (Figures 3.1 and 3.2), referred to in this chapter as the Mohawk River site. The water supply wells for the towns of Rotterdam and Schenectady withdraw ground-water from a glacial outwash aquifer

within a few hundred meters of the riverbank, creating a cone of depression that induces infiltration from the Mohawk River. Winslow et al. (1965) collected temperature readings in 51 wells as often as weekly between August 1960 and September 1961 (preliminary results from this study were published by Winslow, 1962). They identified a zone stretching from the river towards the Schenectady well field where annual ground-water temperature variation was greatest, and inferred that it was a zone of relatively high transmissivity. O'Brien (1970) conducted a similar study at the same site between September 1968 and December 1969, and identified the same zone of apparent high transmissivity with the same spatial pattern in aquifer temperature signals. O'Brien (1970) also made temperature measurements in shallow soil borings, which are discussed further in Chapter 4.

In this chapter we develop a numerical model of thermal transport on the aquifer scale (hundreds to thousands of meters) at the Mohawk River site. By investigating the sensitivity of the temperature signal to spatial variations in the transmissivity and infiltration flux, we determine that the observed zone of high annual temperature variation is caused by a known thickening of the aquifer, that much of the infiltration from the river occurs above Lock E-8, and that induced infiltration represents less than half of the water withdrawn from the aquifer.

3.2 Mohawk River Site

3.2.1 Geological History

Between 12.2 and 12.6 thousand years BP, near the end of the Late Wisconsinan (Woodfordian) glaciation, the Mohawk River Valley became the spillway for Glacial Lake Iroquois (Muller and Calkin, 1993). The paleo-Mohawk River fed into a glacial

lake in the Hudson River Valley. This lake had four distinct levels, which Wall and LaFleur (1994) designated, in decreasing order of age and elevation, as Lake Albany, Lake Albany II, Lake Quaker Springs, and Lake Coveville. While the relative ages of these lakes are well established, their absolute ages have not been determined. The total length of time that Lake Iroquois drained through the paleo-Mohawk has been estimated to be 500 years (Spectra, 2001). During this prolonged discharge, the paleo-Mohawk seems to have eroded away any older fluvial or glacio-fluvial sediments. The base of the sedimentary sequence in the valley is either bedrock (the Schenectady Formation shale) or low-permeability till.

During the Lake Albany phase, a glacial delta formed in the study area where paleo-Mohawk spilled into the lake. The sands and silts deposited in this delta underlie much of the city of Schenectady, and are present at the Southern end of the study site.

As the lake level fell, a channel was incised through the delta sediments. In the study area, the new channel flowed along the course of the modern Mohawk River. During the Lake Quaker Springs stage, the Scotia Gravel was deposited in this channel. The clasts in this unit, which range from 1 to 10 cm in radius, were remobilized from a similar outwash deposit upstream at Little Falls, NY. Manning equation analysis using the channel geometry and the clast size suggests that the discharge of the paleo-Mohawk would have to have been ~45,000 m^3/s, six times greater than Niagara Falls (Wall, 1995). Sedimentary structures in the Scotia Gravel indicate that it was deposited over a long period of discharge rather than during a series of hlaups (Wall and LaFleur, 1994). Once the retreating ice sheet opened the St. Lawrence River, the Great Lakes Basin no longer drained through the Mohawk River Valley, and the flow of the paleo-Mohawk was

greatly reduced. The heterogeneity observed in the well logs at the site suggests that the Scotia Gravel was reworked by fluvial processes, creating an informal geologic unit defined as the Scotia Channel Deposits in the report by Spectra (2001). Up to 7 m of silt and sandy silt flood deposits overlie the channel deposits at the site.

3.2.2 Hydrostratigraphy

The principal aquifer at the site consists of the Scotia Channel Deposits. This aquifer is bounded to the west by the bedrock wall of the valley and to the south by the silts and sands of the Schenectady Delta Deposits (Figure 3.2). The thickness of the gravel at the site ranges from 0 to 20 m, with the greatest thicknesses occurring above a thalweg, or narrow glacial valley incised into the bedrock.

The Schenectady Delta Deposits are finer-grained than the Scotia Channel Deposits, but their sandy beds may be highly permeable. The sandy soils that develop above this unit allow for high infiltration rates, so no stream channels have developed to carry runoff to the Mohawk River. Instead, streams from the highlands drain to wetlands, which recharge the aquifer. The Schenectady Delta unit is not recharged by the Mohawk River, which is a gaining stream everywhere that pumping has not resulted in induced infiltration (Spectra, 2001).

The modern flood deposits above the aquifer act as a confining layer to some extent (see the discussion of storage in section 3.4.2). There are gravel channels and lenses within these deposits (see Chapter 4, particularly the cross section in Figure 4.6), but the most of the aquifer is separated from the surface by 3 to 7 m of finer-grained sediments.

At the base of the aquifer is a basal till known as the Hells Hollow unit (Wall and LaFleur, 1994). This till is compact and clay-rich, and any flux across it would not form a significant component of the aquifer budget.

3.2.3 Induced Infiltration

The interactions between the aquifer and the Mohawk River are complex. During the navigation season, which begins in early May, the river's stage is controlled by locks, with the elevation of the water surface held at ~68.9 m above Lock E-8 and ~64.6 m below it. In mid-November the water level above the lock is reduced to ~64.9 m, and in mid-January the water level below the lock is reduced to ~64.0 m. The change in river stage results in distinctly different water levels in the aquifer during the navigation and non-navigation seasons (Figures 3.3 and 3.4). This seasonal variation in induced infiltration is reinforced by the temperature dependence of the viscosity of water (e.g., Constantz et al. 1994). Floods can occur during the non-navigation season, but their effect on water levels in the aquifer lasts only a few days (Winslow et al. 1965). The pumping centers withdraw ground-water from storage during the non-navigation season, lowering the water-table, and that storage is replenished during the navigation season, raising the water-table.

Winslow et al. (1965) noted that the head in the aquifer above the lock is often higher than the stage of the river below the lock, confirming that infiltration occurs above the lock. They observed that the riverbed below the lock was covered by up to 1.2 m fine-grained riverbed sediments, and concluded that very little infiltration occurred there.

A pumping test using the water supply wells at the site (Malcolm Pirnie, 1989) showed that, with a pumping rate of ~140,000 m^3/day, the cone of depression extended to the far

northeastern bank of the river, indicating that the river is not a true flow boundary. However, the drawdown on the far bank was slight (0.15 m) and it extended less than 100 m from the bank. The pumping test was performed in February of 1988, when infiltration rates would be low due to low river stages and cold water temperatures.

Very low levels (1 ppb or less) of volatile organic compounds (VOCs) were intermittently detected in the Schenectady and Rotterdam pumping wells before 1997 (pumping rates reached their maximum in 1996 and then fell to their current levels). These compounds can be traced to an industrial park across the river (Alpha Geosciences, 2001), indicating that the capture zone of these wells can extend to the far bank of the river. As the VOCs were only intermittently detected at low concentrations, it seems likely that the pumping centers only capture water from the far bank of the river when pumping rates are high and infiltration rates are low.

3.2.4 Water Budget

The Rotterdam and Schenectady pumping stations withdraw roughly 70,000 m^3 of ground-water each day, with 90% of that total pumped by Schenectady. The water is derived from induced infiltration from the river, recharge from precipitation, and flow from the lower-permeability sands to the south.

The average annual precipitation in the Schenectady area is 0.9 m, which is distributed fairly evenly over the year. Winslow et al. (1965) used monthly ET calculations to find that 0.27 m/yr of that total were available for surface runoff and aquifer recharge. As the area around the Mohawk River site is rather poorly drained, we used a recharge rate of 0.3 m/yr, which corresponds to a flux of 790 m^3/day, or just over 1% of the withdrawal

rate. It was not possible to measure stormwater runoff derived from this poorly-drained region to further constrain recharge estimates.

The proportion of the water withdrawn from the aquifer by the two pumping wells has not been resolved. Malcolm-Pirnie (1989) used recharge-boundary analysis (Theis and Conover, 1963) to estimate that 72% of the water pumped from the two well fields was induced infiltration. However, this estimate was based on a pumping rate (1.6 m^3/s) twice the normal value. In addition, the cone of depression reached the far bank of the river during their test, indicating that, contrary to the assumptions of their model, the river was not acting as a recharge boundary.

We have used geochemical mixing lines (e.g., Mazor, 2004) to estimate the quantity of induced infiltration from the Mohawk River to the pumping wells. In July 2005, samples were collected from the Mohawk River, three of Rotterdam's pumping wells (Rotterdam Well 1, Rotterdam Well 3, and Rotterdam Well 4), and city of Schenectady's water supply (we were not granted access to Schenectady's well field, so the sample was collected from an end user of the city's water) (See appendix C). Four samples were taken from the river in order to minimize the effect of river chemistry fluctuations. Rotterdam Wells 1, 2 and 3 are between the river and Rotterdam Well 4, so it is reasonable to assume that Rotterdam Well 4 does not receive a significant fraction of river water. Thus, on each mixing line, the chemical constituents measured in Rotterdam Well 1, Rotterdam Well 3, and the Schenectady municipal water supply fall on a mixing line between the river water and the water not derived from the river. Figure 3.5 shows the mixing lines for chloride concentration, alkalinity, total dissolved solids, calcium concentration and silica concentration. Table 3.1 shows the fractions of river water that

can be inferred for these samples based on these constituents. As estimates based on a single constituent may vary due to analytical errors or secondary processes, it is best to use the average of a number of estimates. According to these analyses, the average fraction of river water in Schenectady wells is 0.26. As the samples for this analysis were collected in the summer months, when infiltration is high, it may represent an overestimate of the fraction of river water on an annual basis.

It is important to note that the river is dredged periodically, so data regarding river-aquifer interactions from different eras may be representative of different conditions. However, the estimated fraction of river water in 2005 (26%) provides a reasonable starting point for the simulation of the aquifer at the time of the Winslow study (Winslow et al. 1965).

3.3 Temperature Data

There have been two major studies that have collected temperature data at the Mohawk River site in an effort to characterize the flux to the aquifer. Winslow et al. (1965) measured temperatures weekly in 51 wells across the site between August 1960 and September 1961. O'Brien (1970) measured temperatures in as many as 44 wells eight times between September 1968 and December 1969. O'Brien (1970) also measured soil temperatures in 1.8 m deep borings over the same area. In the intervening years, virtually all of the wells used in these studies have been destroyed, many by the construction of Interstate 890 across the site (Figure 3.1). As a new set of temperature measurements with modern sensors would have fewer than 10 wells to work with, we have chosen to use these existing data sets.

The report by Winslow et al. (1965) does not include all of the temperature data collected, but instead a map of the annual range in temperature at each well. These data, reproduced in Figure 3.6, show a distinct spatial pattern. The temperature variation is high near the river (17.2 to 20.6 °C), lower in the lower permeability sediments to the south (1.7 to 4.5 °C) and near the bedrock valley wall (5.0 to 9.4 °C). There is also a plume of high temperature variation (10.0 to 16.1 °C) leading from the river to the Schenectady well field. Winslow et al. (1965) inferred that this plume represented a zone of high transmissivity.

O'Brien (1970) measured temperatures in wells and shallow soil borings (discussed in Chapter 4). This data set is less complete than the Winslow data set, as fewer than 25 wells were included during the first five sampling rounds, and the last three rounds only span the period from August to December of 1969. However, unlike the Winslow data set, O'Brien (1970) includes all of the measured temperatures. He observed the same plume of high temperature variation seen in Figure 3.6, and also attributed it to a high transmissivity zone.

O'Brien (1970) measured profiles of temperature variation with depth in each well at each sampling period (a sample set of profiles is shown in Figure 3.7). The temperature varies with depth, and seasonal temperature changes occur at different times and with different magnitudes at different depths. These vertical variations indicate that the flux through the aquifer (and therefore the hydraulic conductivity) varies with depth. Thus, the 2-D model used in this chapter cannot fully reproduce the behavior of the aquifer at the scale of meters.

3.4 Aquifer Model

3.4.1 Numerical Model

Thermal transport in an aquifer is governed by:

$$\nabla^2 \frac{\kappa}{\rho c} T - \frac{\rho_f c_f}{\rho c} \nabla \cdot (\mathbf{v}\, T) = \frac{\partial T}{\partial t} \qquad (3.1).$$

In equation 3.1, κ is the thermal conductivity of the saturated aquifer, T is temperature, ρ_f and c_f are the density and specific heat capacity of the fluid, $\mathbf{v}$ is the Darcy flux, and ρ and c are the volumetrically-averaged density and specific heat capacity of the aquifer sediments and fluid. This equation assumes that the aquifer materials have the same temperature as the fluid, a reasonable assumption when modeling annual temperature variations.

Anderson (2005) compiled a list of eight codes that are freely or commercially available for the simulation of coupled ground-water flow and heat transport. All of these codes simulate thermal transport using a finite element or finite difference approximation to Equation 3.1. A stability criterion for these models is that the thermal Peclet number, *Pe*:

$$Pe = \frac{\rho_w c_w q \Delta x}{\kappa} \qquad (3.2) \quad ,$$

where Δx is the characteristic dimension of the spatial discretization of the model domain. When *Pe* is less than 2, the differential equation is elliptic (diffusion-dominated), and finite difference and finite element models perform well. When *Pe* is greater than 2, the differential equation becomes hyperbolic (advection-dominated), and finite difference and finite element models produce unrealistic oscillations. In permeable aquifers, where advective heat transfer dominates, it can be difficult to create a model with $Pe<2$. At the Mohawk River site, for example, where our model shows that the flux along the bedrock

valley is roughly 5 x 10^{-5} m/s, a finite difference model of thermal transport would need a grid finer than 0.02 m. Near the well fields, the fluxes are even greater. Finer meshes also require smaller time steps, further adding to the computational burden.

The method of characteristics, or particle tracking, can also be used to model differential equations with the form of Equation 3.1. The key to the method of characteristics is to solve the advective and conductive terms of equation 3.1 separately. At each time step, the movement of particles through the aquifer is used to calculate the Lagrangian derivative of temperature, and then a finite difference model is used to calculate the conductive heat transfer.

While the method of characteristics is commonly used to simulate contaminant transport, it has not, to our knowledge, been used to simulate thermal transport at the aquifer scale. We thus wrote our own code (mohawkparticletrack.m, given in Appendix B), following the general structure used by Konikow and Bredehoeft (1970) for solute transport. At each time step, the code simulates flow using a 2-D finite difference grid, then propagates the particles through the resulting velocity field. After the particles have been moved, the diffusive portion or Equation 3.1 is solved.

The heat transport model is explicitly coupled to the flow model by the presence of the Darcian flux, **v**, in Equation 3.1. The flow model is coupled to the heat transport model by the temperature dependence of *K*. Hydraulic conductivity is inversely dependent on the viscosity of water, which varies by a factor of two between 0 and 25 °C. By fitting a polynomial to data from Dingman (1994), this relationship can be approximated as

$$\mu = 6.978\times10^{-7}T^2 - 5.310\times10^{-5}T + 1.777\times10^{-3} \qquad (3.3)$$,

where μ is viscosity in N s m^{-2}. Equation 3.3 is valid within the temperature range of the data used for the fit (0 to 30 °C). The effect of temperature on the density of water can also affect the coupling of ground-water flow and heat flow. However, between 0 and 30 °C density changes by less than 0.5%, so the effect of density differences due to temperature is not included in the model.

The code used in this paper can only be used to simulate 2-D aquifers, either confined or subject to the Dupuit assumption. The temperature data collected by O'Brien (1970) vary with depth, and suggest that flow and thermal transport at the Mohawk River site are fully 3-D processes. Thus, the goal of the current study is not to fully calibrate a model to the available data, but to explore the hydrogeologic conditions required to develop a temperature plume similar in essential characteristics (timing, magnitude, dimensions) to the one observed by Winslow et al. (1965) and O'Brien (1970). A secondary goal is to demonstrate the feasibility of the method of characteristics for modeling thermal transport in highly advective aquifers.

3.4.2 Aquifer Properties

Aquifer thermal properties vary by much less than hydraulic conductivity, so they are typically modeled as homogenous within geologic units. The volumetric heat capacity of saturated gravel, ρc, is typically considered to be the volumetrically-weighted sum of the heat capacities of the matrix material and of water. Lapham (1989) presents calculated values of ρc ranging from 2.1-3.6 x 10^6 J $°C^{-1}$ m^{-3}, but the upper and lower limits correspond to sediments with exceptionally low and high porosities. We used a value of 3.2 x 10^6 J $°C^{-1}$ m^{-3} in our model. The measured values for the thermal conductivity of

saturated coarse-grained sediments, κ, range from 1.88 to 2.69 W m^{-1} $°C^{-1}$ (Markle et al. 2006). The model uses a value of 2.0 W m^{-1} $°C^{-1}$.

Several estimates of the transmissivity of the aquifer at the Mohawk River site are available. Winslow et al. (1965) reported the results of earlier pumping tests, which found that the transmissivity ranged from 0.7-2.2 m^2/s. O'Brien (1970) analyzed several USGS pumping tests, and found that transmissivity ranged from 0.4- 2.2 m^2/s. O'Brien (1970) also used flow net analysis to estimate transmissivities of 0.1- 2.5 m^2/s. More recently, Malcolm-Pirnie (1989) analyzed the results of a pumping test to determine that the transmissivity of the aquifer ranged from 0.45-0.64 m^2/s, with hydraulic conductivities between 0.015 and 0.042 m/s, with an average value of 0.027 m/s. As the Malcolm-Pirnie test had the longest duration (72 hours) we chose to use their average hydraulic conductivity in our model.

Winslow et al. (1965) used a large number of drill logs to map the thickness of the principal aquifer across the site. They found the gravel was thickest (~19 m) in the thalweg running across the site, and that it thinned towards the site boundaries. Our model uses a thickness map (Figure 3.8) contoured from their values. All thicknesses less than 2 m were set to 2 m to avoid overly restricting flow in data-poor areas, and the thickness of the Schenectady delta unit was set to 5 m.

With the exception of values based on a small number of data measurements, the pumping test compiled and analyzed by O'Brien (1970) found storativities of 0.01 to 0.13. We chose to use a single specific yield of 0.1. This value is lower than the typical values of specific yield for gravel (e.g., Fetter, 1994), but the bimodal grain size

distribution in the cobble-and-sand aquifer is likely to result in a relatively low porosity (e.g., Koltermann and Gorelick, 1995).

3.4.3 Boundary Conditions

The finite difference grid used to model the Mohawk River site is bounded by the river to the east, the valley wall to the west, and the Schenectady delta deposits to the south. A 30 m grid size was chosen as a compromise between computational speed, which is greater with coarser grids, and numerical accuracy, which is greater with finer grids. Note that this 30 m grid corresponds to a Peclet number of ~3000 in the bedrock valley. The valley wall is modeled as a no-flow boundary. While the hydraulic conductivity of the bedrock may not be zero, it is several orders of magnitude less than the hydraulic conductivity of the sediments. The Mohawk River site model is insensitive to the type of thermal boundary condition used for the valley wall. The models presented in this chapter were created using a zero heat flow condition.

As seen in Figures 3.3 and 3.4, there is a steep hydraulic gradient across the Schenectady Delta unit at the south of the model during both navigation and non-navigation seasons. The portion of the model grid that represents this unit has a lower hydraulic conductivity than the primary aquifer, and the model's southern boundary is of the constant head type. We adjusted the head at the boundary to match the observed hydraulic gradient south of the Schenectady pumping wells. While this approach does not fully represent the hydraulic processes within the Schenectady Delta unit, it captures their first order impact on the flow system in the aquifer to the north. The data show that the temperatures in the Schenectady Delta unit vary by up to 4.5 °C, much less than the measured variations in the portions of the aquifer affected by river recharge. As the phase and spatial variability

of this oscillation are unknown, we chose not to include it in our model. The southern boundary is held at a constant temperature.

Ground-water surface-water interactions are complex, 3-D, and vary greatly in space and time. As discussed in sections 3.2.3 and 3.2.4 above, the magnitude and spatial distribution of the induced infiltration from the Mohawk River are not well understood. Thus, our treatment of the river boundary is not intended to represent these processes exactly, but rather to introduce a flux of variable-temperature river water into the aquifer. The two characteristics of river infiltration we chose to represent were head dependence and temperature dependence. Thus, the specified flux introduced into a river boundary cell is

$$q_{river} = C(stage - h)\frac{\mu(T_{river})}{\mu(T_{ref})} \qquad (3.4) \quad ,$$

where *stage* is the elevation of water in the river, *h* is the head in a cell on the river boundary, T_{river} is the temperature of the river, T_{ref} is the reference temperature at which the hydraulic conductivities are reported (10 °C in this model), and the viscosities are calculated using Equation 3.3. The constant of proportionality, *C*, is a lumped parameter relating flux to head difference. As *C* is similar to riverbed conductance in the MODFLOW river package (Harbaugh et al. 2000), we refer to it as a conductance. As described above, the river stage varies with time, and is different above and below the lock. Winslow et al. (1965) observed that, at the time of their field work, the riverbed downstream of the lock was blanketed by up to 1.2 m of fine-grained sediment, and that consequently very little river water was able to infiltrate. We therefore used two *C* values in our model: below the lock and one ten times greater above the lock. The river is modeled as a time-varying temperature boundary. The temperature signal is a sinusoid

based on the data shown in Figure 4.11, truncated to reflect the fact that the river does fall below 0 °C.

3.4.4 Model Evaluation

We ran the Mohawk River site model more than 100 times to assess the sensitivity of the temperature signal to model parameters. As noted above, the aquifer at the site has a complex 3-D structure, and the modeled interactions between the Mohawk River and the aquifer are greatly simplified. As a result, we did not attempt to formally calibrate the model to the available data. Instead, we adjusted the fluxes from the southern delta deposits and the river boundary to meet two conditions:

1. The modeled heads on August 3rd and December 29th were in reasonable agreement (within roughly 0.3 cm) with Figures 3.3 and 3.4.
2. The flux from the river equaled 20-30% of the water withdrawn by the pumping wells, in accordance with the geochemical data.

We adjusted the river boundary flux by varying C and the flux from the south by varying the hydraulic conductivity and thickness of the Schenectady delta deposits. We found that our criteria were met using a C of 1.7 x 10^{-5} m/s above the lock and 1.7 x 10^{-6} m/s below, and Schenectady Delta deposits with a thickness of 5 m and a hydraulic conductivity of 0.0135 m/s (one half the hydraulic conductivity of the aquifer). This combination resulted in a total induced infiltration equal to 20% of the withdrawn water. The modeled water-table configurations are shown in Figures 3.9 and 3.10.

3.4.5 Results

Figure 3.11 compares the modeled annual temperature variation in the aquifer with the annual temperature variations observed by Winslow et al. (1965). The model reproduces

the geometry and the magnitude of the observed plume reasonably well. It appears that the plume is controlled by the increased thickness of the aquifer in the southward extension of the bedrock valley (Figure 3.8). The model significantly over-predicts the temperature variation north of the Schenectady pumping center close to the valley wall. The aquifer in this area is thin, so fewer exploratory wells have been drilled there, leaving its geometry and properties poorly constrained. Thus, the low observed temperature variations could be due to a facies change at the edge of the channel resulting in a zone of low transmissivity, a promontory in the bedrock cutting the area off from the infiltration zone above the lock, or simply an abrupt and irregular thinning of the aquifer. Only small portion of the infiltrating river water flows through the area close to the bedrock wall, so the failure of the model in this area should not affect the model as a whole.

3.5 Discussion

3.5.1 Temperature Variation as a Tracer of Transmissivity Variations

The results shown in Figure 3.11 show that, as inferred by Winslow et al. (1965) and O'Brien (1970), the zone of high annual temperature variation represents a high transmissivity pathway. However, neither of those studies attributed this zone to the known increased thickness of the aquifer beneath it- both studies, in fact, specifically note that the plume is not aligned with the deepest part of the bedrock valley. The Rotterdam pumping center captures low temperature variation water from the south and pulls it into the thickest part of the aquifer, so the plume of high temperature variation water does not appear to travel along the bedrock valley. This study suggests that spatial patterns in aquifer temperature variations do contain information about high transmissivity zones that act as preferential pathways of surface-water infiltration, but

they are also affected by other factors. Interpretations of spatial patterns in aquifer temperature variation should therefore be supported by numerical modeling.

3.5.2 River-Aquifer Interactions

Our modeling shows that the magnitude of the temperature variation in the plume of infiltrated river water is partly controlled by the magnitude of the induced-infiltration flux. Figures 3.12 and 3.13 show the annual aquifer temperature variations modeled using river boundary fluxes that totaled 11% and 50% of the withdrawal, respectively. While the lower infiltration plume (Figure 3.12) is similar to the plume in Figure 3.1, the plume's temperature variation in the high infiltration case (Figure 3.13) is much greater than the other model results or the field data. Based on these results, the induced infiltration flux could represent a lower fraction of the water budget than suggested by the chemistry data in Table 3.1, but it must be lower than one-half of the total.

The magnitude of the temperature variation in the plume is also sensitive to spatial patterns in induced infiltration. Figure 3.14 shows the annual variation in aquifer temperature generated using a C value of 1.3×10^{-5} m/s along the entire length of the river boundary. The geometry of the plume is similar to Figure 3.6, but the modeled temperature variations (~20 °C) are much greater than the observed values. This result implies that the attenuated temperature variation observed in the plume of infiltrated river water is dependent on the greater path length from the lock to the Schenectady wells. Note that the modeled temperature variations north of the Schenectady pumping center and close to the valley wall are in much better agreement with the data than are the modeled variations in that region in Figure 3.11. However, we have concluded that the evaluation of models of the Mohawk River site should be weighted more heavily by their

performance near the river and pumping wells than by their performance in areas that are poorly constrained and experience little flow.

3.6 Conclusions

The modeling exercise described above shows that the plume of high annual temperature variation observed by Winslow et al. (1965) and O'Brien (1970) is caused by the thickening of the aquifer in a bedrock valley. No variations in hydraulic conductivity are required to match the first order patterns in the annual temperature variation data, although such variations are not ruled out by results. While the model performs poorly north of the Schenectady pumping centers near the valley wall, that portion of the aquifer is not well-characterized, and has a minimal impact on the rest of the flow system.

The annual temperature variation data proved able to constrain the magnitude and spatial variation of the flux from the river. Our results suggest that much of the infiltration in 1960 originated above Lock E-8, a conclusion also reached by Winslow et al. (1965). The model also suggests that less than 50% of the water withdrawn by the pumping centers infiltrated from the river. Our geochemical analysis indicates that this result holds true today. If the bulk of Schenectady and Rotterdam's water comes from the Schenectady delta deposits to the south, then it is important that the wetlands that recharge the unit are adequately protected. The NYDEC is currently studying the interchange between the aquifer and the wetlands using stable isotopes as tracers. Given the apparent success of our water chemistry study, it seems likely that a larger scale study using our approach with samples collected in more wells and at different times of the year could accurately constrain the water budget of the aquifer.

To our knowledge, this work represents the first application of a method-of-characteristics particle-tracking model of aquifer temperature at the field scale. This approach should be useful at other high transmissivity sites where high thermal Peclet numbers make finite element or finite difference modeling of the temperature field computationally difficult. The greatest weakness of the current model is the crude representation of the infiltration of river water. A 3-D model that extended beyond the northeastern bank of the river would allow for a more accurate simulation of surface-water-ground-water interactions at the site. However, the current model replicates the first order patterns observed in the available aquifer temperature data in a highly permeable aquifer, demonstrating the feasibility of the approach.

	Rotterdam 1	Rotterdam 3	Schenectady Tap Water
Chloride	0.59	0.30	0.25
Alkalinity	0.39	0.30	0.27
Total Dissolved Solids	0.48	0.36	not measured
Calcium	0.52	0.35	0.28
Silica	0.39	0.24	0.24
Average	**0.47**	**0.31**	**0.26**

Table 3.1. Estimated fractions of river water pumped by the city of Rotterdam and the city of Schenectady based on mixing line analysis (Figure 3.5) using July 2005 water samples.

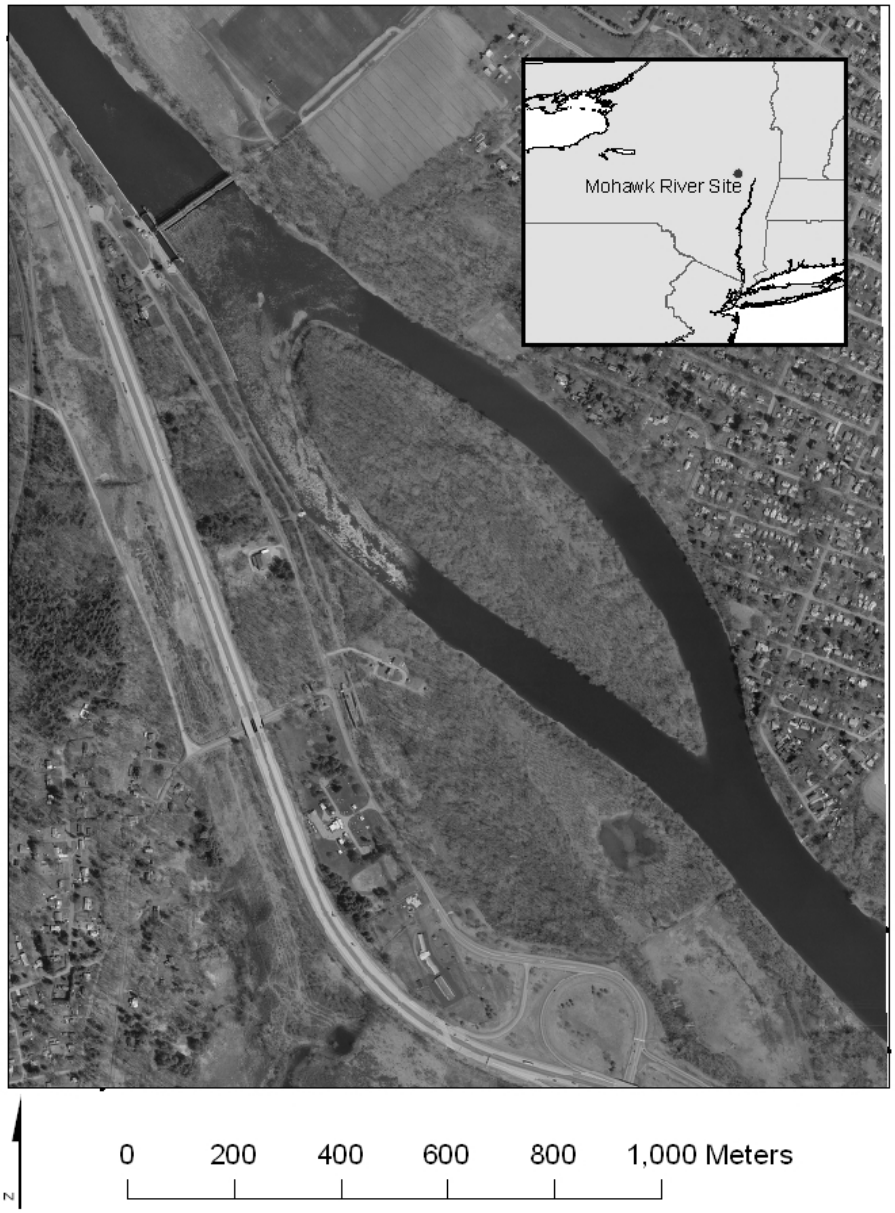

Figure 3.1. Aerial imagery of the Mohawk River site, with an inset indicating its position in New York state. Interstate 890, which runs from north to south on the west bank of the river, was not yet built at the time of the Winslow et al. (1965) and O'Brien (1970) studies.

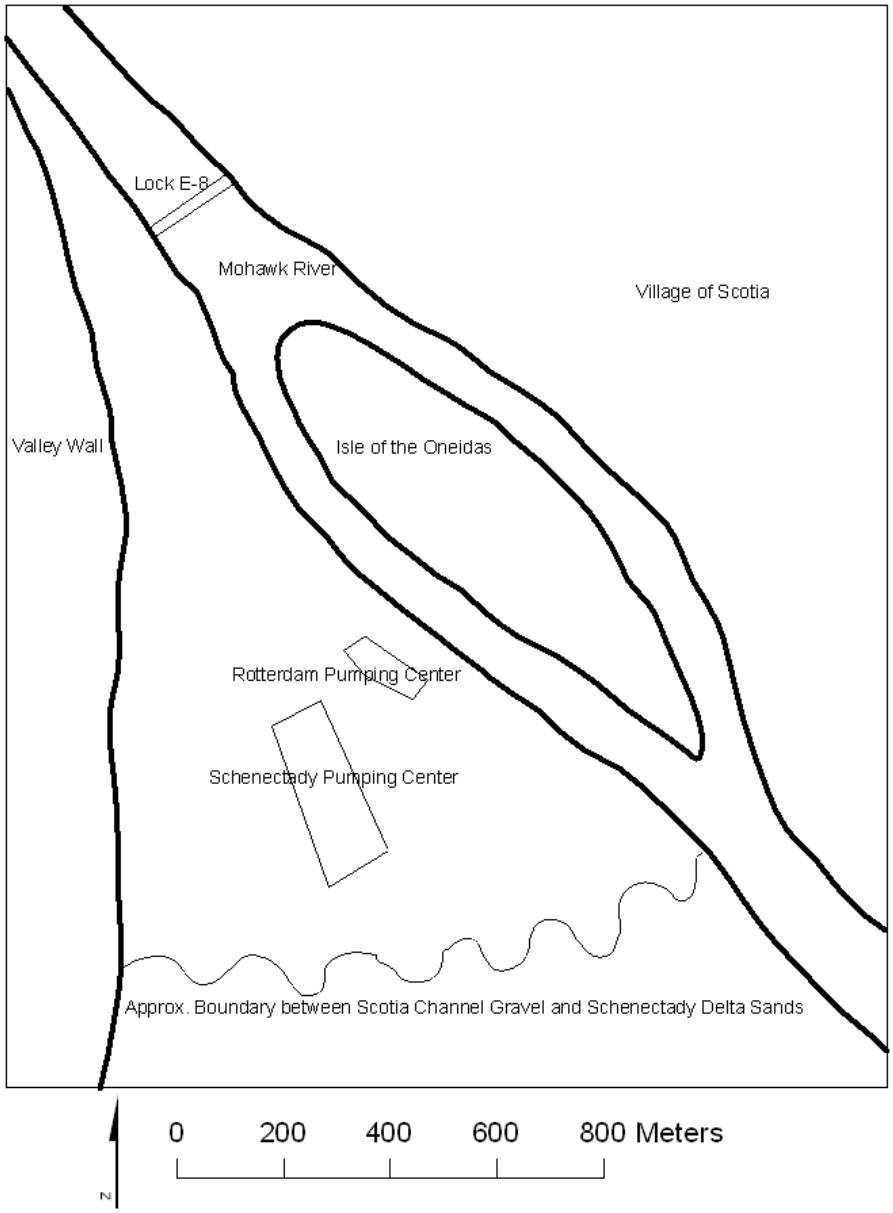

Figure 3.2. Annotated sketch of the Mohawk River site indicating key features.

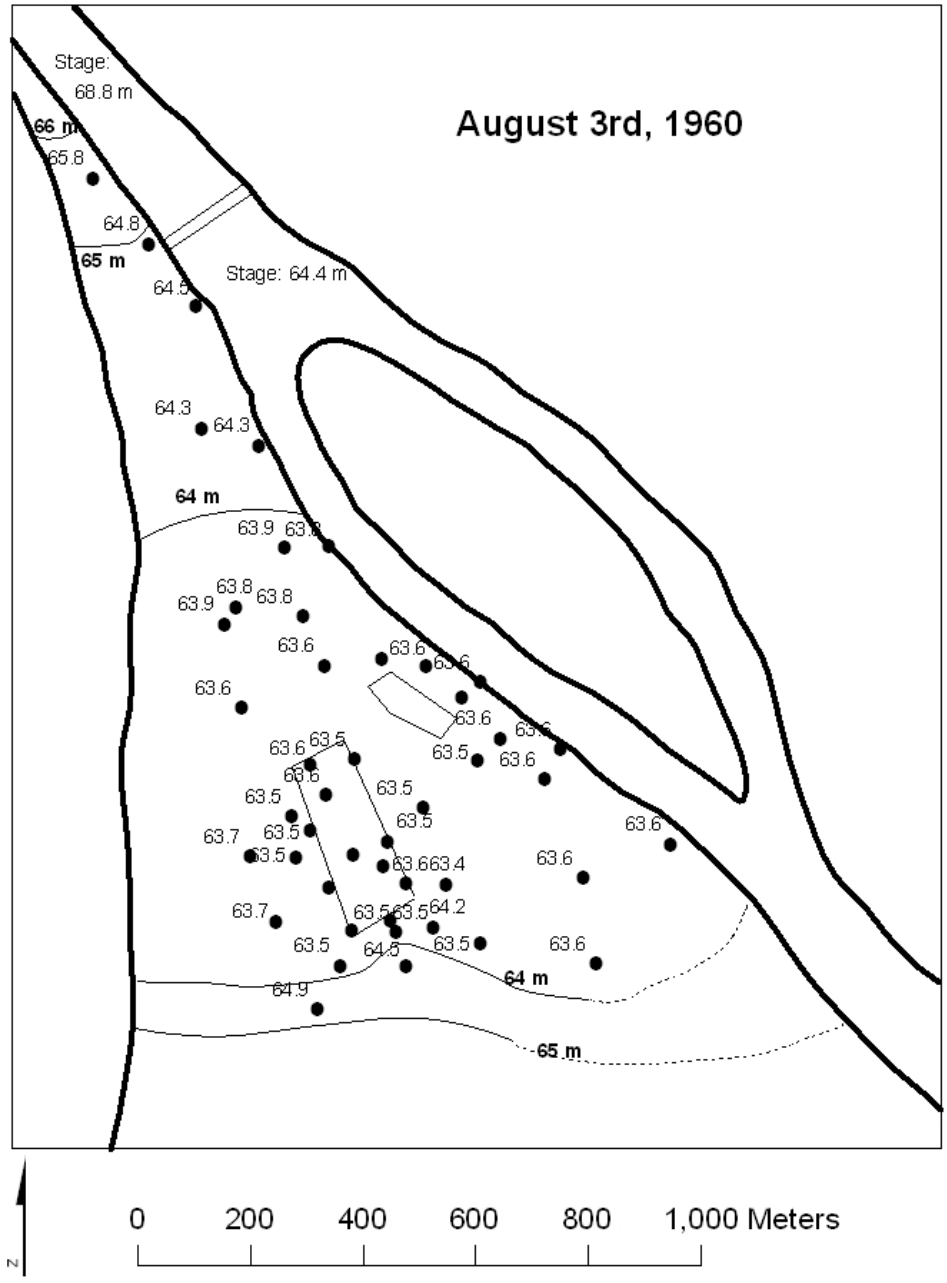

Figure 3.3 Water-table elevations, in meters above sea level, measured on August 3rd, 1960. Data taken from Winslow et al. (1965).

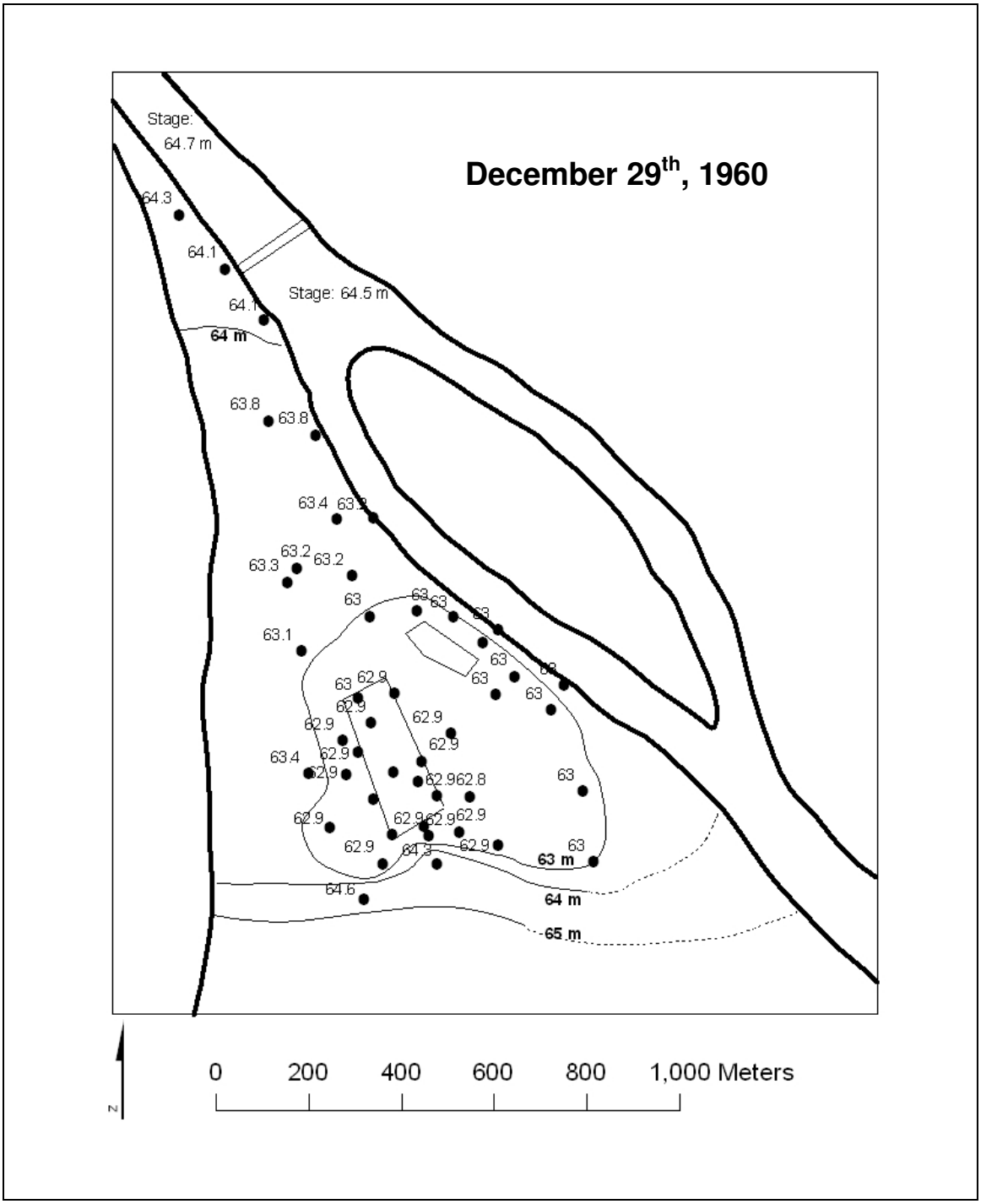

Figure 3.4. Water-table elevations, in meters above sea level, measured on December 29th, 1960. Data taken from Winslow et al. (1965).

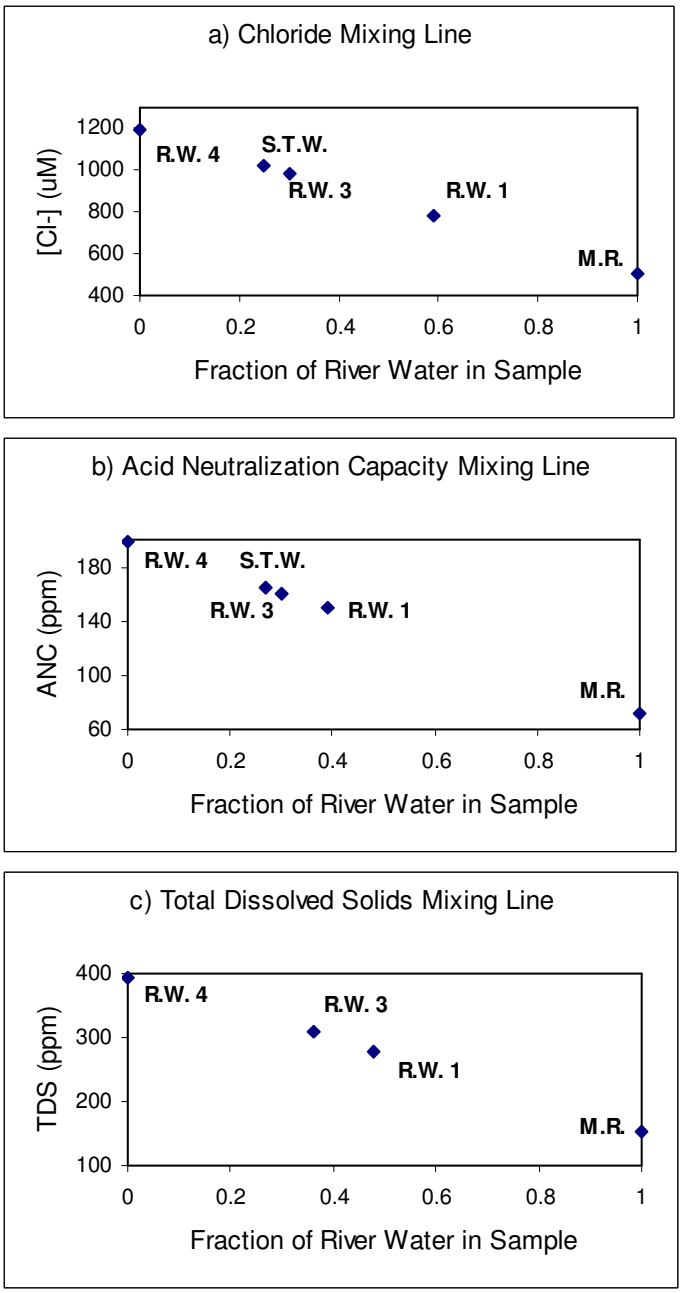

Figure 3.5. Mixing lines for geochemical parameters of water samples taken from Rotterdam Well 4 (R.W.4), Rotterdam Well 3 (R.W. 3), Rotterdam Well 1 (R.W. 1), Schenectady tap water (S.T.W.) and the Mohawk River (M.R.). The *y*-values on these plots are measurements, and the *x*-data are calculated so that the samples fall on a straight line between the two end members (R.W. 4 and M.R.). The *x* values can then be compared to determine the fraction of each end member in the sample (Table 3.1).

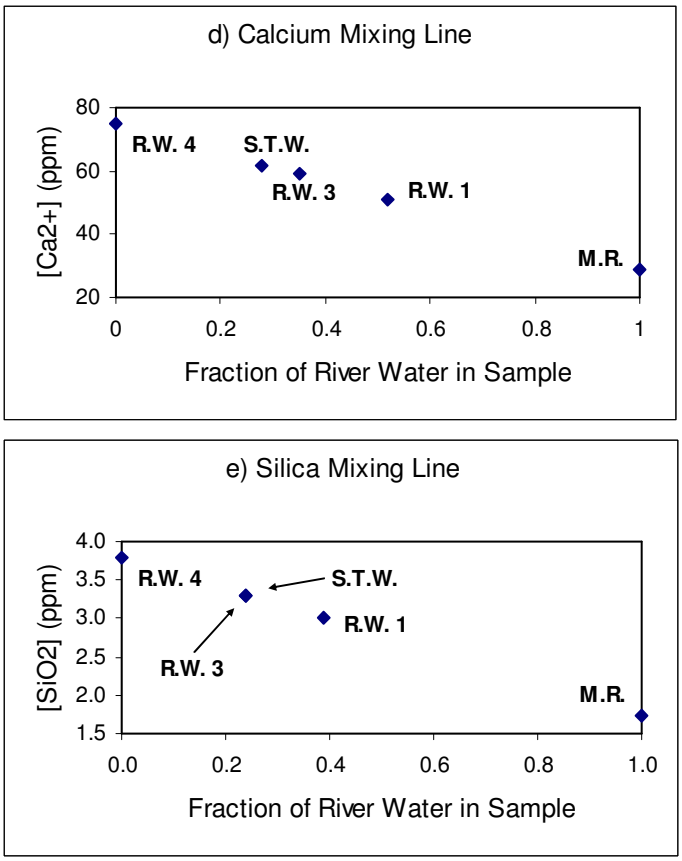

Figure 3.5 (cont'd). Mixing lines for geochemical parameters of water samples taken from Rotterdam Well 4 (R.W.4), Rotterdam Well 3 (R.W. 3), Rotterdam Well 1 (R.W. 1), Schenectady tap water (S.T.W.) and the Mohawk River (M.R.). The *y*-values on these plots are measurements, and the *x*-data are calculated so that the samples fall on a straight line between the two end members (R.W. 4 and M.R.). The *x* values can then be compared to determine the fraction of each end member in the sample (Table 3.1).

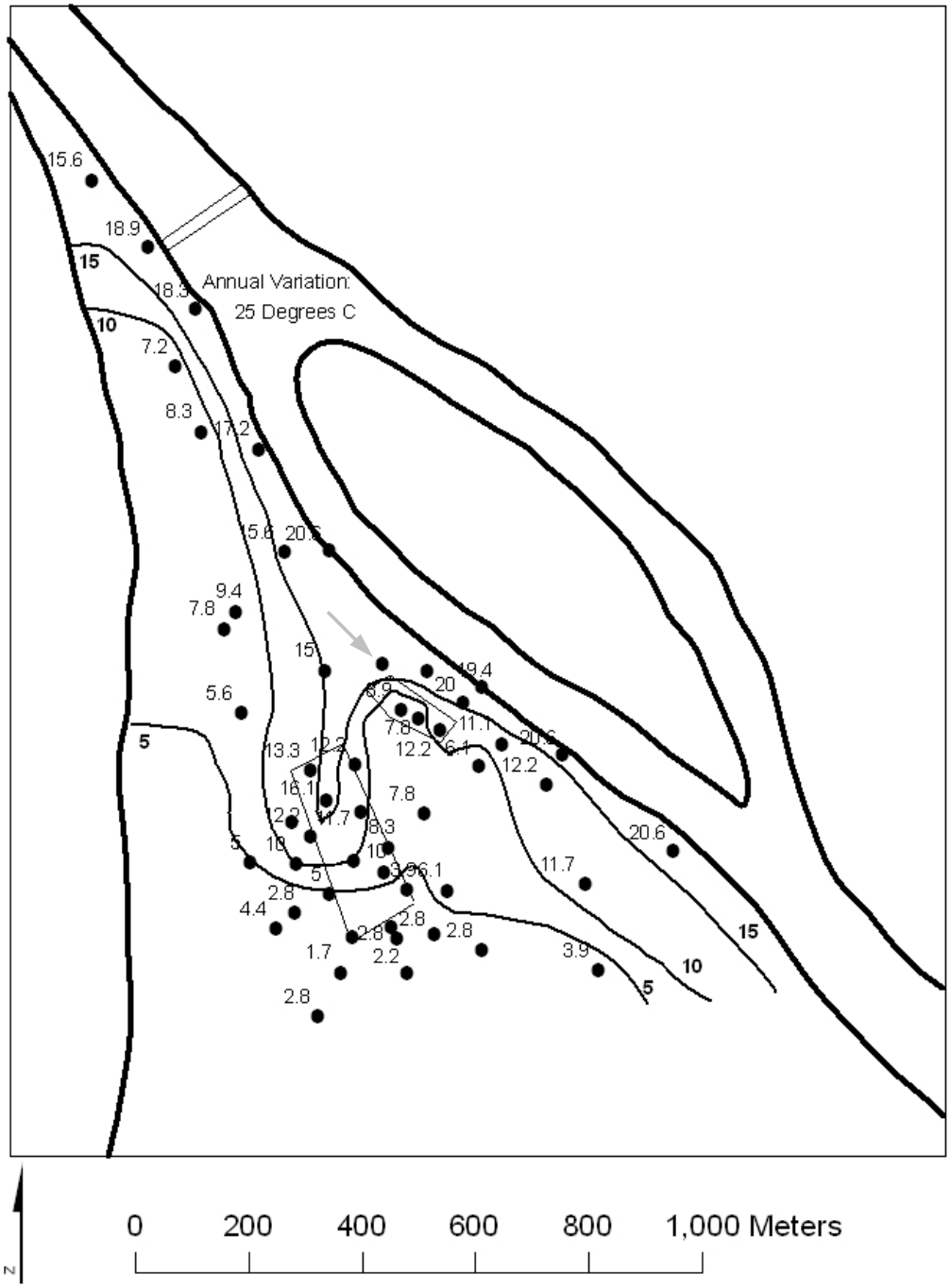

Figure 3.6. Annual temperature variation in °C observed from summer 1960 to summer 1961 in monitoring wells and pumping wells at the Mohawk River site. Note the plume of high temperature variation extending from the river to the Schenectady pumping wells. Data taken from Winslow (1965). Well 61 is indicated with a gray arrow.

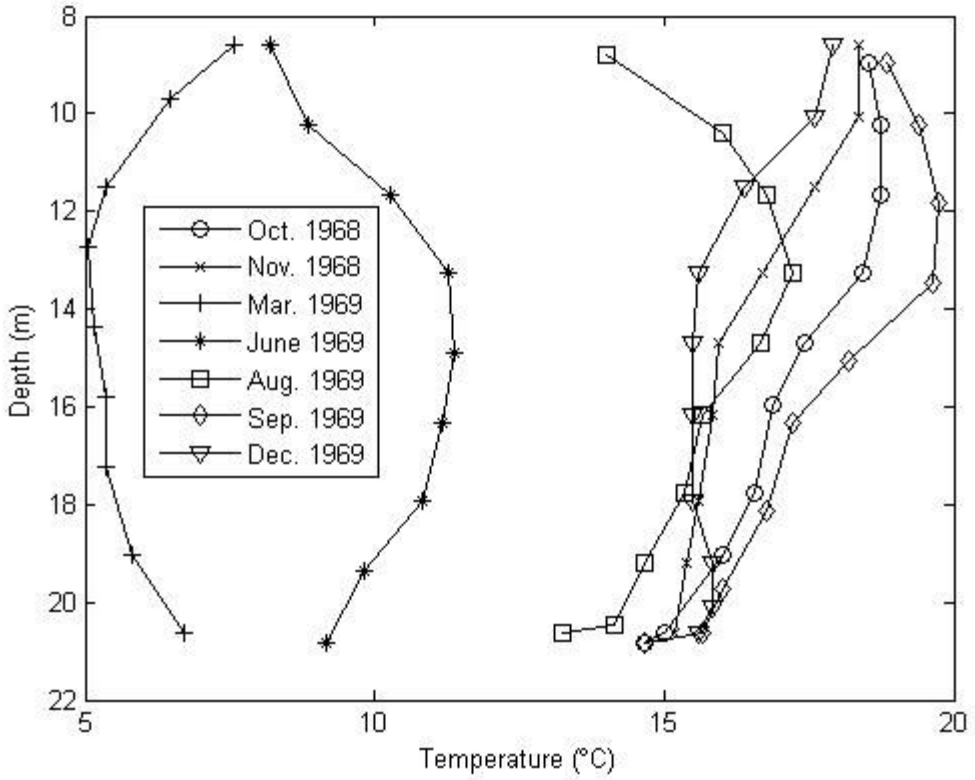

Figure 3.7. Depth profiles observed in well 61 (indicated with an arrow in Figure 3.6) between October 1968 and December 1969. Seasonal temperature changes are greatest and occur the earliest at the most permeable depths. The log for this well indicates undifferentiated sand and gravel between 6.4 and 18.2 m.

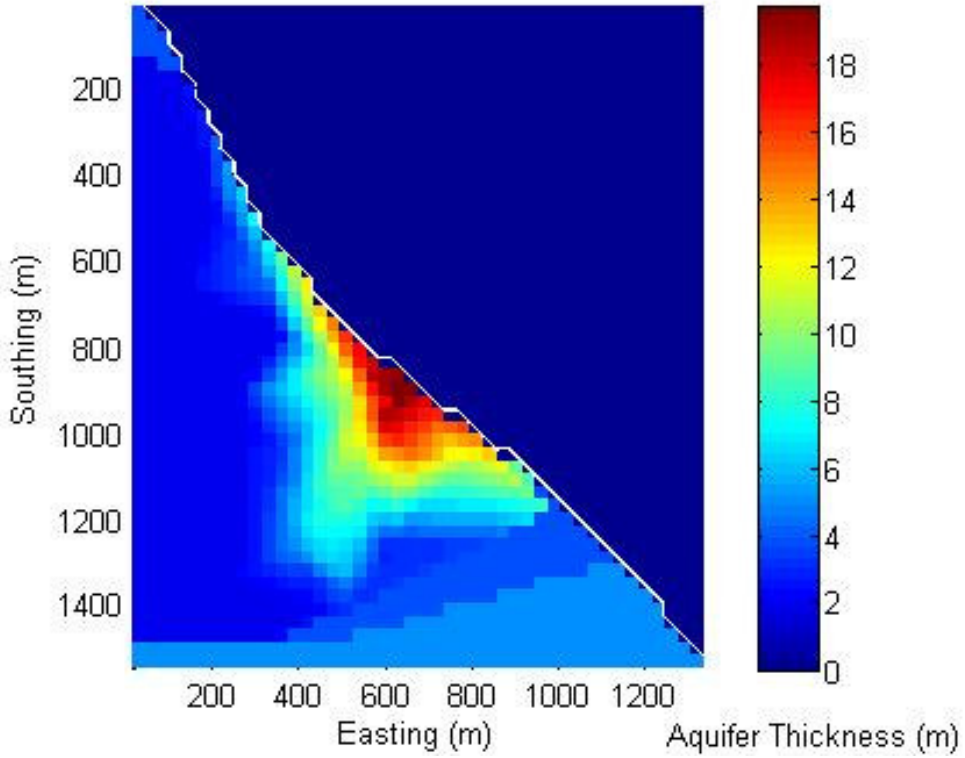

Figure 3.8. Contoured map of aquifer thickness, using thicknesses compiled by Winslow et al. (1965). The Schenectady Delta deposits have been assigned a thickness of 5 m. The white line represents the modeled river recharge boundary.

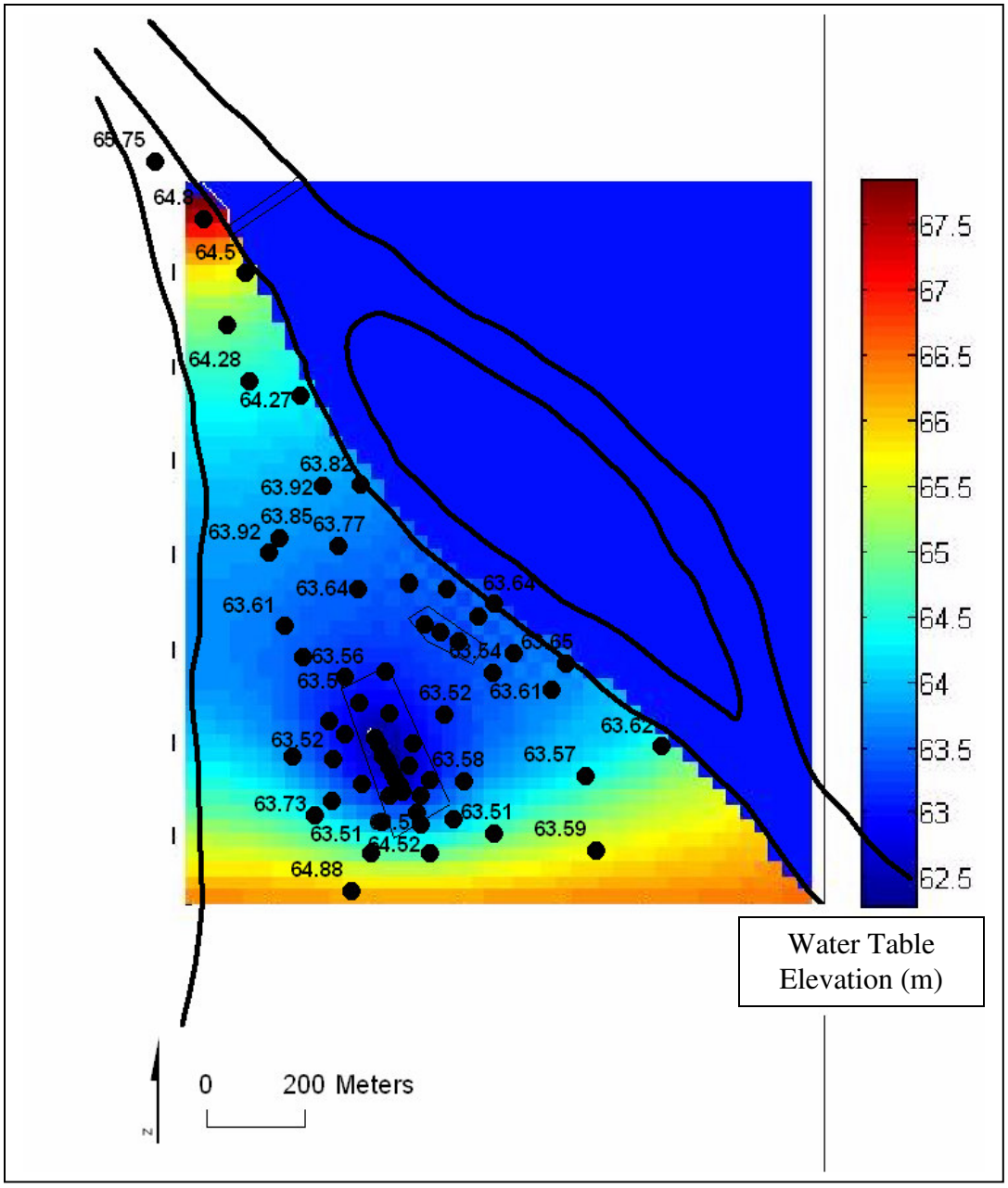

Figure 3.9. Modeled head for August 3rd, 1960. These results compare reasonably well to Figure 3.3, where the water-table in the region of the pumping wells is between 63.5 and 63.9 m above sea level.

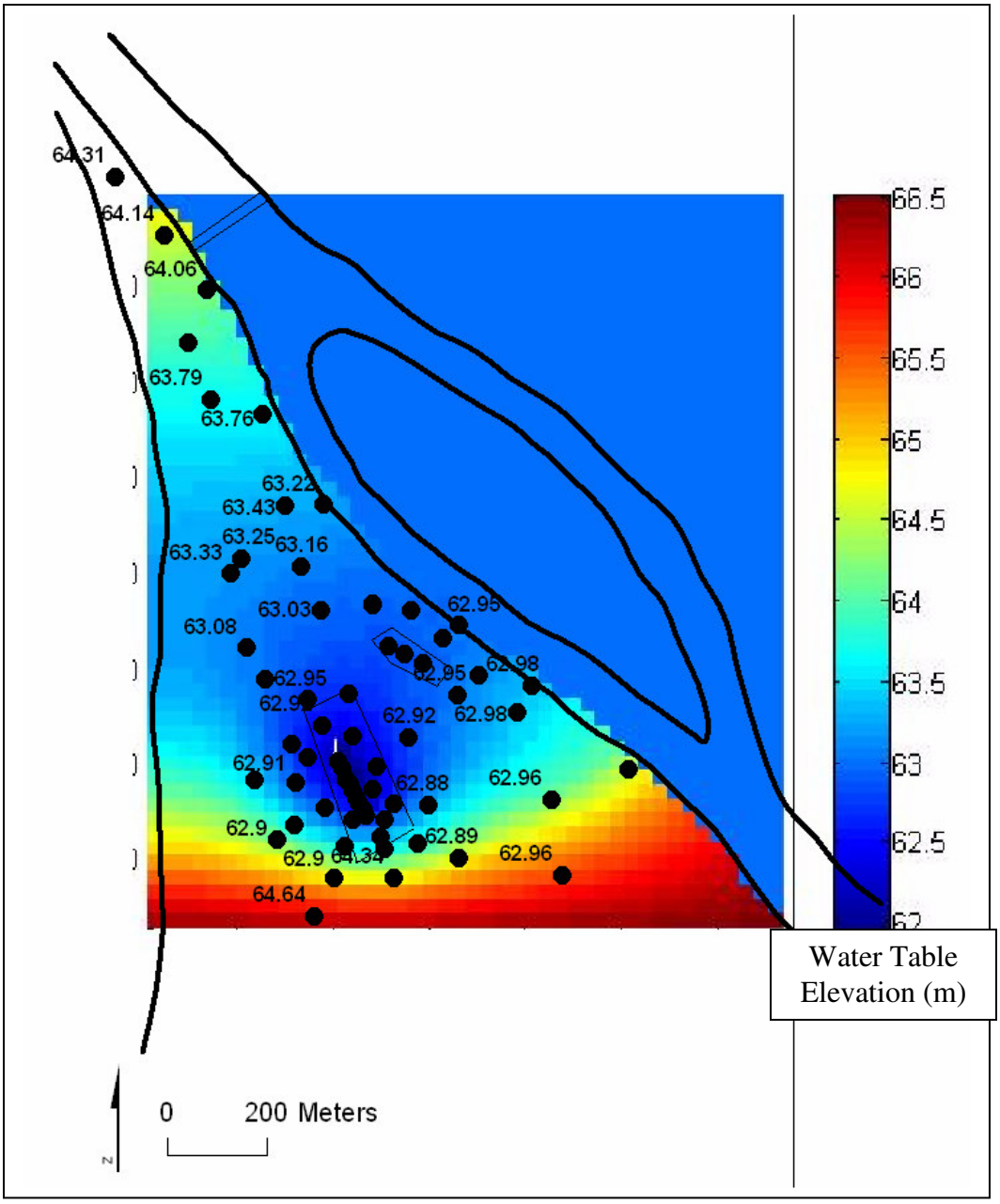

Figure 3.10. Modeled head for December 29th, 1960. These results compare reasonably well to Figure 3.4, where the water-table in the region of the pumping wells is between 62.9 and 63.4 m above sea level.

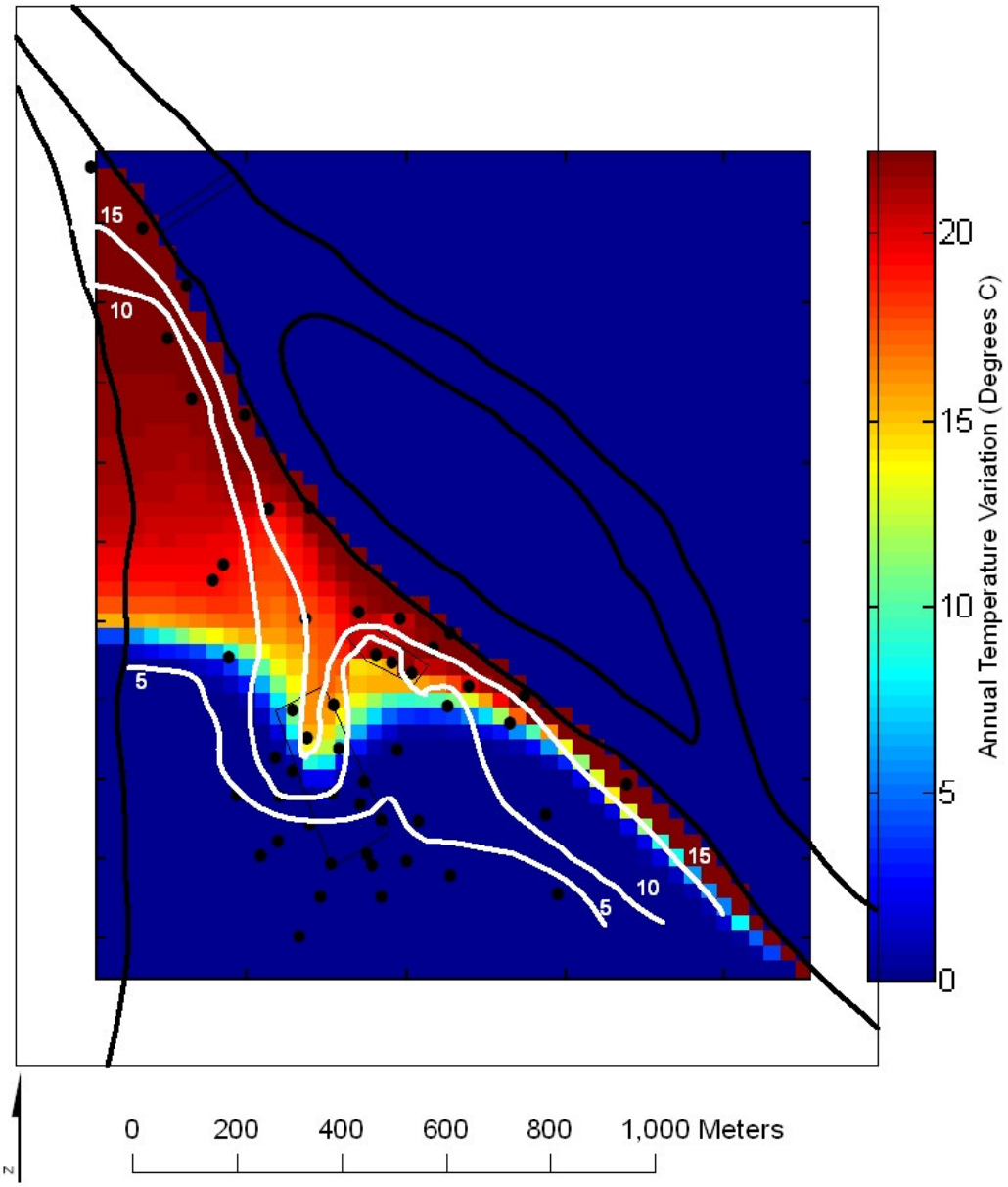

Figure 3.11. Modeled annual temperature variations at the Mohawk River site. The contour lines from Figure 3.6 have been plotted to aid in comparison. The model does not attempt to replicate the small temperature variations in water flowing from the Schenectady Delta deposits. The model reproduces all of the salient features of the data except in the region north of the Schenectady pumping center and close to the valley wall, where the modeled temperature variations (16 to 20 °C) are much greater than the observed variations (7.8 to 9.4 °C). This mismatch may be due to poorly-constrained variations in aquifer depth near the valley wall.

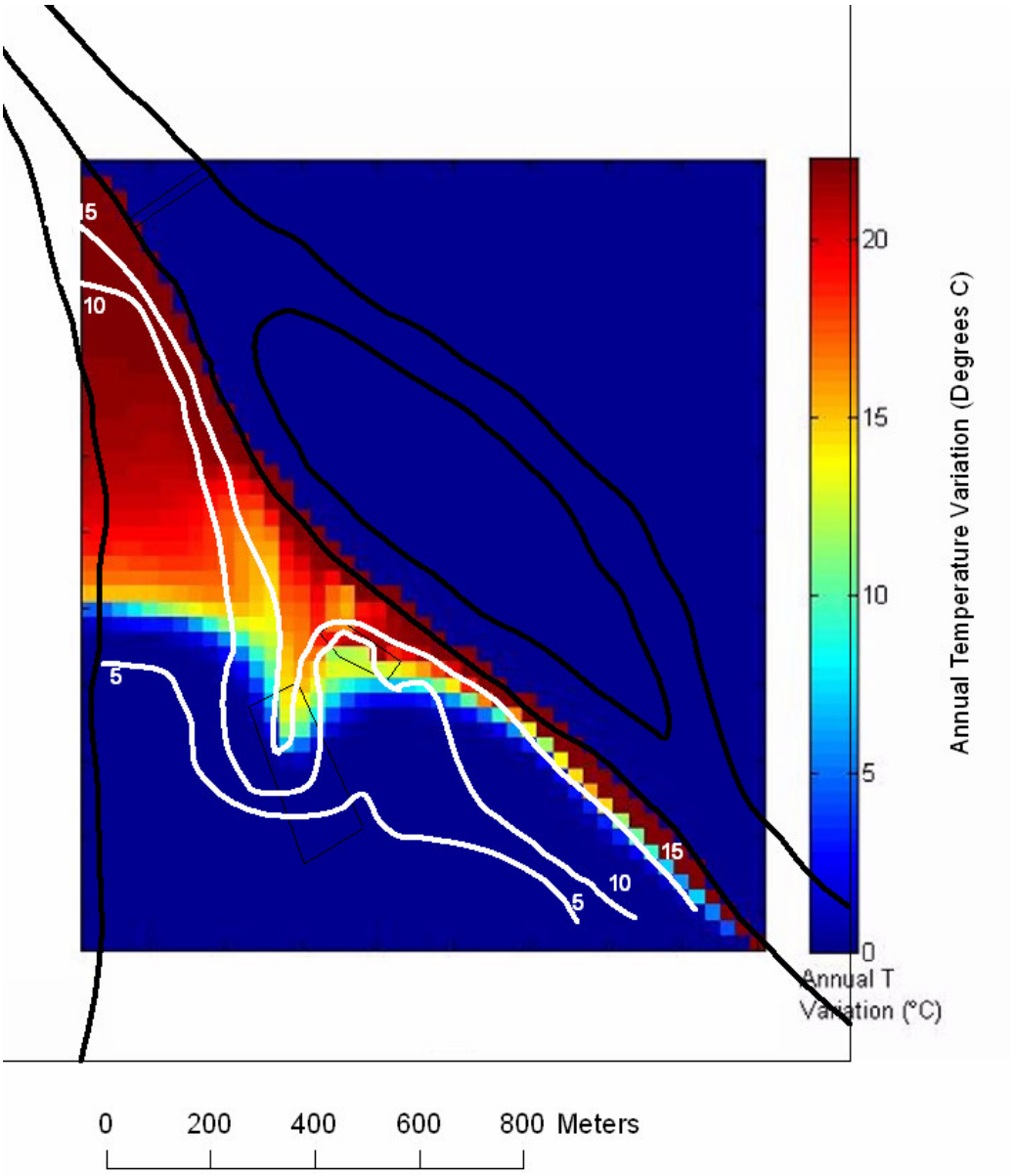

Figure 3.12. Modeled annual temperature variations for a scenario where induced infiltration makes up 11% of ground-water withdrawals. The magnitude of the temperature variation in the plume of warm water is slightly less than in the case when induced infiltration makes up 20% of ground-water withdrawals (Figure 3.11).

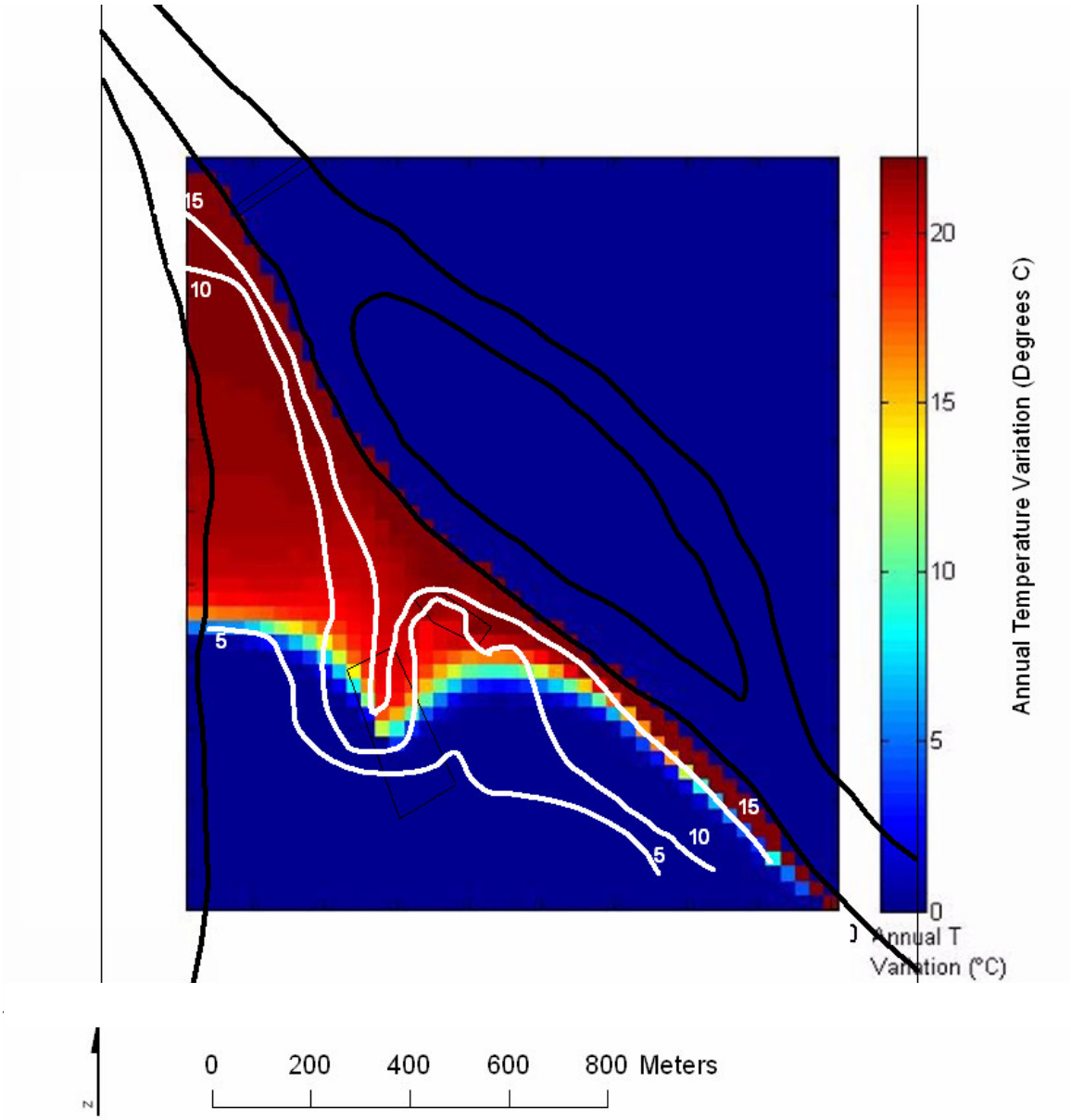

Figure 3.13. Modeled annual temperature variations for a scenario where induced infiltration makes up 50% of ground-water withdrawals. The magnitude of the temperature variation in the plume of warm water is greater than is observed in the data (Figure 3.6).

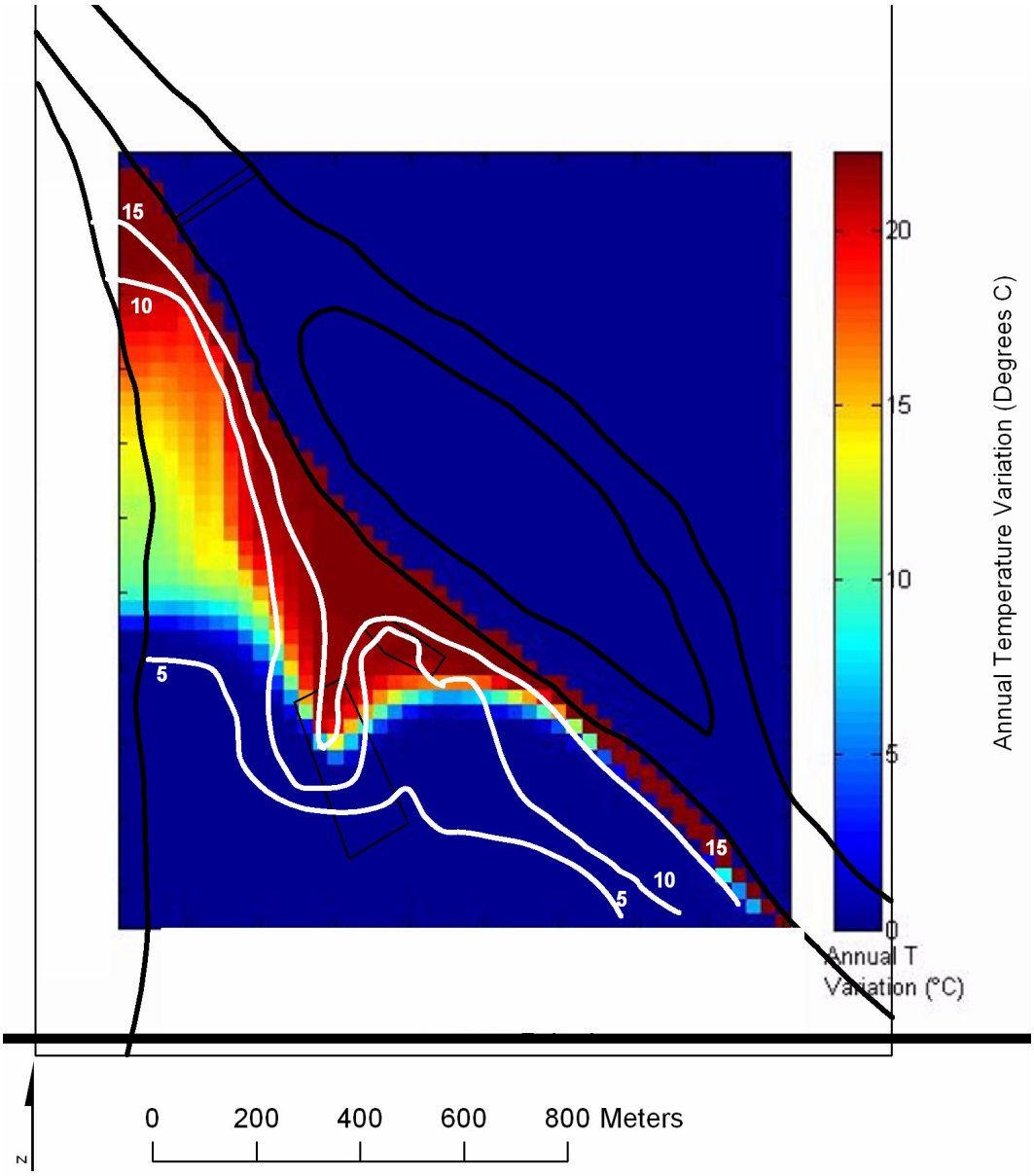

Figure 3.14. Modeled annual temperature variations for a scenario where only one conductance value is used for the entire river boundary. The magnitude of the temperature variation in the plume of warm water is greater than is observed in the data (Figure 3.6).

Chapter 4

Detecting Preferential Pathways of Surface-water Infiltration Using Annual Variations in Soil Temperature

Abstract

Annual temperature variations in ground-water can be used as a tracer for infiltrated surface-water. If the spatial distribution of these measurements is sufficiently dense, then high transmissivity zones acting as preferential flow paths for infiltrated surface-water can be identified. A limitation of this method is that ground-water temperature can be measured only in wells or in natural discharge points. For some shallow aquifers, however, this annual temperature variation can be seen in temperature measurements taken in shallow soil borings. By collecting temperature data in a large number of shallow soil borings, preferential flow paths in shallow soil borings can be mapped. In this paper we model soil temperature variations, investigate the range of conditions under which aquifer temperature variations can be detected, and demonstrate the technique with a data set from a site along the Mohawk River near Schenectady, New York.

4.1 Introduction

Ground-water temperature is increasingly being recognized as a valuable tracer (for reviews of the recent literature, see Anderson, 2005). In particular, diurnal and annual temperature variations in surface-water bodies result in aquifer temperature variations that are a tracer for surface-water- ground-water exchange. Temperature records at different depths beneath surface-water bodies can be used to estimate leakage (e.g., Lapham, 1989; Constantz et al. 2002; Silliman et al. 1995; Niswonger and Prudic, 2003).

Temperatures measured in wells near sources of surface-water infiltration can be used to constrain aquifer properties (e.g., Ronan et al. 1998; Niswonger and Prudic, 2003; Su et al. 2004). Winslow et al. (1965) used temperature measurements in ~50 wells over an area of less than 1 km^2 to identify a high transmissivity zone that acted as a preferential pathway for induced infiltration from the Mohawk River near Schenectady, NY. One limitation of ground-water temperature measurements is that they can be measured only in wells or at natural discharges, making a study on the scale of Winslow et al. (1965) expensive and logistically difficult.

Temperatures in soils and sediments can be influenced by conductive and convective heat transfer from underlying aquifers. Therefore, temperature measurements in shallow borings can be used to obtain inexpensive spatially extensive information about ground-water temperature. Shallow temperature measurements have long been used as a reconnaissance technique for geothermal exploration (e.g., Kintzinger, 1956; Olmsted, 1977; LeSchack and Lewis, 1983). Cartwright (1968), Birman (1969), and Bair and Parizek (1978) noted that soil temperatures above shallow aquifers of constant temperature were less affected by atmospheric temperature variations than soil temperatures above less permeable material. Cartwright (1974) found that soil temperatures above discharge areas varied less than soil temperatures above recharge areas. Ebaugh, Parizek and Greenfield (1978) and Parizek and Bair (1990) used shallow soil temperature patterns to locate karst channels. These studies have used persistent spatial patterns in shallow temperatures to delineate their targets, but they have not considered the effect of annual variations in aquifer temperature.

In this paper, we propose that the effect of aquifer temperature variations due to surface-water infiltration can be seen in shallow temperature data, and that temperatures measured in a network of soil borings can be used to detect preferential flow paths in the aquifer below or within the soils themselves. However, the other factors affecting soil temperature must be identified, modeled, and subtracted before these data can be interpreted. In this paper, we develop a model of soil temperature variation and investigates the detectability of the effect of aquifer temperature variations. We apply the method to soil and aquifer temperature data collected by O'Brien (1970) at the Mohawk River site studied by Winslow (1965).

4.2 Field Study- Mohawk River Site, NY

4.2.1 Site Description

To investigate annual variations in soil temperature in a field setting, we use data collected by the Mohawk River near Schenectady, NY (Figure 4.1). The Schenectady and Rotterdam well fields are located on the Southwest bank of the Mohawk River adjacent to the Isle of the Oneidas (Figure 4.1). Because the two well fields are separated by only 200 m, they create a single more regional cone of depression. The aquifer is extremely productive, with transmissivity estimates in the range of 0.1-2.5 m^2/s (e.g., O'Brien, 1970; Spectra, 2001).

The geology of the site is discussed extensively in chapter 3. The Glacio-Mohawk River was a major outlet for glacial melt water at the end of the most recent glaciation (e.g., Wall and Lafleur, 1994), depositing tens of meters of coarse outwash sediments known as the Scotia gravel. In the vicinity of the well fields, this gravel has been reworked by later alluvial processes to form a unit known as the Scotia Channel Deposits (Spectra, 2001).

The unit is 10-20 m thick beneath much of the site shown in Figure 4.1, although the sediment fines to the south and the unit thins as it nears the valley wall. The aquifer is overlain by a layer of younger, fine-grained flood deposits ranging in thickness from 2-20 m.

The many drill logs at the site show that the sediment overlying the Scotia gravel has a complex depositional history, with facies variations over horizontal distances of tens of meters. In much of the watershed, this layer is fine-grained and can be considered an aquitard. However, as Figure 4.2 shows, there are gravel channels that provide high permeability pathways through the overburden.

Winslow et al. (1965) studied the Mohawk River site in detail. They recorded ground-water temperatures in observation wells ten times between August 1960 and August 1961. These data showed a preferential flow path (Figure 3.6) from the river to the pumping wells where the groundwater temperature varied by 10-20 °C, as opposed to a variations as little as 2 °C in the rest of the aquifer. A similar pattern was observed in well temperature data collected by O'Brien (1970).

4.2.2 Soil Temperature Data

O'Brien (1970) collected temperature data in 90 1.83 m borings (shown in Figure 4.1) and 22 0.91 m borings at eight times between September 1968 and December 1969 (not all borings were included in each sampling round). The borings were hand-augered and covered at the surface, and the temperature measurements were made with a thermistor probe with an accuracy of 0.2 °C. Figure 4.3 shows the pattern of temperatures at a depth of 1.83 m in March (Figure 4.7a) and August (Figure 4.7b) of 1969. We have chosen to use this data set because the large number of wells (most of them now destroyed) allowed

the aquifer temperature to be recorded with sufficient spatial resolution to resolve the preferential flow path. The soil temperature data have excellent spatial coverage, sufficient measurement accuracy, and adequate temporal resolution. Since 1969, Interstate 890 has been built over the site, and much of the remaining area has been covered with dredged sediments, making it impossible to collect a new data set with the same level of spatial coverage.

4.3 Analysis of Soil Temperature Variations

4.3.1 Analytic Solution

Consider a homogenous soil layer bounded by the land surface at $z = 0$ and the top of a confined aquifer *at* $z = z_0$. One-dimensional conductive heat flow in this soil is governed by the diffusion equation:

$$D\frac{\partial^2 T}{\partial z^2} = \frac{\partial T}{\partial t} \quad , \qquad (4.1)$$

where T is temperature in °C and D is the soil's thermal diffusivity in m^2/s.

The thermal diffusivity of a material is the ratio of its thermal conductivity to the product of its density and its specific heat capacity:

$$D = \frac{\kappa}{\rho c} \qquad (4.2),$$

where κ is the thermal conductivity of the soil in J/m/sec/°C, ρ is its density in kg/m^3, and c is its specific heat in J/°C/kg. The thermal diffusivity may also include a velocity term to account for advective dispersion (e.g., de Marsily, 1986), but this term is insignificant for typical annual recharge rates.

Equation 4.1 can be solved by defining temperature signals for the surface and the aquifer. If we approximate these signals as sinusoidal waves, then the analytical solution is (O'Brien, 1970):

$$T(t,z) = T_s + \frac{(T_a - T_s)z}{z_0} + A_s \exp\left(-z\sqrt{\frac{\pi}{DP}}\right)\sin\left(\frac{2\pi}{P}\left(t - \sqrt{\frac{P}{\pi D}}\frac{z}{2}\right) + \varphi_s\right) + A_a \exp\left(-(z_0 - z)\sqrt{\frac{\pi}{DP}}\right)\sin\left(\frac{2\pi}{P}\left(t - \sqrt{\frac{P}{\pi D}}\frac{(z_0 - z)}{2}\right) + \varphi_a\right) \quad (4.3)$$

where T_s is the average surface temperature in °C, T_a is the average aquifer temperature in °C, A_s is the amplitude of the surface wave in °C, A_a is the amplitude of the aquifer wave in °C, φ_s is the phase of the of the surface wave in radians, φ_a is the phase of the aquifer wave in radians, and P is the period of the waves (one year for annual variation) in seconds.

4.3.2 Data Analysis

The analytical solution in Equation 4.3 consists of three parts: a time-invariant term related to the average surface and aquifer temperatures, the effect of the annual variation in surface temperature, and the effect of the annual variation in aquifer temperature (Figure 4.4). The aquifer temperature effect increases the magnitude and changes the phase of the signal. The first two terms must be subtracted from the data to study variations in the third term.

The time-invariant term of Equation 4.3 depends on the average surface and aquifer temperatures and the depths of the measurement point and the top of the aquifer. However, when analyzing the annual temperature variation in these data we may simply subtract the mean value of the soil temperature measurements over a year.

The thermal diffusivity and surface temperature signal must be known to subtract the effect of the surface temperature variation. Thermal diffusivity at the relevant scale can be determined by modeling the observed annual or diurnal soil temperature signal caused by surface temperature variation. Deterministic models relating surface temperature to atmospheric temperature (e.g., LeSchack and Lewis, 1983; Yeh and Luxmoore, 1983) require many parameters related to both the climate (e.g., dew point, cloud cover, wind speed) and the soil surface (e.g., aerodynamic surface roughness, albedo). A more empirical approach is described by Smerdon et al. (2004), who fit temperature records from various depths at four sites using the first two terms of Equation 4.3 to determine a sinusoidal surface soil temperature signal at four different sites. They found that the soil surface temperature lagged atmospheric temperature by 4.6 to 8.4 days, and was attenuated by 7.6 to 22.5%. They attributed the variability in attenuation to days of snow cover, with the lowest value found at Cape Hatteras, North Carolina, and the highest value found at Fargo, North Dakota. If we consider an annual atmospheric temperature wave with an amplitude of 15 °C, and a D of 4×10^{-7} m^2/s (a reasonable value for soil), then these lower and upper bounds of attenuation would, change the amplitude of the surface temperature wave at 2 m depth by 0.4 and 1.2 °C, respectively.

4.3.3 Other Factors Affecting Soil Temperature

Surface temperatures can change greatly over the course of a day. Because these variations propagate as a diffusive wave, however, they are attenuated with depth. If we assume that D is 4×10^{-7} m^2/s, then the daily wave is attenuated by 90% at a depth of 0.24 m, while the annual wave is attenuated by 90% at 4.6 m. Thus, most temperature measurements in soil borings are affected by the annual variation but are below the

depths at which the diurnal variation is significant. Similarly, while the true surface temperature signal is not a perfect sinusoid, short period variations are attenuated with depth.

Many of the parameters affecting atmosphere-soil coupling, such as wind speed and insolation, are affected by land cover. Studies of logged areas show that forests may decrease the magnitude of surface temperature by 1-2 °C (e.g., Lewis and Wang, 1998). The magnitude of the effect depends greatly on site specific conditions. O'Brien (1970) investigated this at the Mohawk River site by measuring soil temperatures along a profile of borings crossing from open ground to forest at the Mohawk River site described later in this paper. He made the measurements in early September, when soil temperatures were near their highest, and found that the temperature at 1.8 m depth was cooler in the forest by up to 0.33 °C.

Geothermal heat flow is an important factor in many subsurface thermal settings, and some soil temperature studies are designed specifically to locate geothermal anomalies (e.g., LeSchack and Lewis, 1983). However, this study considers temperatures in the region between the surface and the shallowest aquifer, so variations in geothermal heat flux are viewed as changes in the aquifer temperature.

Recharge through the soil profile will result in advective heat transfer. If the seepage velocity does not change with depth, then the governing equation is

$$D\frac{\partial^2 T}{\partial z^2}+\frac{\rho_w c_w}{\rho c}q_d\frac{\partial T}{\partial z}=\frac{\partial T}{\partial t} \qquad (4.4)$$

where q_d is the seepage velocity of ground-water through the soil in m/s, and ρ_w and c_w are the density and specific heat of water, with units of kg/m^3 and J °C^{-1} kg^{-1}, respectively. In general, recharge increases the heat transfer from the surface, reducing

the attenuation of the surface temperature wave. We tested the significance of these effects by using a finite element model of Equation 4.4 to simulate the annual temperature wave at 2 m depth for recharge rates ranging from 0.02 to 1 m/yr. Figure 4.5 shows the RMS difference between these simulations and the solution without recharge (Equation 4.3). The surface and aquifer temperature signals, soil thermal properties, and depth to the aquifer chosen for this model influence the results. In this case, however, the RMS misfit caused by 0.2 m/yr of recharge is roughly 0.1 °C.

Spatial variations in soil thermal properties could be misinterpreted as spatial variations in aquifer temperature. Typical values for the thermal properties of various geological materials have been compiled by Anderson (2005) and Bair and Parizek (1978), and are discussed in detail by Lapham (1989). Thermal diffusivity values of soils typically range over roughly an order of magnitude. There has been little work done on the heterogeneity of soil thermal properties at the site scale. Markle et al. (2006) found that the apparent thermal conductivity in a saturated glacial outwash aquifer had a standard deviation of 5% of the mean value, but that there were greater differences between sedimentary units. Figure 4.6 shows the RMS error that would result from using incorrect thermal diffusivities to simulate the temperature signal shown in Figure 4.4 (for the case where both the surface temperature and aquifer temperature vary). Using a value of D within ~25% of the true value results in a misfit of 0.5 °C or less, suggesting that slight variations in the D values used to calculate the surface temperature correction are acceptable. Greater excursions from the true value result in greater misfits.

4.3.4 Aquifer Temperature Signal Detectability

In general, the factors described above affect soil temperatures by less than 1 °C. Thus, it is reasonable to assume that signals with a magnitude of 2 °C or greater can be distinguished from background variation. Figure 4.7a shows the magnitude of aquifer temperature variation (A_a) required to reach this detectability threshold as a function of height above the top of the aquifer (z_0) for $D = 4 \times 10^{-7}$ m^2/s. The temperature variation in infiltrating surface-water is unlikely to exceed the annual surface temperature variation, which, for the four mid-latitude sites studied by Smerdon et al. (2004), did not exceed 13.8 °C. For the case in Figure 4.7a, an aquifer temperature variation of 13.8 °C is unlikely to be detected by sensors more than 3.8 m above the top of the aquifer. As Figure 4.7b shows, the height above the aquifer at which a 13.8 °C variation in aquifer temperature results in a 2 °C variation in soil temperature increases with increasing values of D. In general, it is unlikely that temperature measurements made at depths more than a few meters above the top of the aquifer will detect variations due to aquifer temperature variations. Therefore, soil borings used for temperature measurements should be made as deep as possible to enhance signal strength.

4.3.5 Analysis of Mohawk Data

To subtract the effect of the variation in surface temperature from the soil temperature data, we must estimate the surface temperature signal and the thermal diffusivity of the soil. Smerdon et al. (2004) estimated these parameters using measurements made at multiple depths. We have followed their approach using measurements made in 0.91 m and 1.83 m borings. We chose eight pairs of 0.91 and 1.83 m borings where the depth of the fine-grained overburden deposits suggested that the temperatures were unlikely to be

influenced by aquifer temperature variations, and determined a best fit model using a grid search algorithm. This approach uses both forested and open boring sites, and as a result we would not expect the resulting temperature model to fit the data exactly. While atmospheric temperature data are not available for the site, Figure 4.8 compares this model to the best fit atmospheric temperature model for measurements at the Schenectady County Airport, 5 km away (O'Brien, 1970). The best fit surface temperature is attenuated and insignificantly delayed relative to the atmospheric signal. The attenuation is 19%, within the range of modeled attenuations at the sites described by Smerdon et al. (2004). The best fit thermal diffusivity is 5.2×10^{-7} m^2/s. While the RMS misfit of this solution is 0.57 °C, thermal diffusivities from $3.7\text{-}6.4 \times 10^{-7}$ m^2/s resulted in misfits of less than 0.7 °C. This uncertainty in the best fit thermal diffusivity is consistent with the low sensitivity to small variations in D found in synthetic models (Figure 4.6).

4.4 Interpretation

Figure 4.9a shows the temperature time series for 1.83 m boring after the modeled effect of surface temperature variation and a constant temperature (selected individually for each time series) have been subtracted. While most of the time series vary within 1°C of zero, several of them oscillate with greater amplitudes roughly in phase with the river temperature (shown in Figure 4.11). Figure 4.9b shows the histogram of the RMS misfit of each time series to the modeled effect of the surface temperature signal. There are three borings that have misfits greater than 2 °C, and seven more that have misfits greater than 1°C (note that a sinusoid with an amplitude of 2 °C has an RMS amplitude of ~1.4 °C). If we plot these anomalous borings on a map (Figure 4.10), we find that all except

boring 64 are located near the bank of the river. As the temperature time series of the borings near boring 64 do not exhibit anomalous misfits, we suspect that that the boring 64 anomaly may be due to measurement errors, boring construction, or local undefined soil conditions. Of the remaining borings, six are clustered within 100 m of each other. As figure 4.9a shows, the temperatures measured in boring 42 vary by up to 6°C from the modeled effect of surface temperature variation. We have inverted the boring 42 temperature record to show that an aquifer at a reasonable depth and with a reasonable temperature signal could produce this variation. In the inversion, we hold the thermal diffusivity of the aquifer constant at 5.2 x 10^{-7} m^2/s, and model the aquifer temperature as a trunctuated sinusoid, where all values less than 0 °C are set to 0 °C (e.g., Lapham, 1989). The best fit model, which resulted in an RMS misfit of 0.77 °C, had a depth to aquifer of 4.1 m. The best fit aquifer temperature signal, shown in Figure 4.11, is reasonably similar to the river temperature time signal. This similarity indicates that a reasonable temperature variation could produce the observed temperature signal.

4.5 Discussion

The relatively shallow depth and limited lateral extent of the detected feature is more consistent with a buried channel such as the gravel lens shown in Figure 4.2 than with a transmissive zone in the deeper aquifer. Gravel is present at a depth of 4.7 m in the northernmost production wells of the Rotterdam well field that may or may not be hydraulically connected with the zone of anomalous shallow temperatures. The depositional environment at the site (glacial outwash reworked by younger alluvial processes) is complex, so the connectivity of different shallow gravels at the site cannot be assumed.

The presumed channel cannot be mapped further than 100 m from the river bank. While Winslow et al. (1965) and O'Brien (1970) were able to detect significant aquifer temperature variations as far as the Schenectady well field, the magnitude of the oscillation decreased with distance from the river. Also, their measurements were made in the deeper glacial outwash aquifer at the depths where the production wells are screened. If the detected channel is isolated from this aquifer by a clay layer as in Figure 4.2, then the cone of depression will not draw water into the channel, and the temperature plume will not extend as far from the river as in the deeper aquifer. Alternatively, it is possible that the high permeability zone does not extend beyond the area in which it was detected, or that the overburden depth above the feature is greater at other locations.

4.6 Conclusions

Soil temperature oscillations due to variations in aquifer temperature can be used to detect preferential flow paths of infiltrating surface-water. These signals are detectable in soil borings a few meters above the top of the aquifer, with the exact value dependent on the magnitude of temperature variation in the aquifer and the thermal conductivity of the overburden. Numerical modeling suggests that vertical flow through the overburden has little effect on the shallow temperature signal for recharge rates on the order of tenths of meters per year.

The analysis of existing data from the Mohawk River site serves as a demonstration of the strengths and weaknesses of the analysis of soil temperatures. The measurements were unable to detect the spatial variations in the temperature of the main aquifer described by Winslow et al. (1965) and O'Brien (1970). However, despite the numerous sources of noise and uncertainty, the effect of the aquifer temperature signal was

detectable in nine borings located over an interpreted shallow channel deposit. The inversion of the temperature time series from the most anomalous boring resulted in an aquifer temperature signal broadly similar to the recorded river temperature signal, and a depth-to-aquifer consistent with our knowledge of the shallow sediments at the site. However, new shallow temperature surveys should not use the methods described by O'Brien (1970). With modern instrumentation (e.g., Stonestrom and Blaschl, 2003; Johnson et al. 2005) sampling frequencies can be orders of magnitude higher. Temperatures should be measured at more depths to better constrain the effect of surface temperature variation. The most important change, however, would be to make the borings as deep as possible rather than at a uniform depth of 1.83 m, allowing smaller aquifer temperature variations at greater depths to be detected.

Moving beyond the detection of preferential pathways for flow, the quantitative analysis of shallow temperature data may prove to be valuable. Ground-water temperature data are valuable in parameter estimation because it is related to flow (e.g., Woodbury and Smith, 1988; Bravo et al. 2002; Su et al. 2004). In shallow aquifers near sources of surface-water recharge, it is possible that the joint inversion of hydrogeological data and spatially extensive shallow temperature measurements could be used to constrain spatial variations in transmissivity.

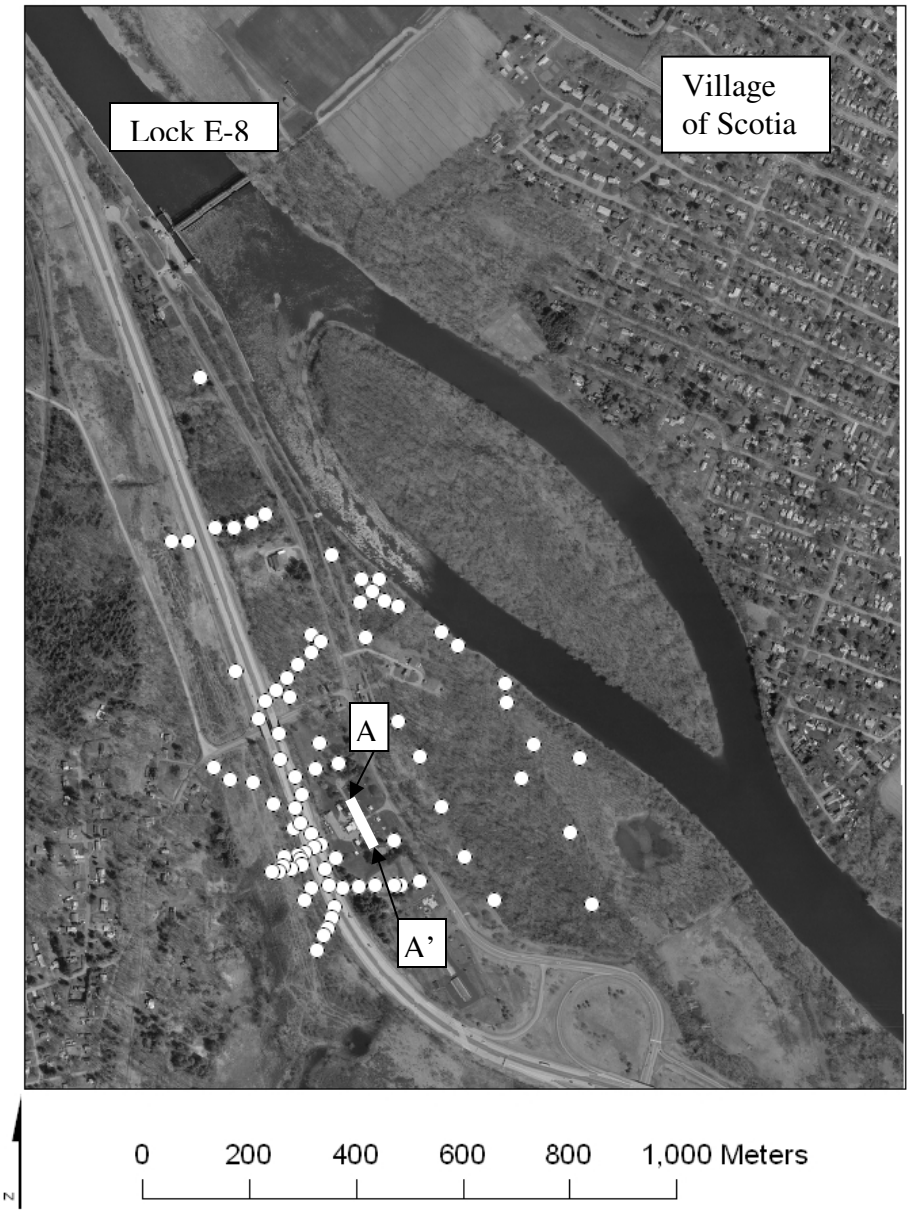

Figure 4.1. Mohawk River Site location map indicating soil boring locations used in this chapter. Additional maps of this site can be seen in Figures 3.1 and 3.2. The location of the cross-section in Figure 4.2 is indicated with a white line.

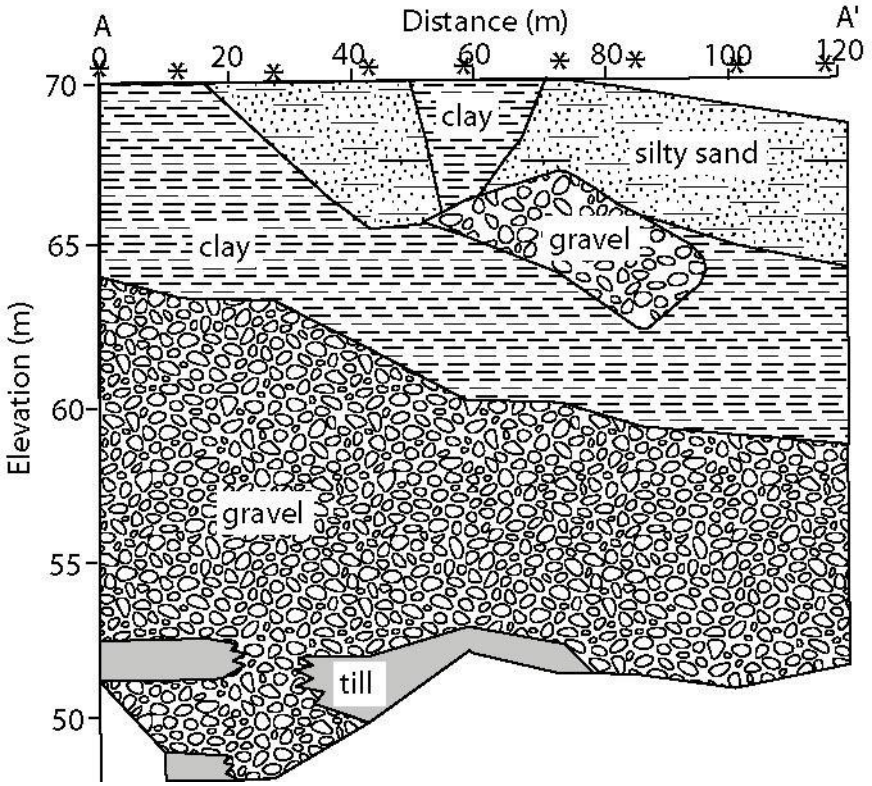

Figure 4.2. Cross section across the City of Schenectady well field. The nine well logs used (positions indicated by asterisks) were compiled by Winslow et al. (1965). The vertical exaggeration is 4:1. Note that the shallow gravel channel is isolated from the deeper aquifer by the clay.

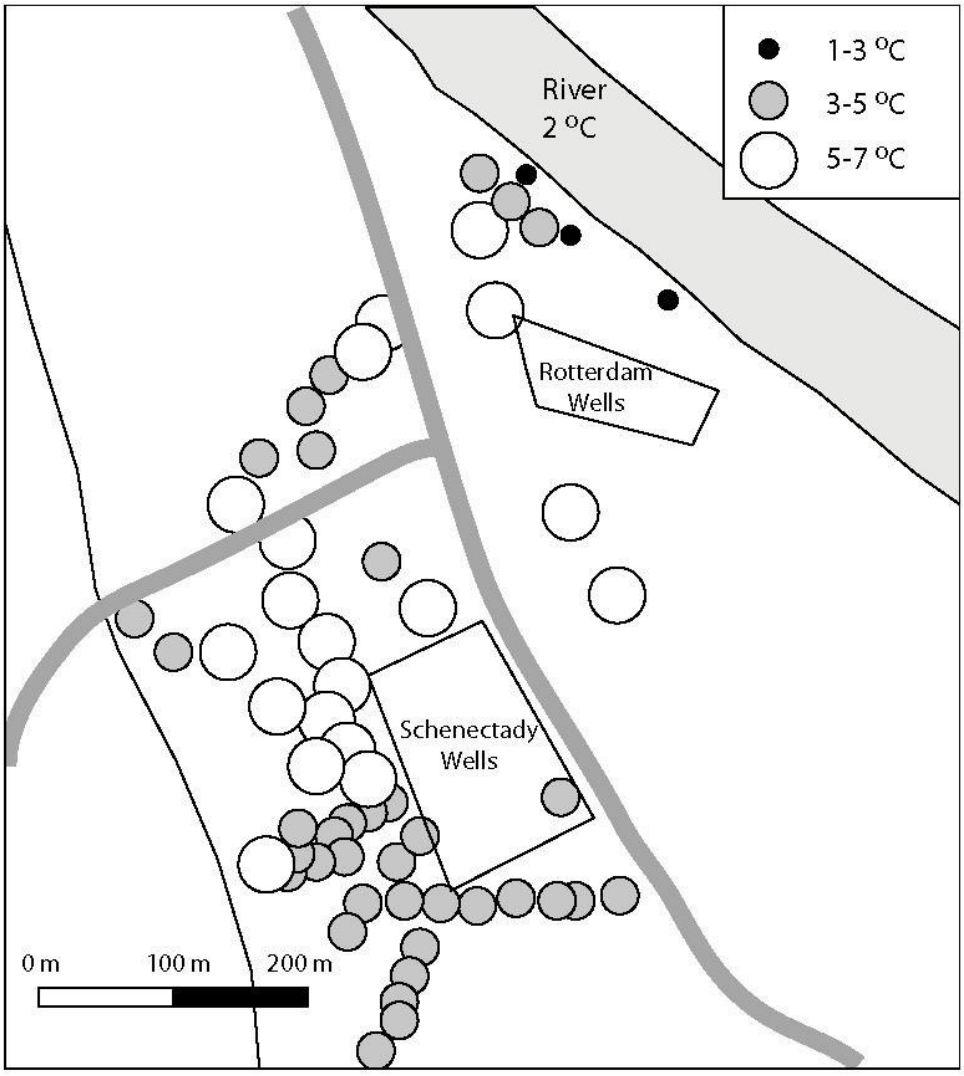

Figure 4.3.a. Soil temperatures recorded by O'Brien (1970) at a depth of 1.83 m in March 1969. Most of the data are between 3 and 7 °C, with three lower values near the river. Many of the higher values (between 5 and 7 °C) are clustered south of the Schenectady well field.

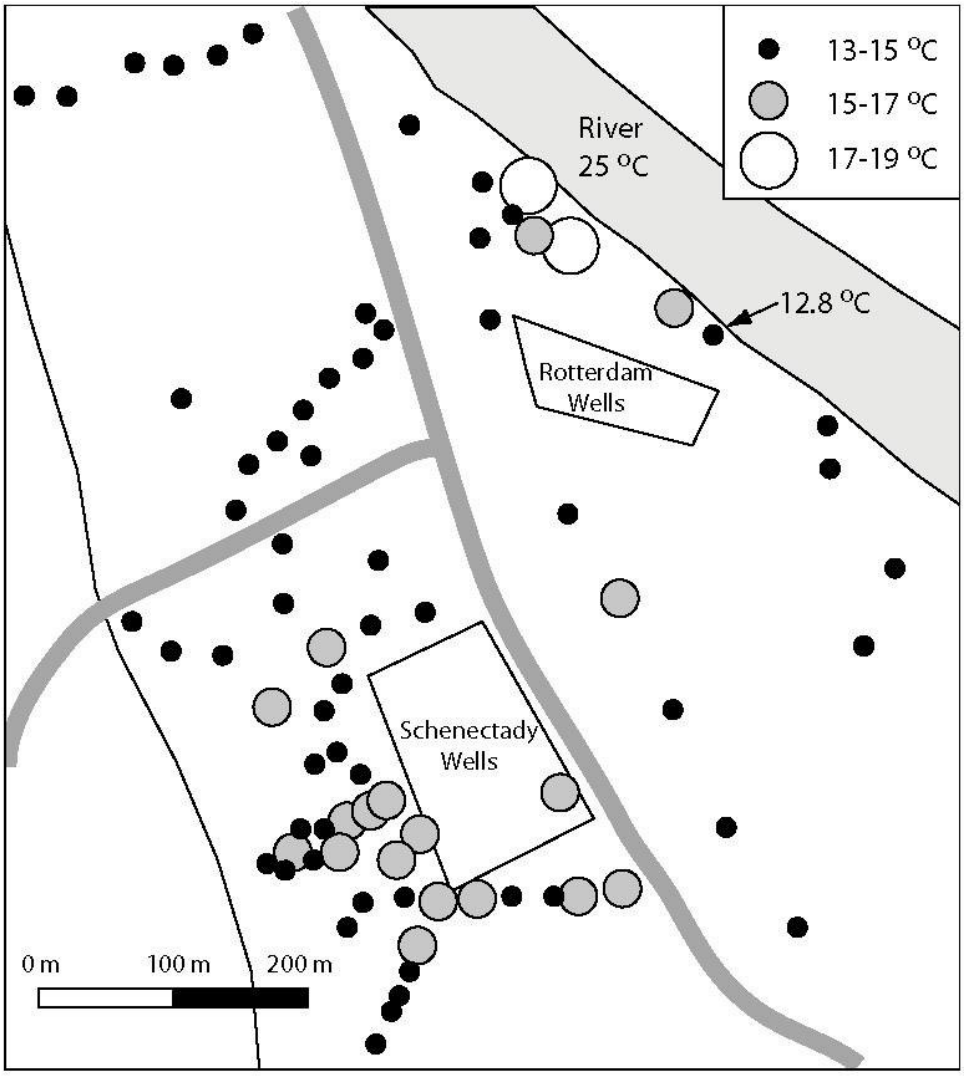

Figure 4.3.b. Soil temperatures recorded by O'Brien (1970) at a depth of 1.83 m in August 1969. Most of the data are between 13 and 17 °C, with two higher values near the river. Note that the many of the borings south of the Schenectady well field that had high temperatures in Figure 4.3a also have higher temperatures (15 to17 °C) in this figure, indicating that they are anomalous due to a time-invariant temperature signal.

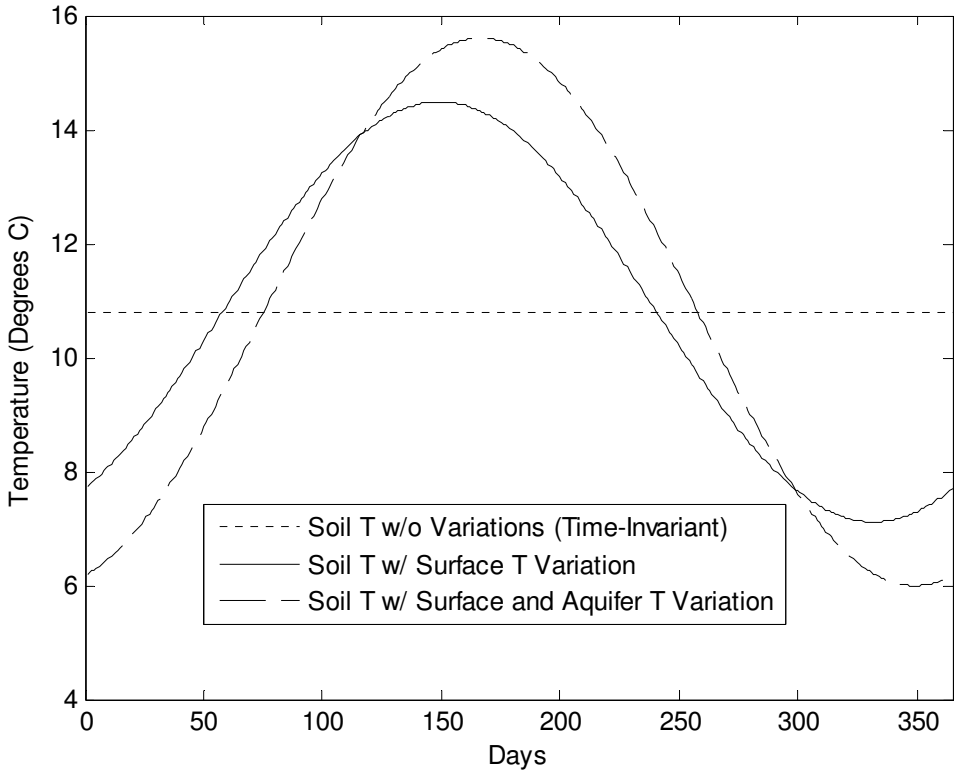

Figure 4.4. Synthetic example of the effect of surface and aquifer temperature variations on soil temperature. In this case, the soil layer is 5 m thick and has a thermal diffusivity of 4×10^{-7} m^2/s, the temperature is measured at a depth of 2 m, the amplitude of the surface temperature variation is 10 °C and the amplitude of the aquifer temperature variation is 7 °C. The effect of the aquifer temperature variation is to increase the magnitude and change the phase of the signal.

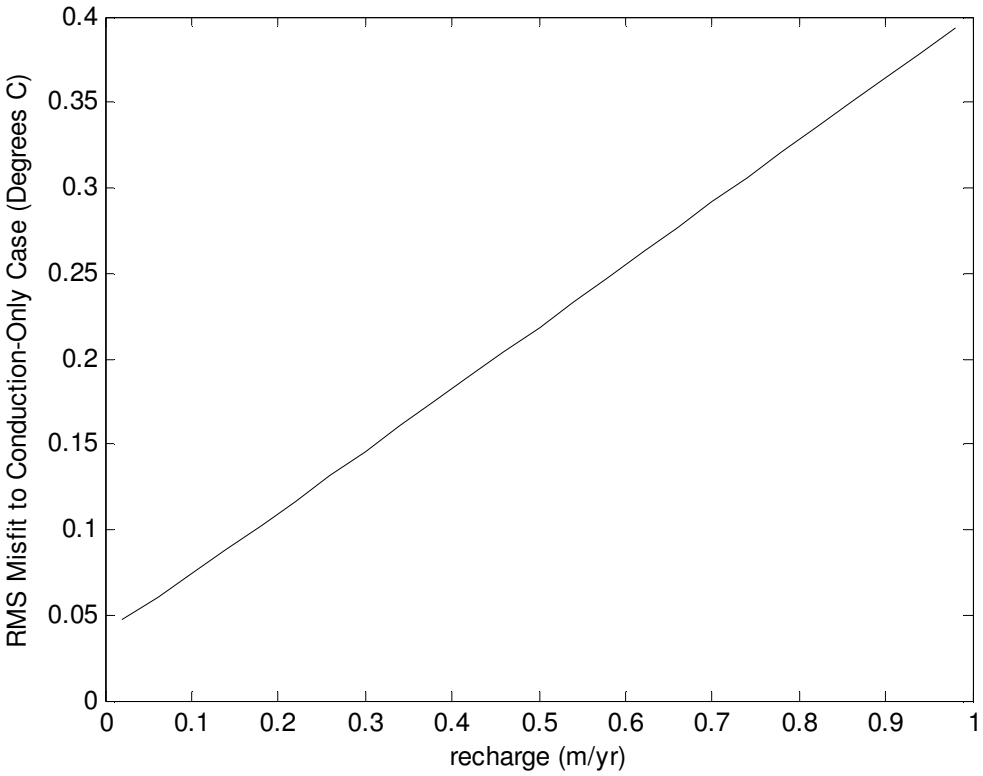

Figure 4.5. Effect of recharge on the temperature signal recorded at 2 m depth, as measured using the RMS misfit to the signal modeled without recharge. The intercept of this line suggests that the error in the numerical model is ~0.05 °C. These results suggest that typical recharge rates will not greatly affect temperatures measured in soil borings.

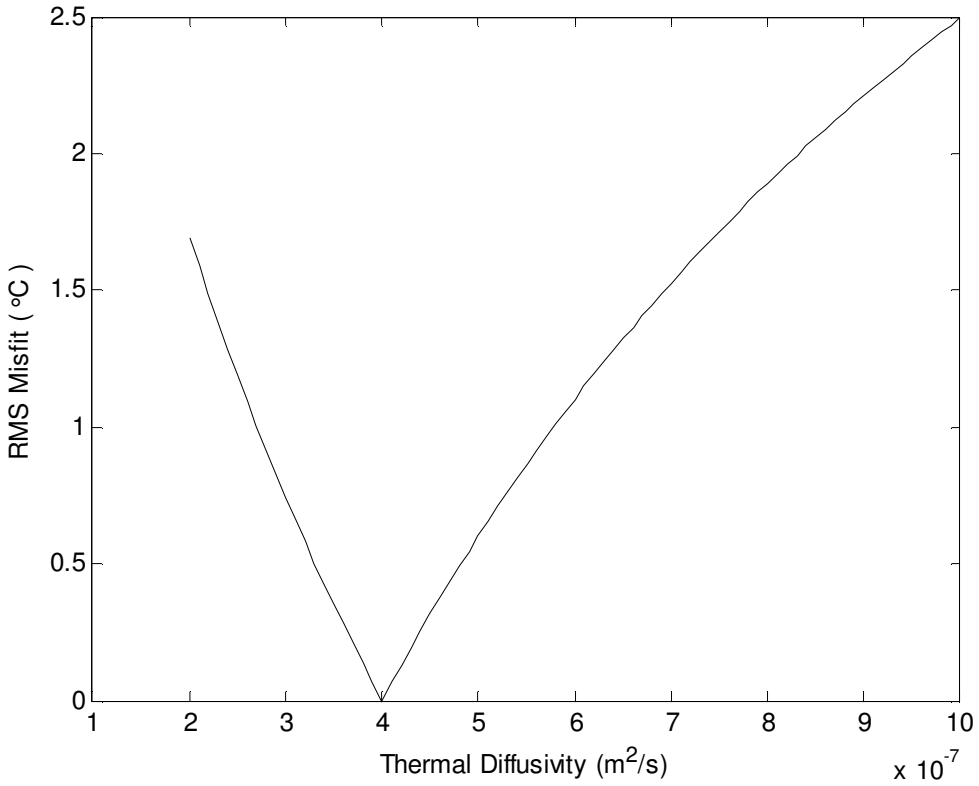

Figure 4.6. RMS error in a modeled temperature signal due to the use of incorrect thermal diffusivity. The true thermal diffusivity in this case is 4×10^{-7}, and all other model parameters are identical to the ones used in Figure 4.4

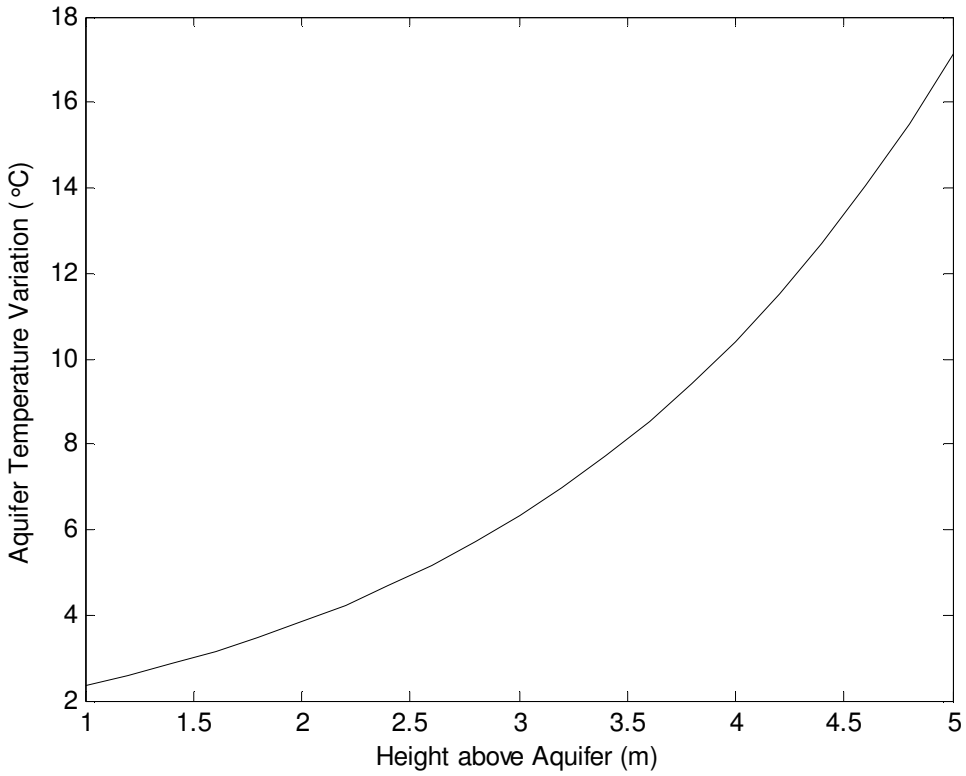

Figure 4.7.a. The amplitude of aquifer temperature variation required to create a 2 °C variation in soil temperature signal as a function of height above the aquifer. While the this curve is affected by the thermal diffusivity used in the calculations (4 x 10^{-7} m^2/s, in this case), it is unlikely that temperature signals measured more than a few meters above the top of an aquifer will be able to detect aquifer temperature variations.

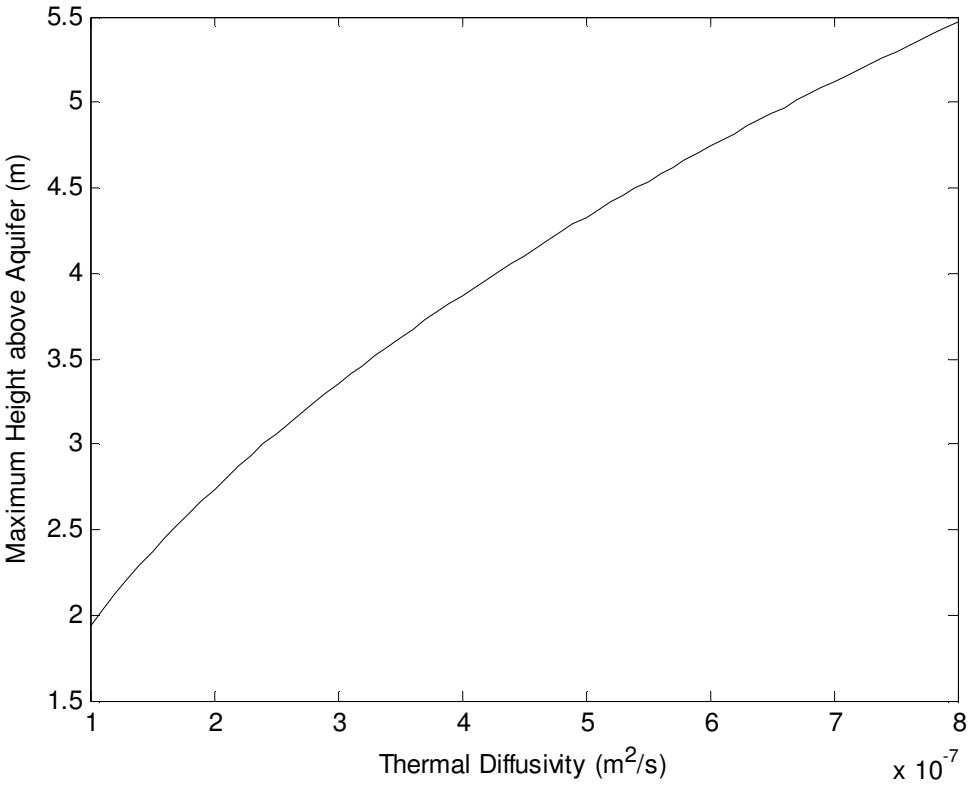

Figure 4.7.b. The greatest height above the aquifer at which the effect of a 13.8 °C variation in aquifer temperature on the soil temperature variation will have an amplitude of at least 2 °C as a function of thermal diffusivity. Soil temperature signals are affected by temperature variations in deeper aquifers when the D of the soil is greater.

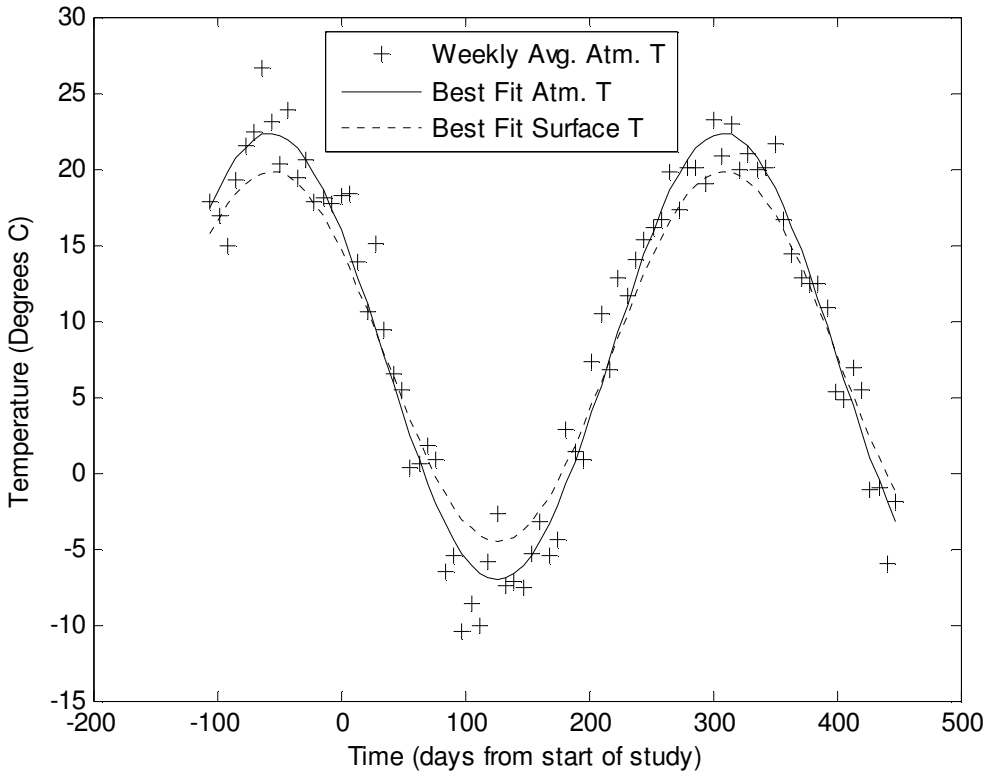

Figure 4.8. The atmospheric and surface temperature variations for the site. The atmospheric temperature data were recorded at the Schenectady Airport. The best fit surface temperature model was determined independently using soil temperature measurements, but, as expected, it is attenuated and very slightly lagged relative to the atmospheric signal.

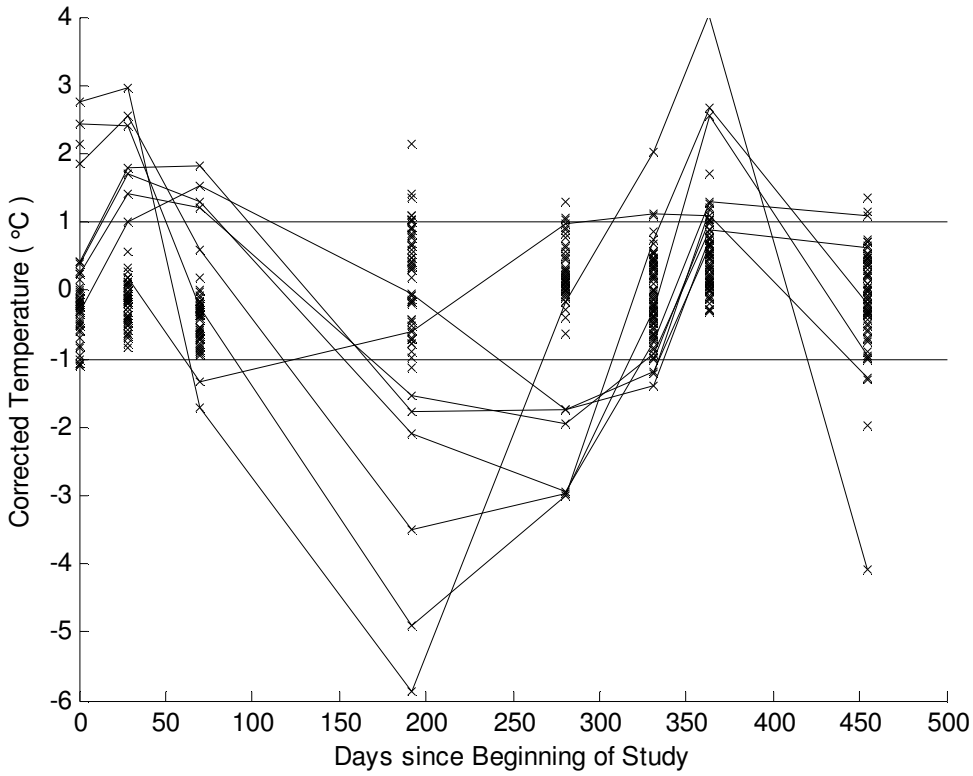

Figure 4.9.a. Temperature time series for each boring after the subtraction of the modeled effect of surface temperature variation. Most of the corrected time series vary from zero by <1 °C. Lines are drawn connecting the data points for the borings where the RMS misfit between the uncorrected series and the modeled effect is greater than 1 °C. The anomaly with the highest magnitude is boring 42.

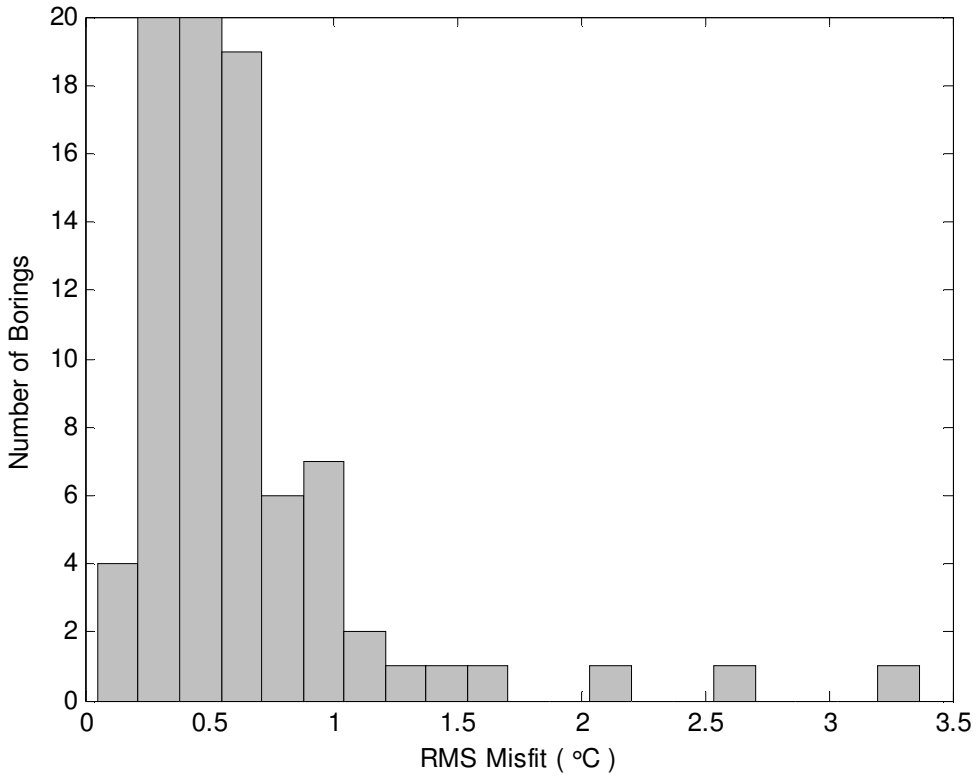

Figure 4.9.b. Histogram of the RMS misfit between the temperatures in each boring and the modeled effect of surface temperature variations. RMS misfits of <1 °C may be due to variability in the surface temperature effect and uncertainty in measurements. We infer that we have detected the effect of the aquifer temperature signal in the 10 borings with misfits >1 °C.

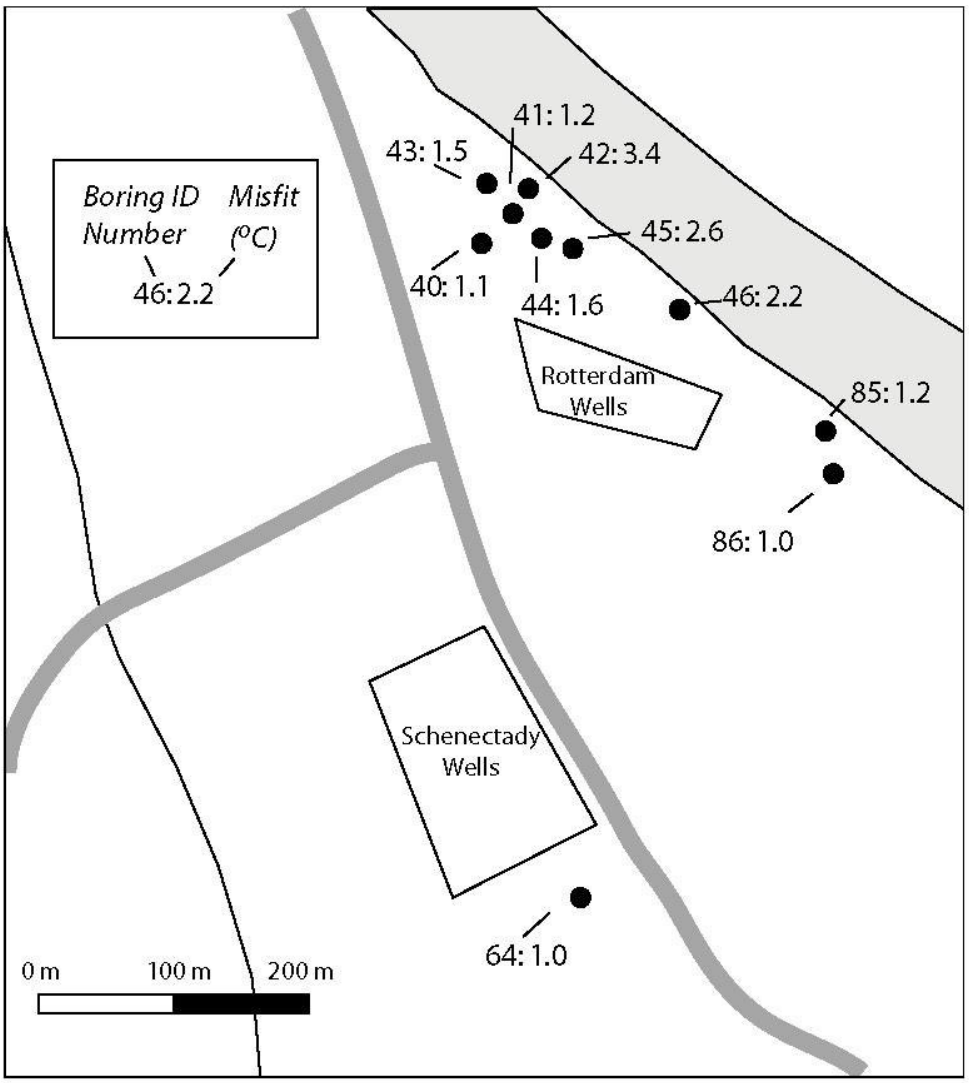

Figure 4.10. The locations of the borings with RMS misfits to the modeled surface temperature effect greater than 1 °C. The aquifer temperature effect has been successfully detected near the bank of the river. Boring 64, which has a misfit only slightly greater than 1 °C, may have a high misfit due to measurement errors.

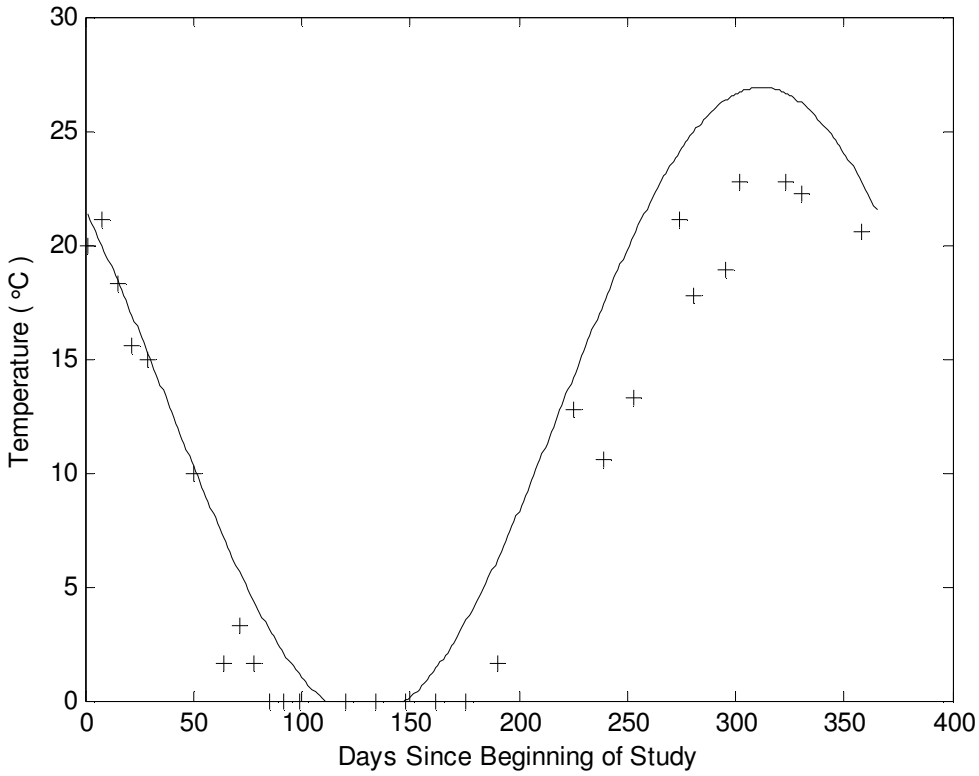

Figure 4.11. Best fit model of aquifer temperature beneath boring 42 (line) and Mohawk River temperature measurements (crosses). The aquifer temperature model is truncated at 0 °C, and is reasonably similar to the river temperature, which should be close to the true aquifer temperature.

Chapter 5

Conclusions

5.1 Summary of Results

5.1.1 Site-Specific Implications

While the focus of the work presented here relates to the use of temperature measurements in the characterization of flow systems, each chapter also produced results of interest to hydrogeologists working in the study areas.

The work described in Chapter 2 resulted in an estimate of the surface-water- ground-water flux from the Rio Grande to the Upper Santa Fe Group Aquifer of 1.2-1.6 m^3 per day per meter of riverbank. This estimate is consistent with the river-aquifer interchange measurements made by the USGS and local governments. Thus, the results of Chapter 2 increase our confidence in the model used to allocate Rio Grande surface water rights. The flux estimate presented in Chapter 2 is specific one stretch of the Rio Grande near the Paseo Del Norte in Albuquerque, New Mexico. The apparent success of this study suggests that aquifer temperature measurements made in chains of piezometers may be a cost-effective method for estimating the river-bottom seepage at the aquifer scale at other locations along the Rio Grande.

The modeling in Chapter 3 suggests that the Rotterdam and Schenectady water supply wells draw less than half of their water from the Mohawk River. This estimate is significantly lower than some existing estimates of the magnitude of induced infiltration at the site. The implication of this finding is that more than half of the water used by Rotterdam and Schenectady is drawn from the sandy aquifer to the south. The most likely source of this water is infiltration from the wetlands to the south of the well fields. The

New York Department of Environmental Conservation is currently engaged in a project to estimate the flux from the wetlands to the aquifer. If their study confirms the results of Chapter 3, then more attention will need to be paid to wellhead protection in the wetlands.

While the soil temperature study in Chapter 4 did not detect the deeper aquifer at the Mohawk River site, it did indicate the presence of a preferential flow path in the overlying fine-grained sediments. While it is unlikely that the flow through this shallow channel is significant compared to the flow through the deeper aquifer, it represents an alternate pathway for river water to reach the wells, and thus should be considered in future studies of surface water influence on the Rotterdam and Schenectady pumping centers.

5.1.2 Broader Implications

A significant contribution of this work is that it doubles, from two to four, the number of studies in which annual temperature variations have been used to characterize surface-water-ground-water interactions at scales that are directly relevant to ground-water modelers (e.g.., hundreds to thousands of meters). Each chapter also made technical advances in the use of temperature signals in hydrogeology.

Chapter 2 presents the first application of the Suzuki-Stallman equation to horizontal, aquifer-scale flux estimation. This analytical solution should be useful for obtaining preliminary results rapidly and for estimating the flux through advective systems that are difficult to model numerically.

Chapter 3 solves the problem of modeling thermal-transport in high-Peclet number regimes using a method-of-characteristics, particle-tracking model. This approach proved

successful in modeling the temperature patterns in an aquifer that would have been difficult to model using a conventional finite-difference or finite-element model. Chapter 4 showed that annual variations in aquifer temperature can be detected in shallow soil borings, and that these data can be used to map preferential flow-paths. A particular contribution of Chapter 4 is the investigation of the range of conditions under which these signals will be detectable.

5.2 Recommendations for Future Work

The principal recommendation that arises from the work presented in this thesis is that annual ground-water temperature variations should be used more widely. Part of the reason that these data are underutilized is that the available models do not perform well in the high-flux flow systems, where annual temperature variations provide the most information. Thus, the availability of a particle-tracking model such as the one described in Chapter 3 would encourage the wider use of temperature data in aquifer characterization. The code presented in Appendix B represents a proof-of-concept for the method, but it is written for use with Matlab, a proprietary software package. A Fortran version of the code would run more quickly and would not require a Matlab license. Future particle-tracking thermal transport models should also be extended to three dimensions, or to multiple, interacting two-dimensional layers.

Another promising direction for future research is the joint inversion of temperature signals and traditional hydrogeological data to estimate hydraulic conductivity. This has already been achieved for steady state temperature signals, but the work presented here has shown that annual variations in temperature may be useful in characterizing surface-water-ground-water interchange. In addition, spatially-dense temperature data collected

either in wells or in soil borings contain information about aquifer heterogeneities. Using such data sets as calibration targets for parameter estimation could help to constrain spatial variations in hydraulic conductivity.

Appendix A

Code Listing for Finite Element Model of Coupled Ground-water Flow and Thermal Transport

The example programs listed here (EgyptTtr.m and genericgeom.m) are Matlab functions designed to perform the simulation described in Appendix D.

function [p,t,Tall,hall]=egyptTtr;

```
Ttable=[0,5,10,15,20,25,30];
mu=[1,.85,.73,.64,.56,.50,.45];
viscfit=polyfit(Ttable,mu,2);
Tref=10;
muref=polyval(viscfit,Tref);


%parameter related to time domain solver (implicit, explicit, etc.)
omega=.5;

%parameters realted to time steps

ntsteps=10*365;
increment=ones(1,ntsteps)*3600*24;
time=cumsum(increment);
recordinginterval=3600*24;
nrecs=floor(max(time)/recordinginterval);
%Grid setup-must match match external file!
xall=[0,200,200,0,0];
yall=[0,0,3,3,0];
%bcflag: 1=constant head, 0=constant flow, -1=no flow
bcflag=[-1,1,-1,2];
nbs=length(bcflag);

%NOTE: around line 150 I got rid of the ability to linearly change ch
%values- only first row counts
bcstartend=[[0,3,0,4];[0,3,0,4]];
biggest=1;
%as above, but 2 is time variable
Tbcflag=[-1,1,-1,2];
Tbcstartend=[[0,25,0,0];[0,25,0,0]];
[p,e,t]=initmesh('genericgeom','Hmax',biggest);
```

```
[Kref,storage]=kfind(p,t);
ncells=length(t);
nnodes=length(p);
hall=zeros(nnodes,nrecs);
Tall=zeros(nnodes,nrecs);
[hold,Told]=getic(nnodes,p);

%%%%%%%%%%%%%%%%%%%%%%%%%%%%%%%%%%%%%%%%%%%%%%%%%%%%%%%%%%%%%%%%

%physical values related to temperature
%rhof is in kg/m^3
rhof=1000;
%Csolid=800;
rhoCsolid=2.7e6;
porosity=0.35;
%Cf is in J/kg/deg C
Cf=4216;
%dispersivi
%rhoCavg=rhof*Cf*porosity+rhoCsolid*(1-porosity);
rhoCavg=3.2e6;
Rf=rhoCavg/(rhof*Cf*porosity);
D=Dfind(p,t);
depth=getdepths(p,t);
%%%%%%%%%%%%%%%%%%%%%%%%%%%%%%%%%%%%%%%%%%%%%%%%%%%%%%%%%%%%%%%%

sglob=zeros(nnodes);
K0glob=sglob;
Tglob2=sglob;
areas=zeros(1,ncells);
betalong=zeros(3,3,ncells);
%set up storage matrix and calcualte triangle areas
for n=1:ncells
   i=t(1,n);
   j=t(2,n);
   k=t(3,n);
   xi=p(1,i);
   xj=p(1,j);
   xk=p(1,k);
   yi=p(2,i);
   yj=p(2,j);
   yk=p(2,k);
   tri=[[1,xi,yi];[1,xj,yj];[1,xk,yk]];
   beta=inv(tri);
   a=beta(2:3,:);
   betalong(1:3,1:3,n)=beta;
```

```
    areas(n)=det(tri)/2;
    slocal=storage(n)*diag(ones(3,1))./3*areas(n);
    sglob(i,i)=sglob(i,i)+slocal(1,1);
    sglob(j,j)=sglob(j,j)+slocal(2,2);
    sglob(k,k)=sglob(k,k)+slocal(3,3);
    K0local=rhoCavg*diag(ones(3,1))./3*areas(n);
    K0glob(i,i)=K0glob(i,i)+K0local(1,1);
    K0glob(j,j)=K0glob(j,j)+K0local(2,2);
    K0glob(k,k)=K0glob(k,k)+K0local(3,3);


    local2=a'*D(n)*a*areas(n);
        Tglob2(i,i)=Tglob2(i,i)+local2(1,1);
        Tglob2(i,j)=Tglob2(i,j)+local2(1,2);
        Tglob2(i,k)=Tglob2(i,k)+local2(1,3);
        Tglob2(j,j)=Tglob2(j,j)+local2(2,2);
        Tglob2(j,i)=Tglob2(j,i)+local2(2,1);
        Tglob2(j,k)=Tglob2(j,k)+local2(2,3);
        Tglob2(k,k)=Tglob2(k,k)+local2(3,3);
        Tglob2(k,i)=Tglob2(k,i)+local2(3,1);
        Tglob2(k,j)=Tglob2(k,j)+local2(3,2);
end

%disp('now iterate through time')
recs=0;
for z=2:ntsteps
    if ceil(time(z)/recordinginterval)==time(z)/recordinginterval
        disp(time(z)/3600/24)
        recs=recs+1;
        recflag=1;
    else
        recflag=0;
    end
 delt=time(z)-time(z-1);
    %set up flow model matrix
glob=zeros(nnodes);

for n=1:ncells
    i=t(1,n);
    j=t(2,n);
    k=t(3,n);
    xi=p(1,i);
    xj=p(1,j);
    xk=p(1,k);
    yi=p(2,i);
    yj=p(2,j);
```

```
    yk=p(2,k);
    tri=[[1,xi,yi];[1,xj,yj];[1,xk,yk]];
    %beta=inv(tri);
    beta=betalong(:,:,n);
    a=beta(2:3,:);
    Ttri=(Told(i)+Told(j)+Told(k))/3;
    %assume K is transmissivity, leave out aquifer thickness
    mutri=viscfit(3)+viscfit(2)*Ttri+viscfit(1)*Ttri^2;
    K(n)=Kref(n)*muref/mutri;

    local=a'*K(n)*a*(areas(n));
    glob(i,i)=glob(i,i)+local(1,1);
    glob(i,j)=glob(i,j)+local(1,2);
    glob(i,k)=glob(i,k)+local(1,3);
    glob(j,j)=glob(j,j)+local(2,2);
    glob(j,i)=glob(j,i)+local(2,1);
    glob(j,k)=glob(j,k)+local(2,3);
    glob(k,k)=glob(k,k)+local(3,3);
    glob(k,i)=glob(k,i)+local(3,1);
    glob(k,j)=glob(k,j)+local(3,2);
end


    q=zeros(nnodes,1);

    gsubset2=(1-omega)*glob-sglob./delt;

    q=q-gsubset2*hold;

    nch=0;
    segnum=e(5,:);
    chnodes=zeros(0,1);
    cfnodes=zeros(0,1);
    for m=1:nbs
       bb=find(segnum==m);

       if bcflag(m)==1

          chnodes=[chnodes,e(1,bb)];
          ch((nch+1):(nch+length(bb)))=bcstartend(1,m);
          nch=nch+length(bb);

       elseif bcflag(m)==0
          len=e(4,bb)-e(3,bb);
          weight=[len(1)/2,(len(1:(end-1))+len(2:end))./2]./(sum(len)-len(end)/2);
          cf=weight.*bcstartend(1,m);
```

```
            cfnodes=[cfnodes,e(1,bb)];
        elseif bcflag(m)==2
            chnodes=[chnodes,e(1,bb)];
            rmndr=time(z)/3600/24-floor(time(z)/7/3600/24)*7;
            if rmndr<5
                ch((nch+1):(nch+length(bb)))=4;
                nch=nch+length(bb);
            else
                ch((nch+1):(nch+length(bb)))=6;
                nch=nch+length(bb);
            end

        end
    end

    gsubset=omega*glob+sglob./delt;

    index=1:nnodes;

    for n=1:length(cfnodes)
        q(cfnodes(n))=q(cfnodes(n))+cf(n);

    end

    for n=1:nch
        m=chnodes(n);
        o=find(index==m);
        gsubset=[gsubset(1:(o-1),:);gsubset((o+1):end,:)];
        q=[q(1:(o-1));q((o+1):end)];
        index=[index(1:(o-1)),index((o+1):end)];
        q=q-ch(n).*gsubset(:,chnodes(n));

    end

    gsubset=gsubset(:,index);

    qstar=q;

    hsub=gsubset\qstar;
    h=zeros(nnodes,1);
    h(index)=hsub;
    h(chnodes)=ch;
hold=h;
if recflag==1
    hall(:,recs)=h;
end
```

```
%%%%%%%%%%%%%%%%%%%%%%%%%%%%%%%%%%%%%%%%%%%%
    %given heads, calculate temperature



    Tglob=Tglob2;
%K0glob=zeros(nnodes);
    for n=1:ncells
        i=t(1,n);
        j=t(2,n);
        k=t(3,n);
        xi=p(1,i);
        xj=p(1,j);
        xk=p(1,k);
        yi=p(2,i);
        yj=p(2,j);
        yk=p(2,k);
        tri=[[1,xi,yi];[1,xj,yj];[1,xk,yk]];
        %beta=inv(tri);
        beta=betalong(:,:,n);
        a=beta(2:3,:);
        hvec=hold([i;j;k]);
        vel=-K(n)*a*hvec;
        %vel=2e-4*2/300*[1;0];

        vv(n)=sqrt(vel(1)^2+vel(2)^2);
        %vv(n)=vel(1);
        %vv(n)=atan2(vel(2),vel(1));
        b=[1/3,1/3,1/3];


        local1=rhof*Cf*b'*vel'*a*areas(n);


        Tglob(i,i)=Tglob(i,i)+local1(1,1);
        Tglob(i,j)=Tglob(i,j)+local1(1,2);
        Tglob(i,k)=Tglob(i,k)+local1(1,3);
        Tglob(j,j)=Tglob(j,j)+local1(2,2);
        Tglob(j,i)=Tglob(j,i)+local1(2,1);
        Tglob(j,k)=Tglob(j,k)+local1(2,3);
        Tglob(k,k)=Tglob(k,k)+local1(3,3);
        Tglob(k,i)=Tglob(k,i)+local1(3,1);
```

```
      Tglob(k,j)=Tglob(k,j)+local1(3,2);



   end



   ncT=0;
   ncHf=0;
   nspecial=0;
   segnum=e(5,:);
   cTnodes=zeros(0,1);
   cHfnodes=zeros(0,1);

   for m=1:nbs
      bb=find(segnum==m);

      if Tbcflag(m)==1

         cTnodes=[cTnodes,e(1,bb)];
         cT((ncT+1):(ncT+length(bb)))=Tbcstartend(1,m);
         ncT=ncT+length(bb);

      elseif Tbcflag(m)==0
         len=e(4,bb)-e(3,bb);
         weight=[len(1)/2,(len(1:(end-1))+len(2:end))./2]./(sum(len)-len(end)/2);
         cHf((ncHf+1):(ncHf+length(bb)))=weight.*Tbcstartend(1,m);
         cHfnodes=[cHfnodes,e(1,bb)];
         ncHf=ncHf+length(bb);
      elseif Tbcflag(m)==2

         cT((ncT+1):(ncT+length(bb)))=10*sin((time(z)-110)/365/3600/24*2*pi)+25;
         cTnodes=[cTnodes,e(1,bb)];
         ncT=ncT+length(bb);

      end
   end



   qH=zeros(nnodes,1);
   gsubset=Tglob;
gsubsetLHS=(omega)*Tglob+K0glob./delt;
gsubsetRHS=(1-omega)*Tglob-K0glob./delt;
   qH=qH-gsubsetRHS*Told;
```

```
    index=1:nnodes;
    if length(cHfnodes)>0
       qH(cHfnodes)=cHf;
    end

    for n=1:ncT
       m=cTnodes(n);
       o=find(index==m);
       gsubsetLHS=[gsubsetLHS(1:(o-1),:);gsubsetLHS((o+1):end,:)];
       qH=[qH(1:(o-1));qH((o+1):end)];
       index=[index(1:(o-1)),index((o+1):end)];
       qH=qH-cT(n).*gsubsetLHS(:,cTnodes(n));

    end

    gsubsetLHS=gsubsetLHS(:,index);

    Tsub=gsubsetLHS\qH;

    T=zeros(nnodes,1);
    T(index)=Tsub;
    T(cTnodes)=cT;
    Told=T;
    if recflag==1

    Tall(:,recs)=T;
    end


end
```

```
%%%%%%%%%%%%%%%%%%%%%%%%%%%%%%%%%%%%%%%%%%%%%%%%%%%%%%%%%%%%%%%%
%DISPLAY

pdesurf(p,t,Tall(:,end-1))
% xx=0:10:1400;
% yy=0:10:2100;
% hgrid=tri2grid(p,t,h,xx,yy) ;
% figure(1)
% surf(xx,yy,hgrid)
% shading flat
```

```
% view(2)
% xlabel('Easting (m)')
% ylabel('Southing (m)')
% colorbar
% axis ij
% axis equal
% axis tight


%%%%%%%%%%%%%%%%%%%%%%%%%%%%%%%%%%%%%%%%%%%%%%%%%%%%%%%%%%%%%%%%
%SUB-FUNCTIONS

function [k,storage]=kfind(p,t);

k=ones(1,length(t))*1e-5;
storage=ones(1,length(t))*.18;

function [qw,wellnodes]=qwellsfind(t);
wellnodes=[500,30];
qw=zeros(2,1);
   if t>0
      qw(1)=-0.00001;
   end
   if t>5e6
      q(2)=-0.02;
   end



function [hinit,Tinit]=getic(nnodes,p);
hinit=p(1,:)'*(3-4)/200+4;
Tinit=ones(nnodes,1)*25;


function D=Dfind(p,t);
D=ones(1,length(t))*(1.8);
function [x,y]=genericgeom(bs,s)


xall=[0,200,200,0,0];
yall=[0,0,3,3,0];
nbs=length(xall)-1;
if nargin==0
  x=nbs;
  return
end
```

```
dl=[0:(nbs-1);1:nbs;ones(1,nbs);zeros(1,nbs)];
altot=0;
for n=1:nbs
   dl(1,n)=0;
   dl(2,n)=sqrt((xall(n)-xall(n+1))^2+(yall(n)-yall(n+1))^2);

%    dl(1,n)=altot;
%    al=sqrt((xall(n)-xall(n+1))^2+(yall(n)-yall(n+1))^2);
%    altot=altot+al;
%    dl(2,n)=altot;
end

if nargin==1
  x=dl(:,bs);
  return
end
x=zeros(size(s));
y=zeros(size(s));
[m,n]=size(bs);
if m==1 & n==1,
  bs=bs*ones(size(s)); % expand bs
elseif m~=size(s,1) | n~=size(s,2),
  error('bs must be scalar or of same size as s');
end

if ~isempty(s)
for q=1:(m*n)
   r=bs(q);
   als=dl(1,r);
   alf=dl(2,r);
   frac=(s(q)-als)/(alf-als);
   x(q)=xall(r)+frac*(xall(r+1)-xall(r));
   y(q)=yall(r)+frac*(yall(r+1)-yall(r));
end
end
```

Appendix B

Code Listing For Finite Difference, Method-of-Characteristics Model of Coupled Ground-water Flow and Thermal Transport

The example program listed here (mohawkparticletrackbest.m) is a Matlab function

designed to perform the simulation that produced Figure 3.11.

```
function [hrecord,Trecord]=mohawkparticletrackbest;
Qriv=0;
conductance=5e-6;
Klow=.0135;
%time parameters, time starts on Jan 1 at 0000h
dt=3600*24*.1;
time=0;
ntend=3650;

recordtimes=[1:1:366]*3600*24;
recordflag=0;

%define domain
dx=30;
ymax=1534;
xmax=1330;

m=ceil(xmax/dx);
n=ceil(ymax/dx);

riverx=[0,67,293,537,975,m*dx];
rivery=[0,79,536,804,1146,n*dx];
active=zeros(m,n);
rivseg=1;
ncell=1;
flag=0;

%define wells
nrotwells=3;
nschenwells=5;
nwells=8;
 wellsi=[17;18;20;14;14;15;16;16];
 wellsj=[32;32;33;[39:43]'];
```

```
%rotterdam pumps 1.9 mgpd, or 0.083 m3/s
rotrate=-0.083/nrotwells;
%schenectady pumps 16.5 mgpd, or 0.722 m3/s
schenrate=-.722/nschenwells;
r=ones(m,n)*.3/3600/24/365;
rnowells=r;
Trecharge=10;


for q=1:nrotwells;
   r(wellsi(q),wellsj(q))=rotrate/dx/dx;
end
for q=1:nschenwells;
   r(wellsi(q+nrotwells),wellsj(q+nrotwells))=schenrate/dx/dx;
end

%define river boundaries b1 and b2
for q=1:n
   yq=(q-.5)*dx;
   if yq>rivery(rivseg+1)
      rivseg=rivseg+1;
   end
   xriv=(riverx(rivseg+1)-riverx(rivseg))/(rivery(rivseg+1)-rivery(rivseg))...
      *(yq-rivery(rivseg))+riverx(rivseg);
   if flag==0
      if rivseg==1
         b1(ncell,1)=ceil(xriv/dx);
         b1(ncell,2)=q;
         ncell=ncell+1;
         if q>2
            if active(b1(ncell-1,1),q-1)==0
               b1(ncell,1)=ceil(xriv/dx-1);
               b1(ncell,2)=q;
               ncell=ncell+1;
            end
         end
      else
         flag=1;
         ncell=1;
      end
   end
   if flag==1
      b2(ncell,1)=ceil(xriv/dx);
      b2(ncell,2)=q;
      ncell=ncell+1;
      if q<48
```

```
        if active(b2(ncell-1,1),q-1)==0
           b2(ncell,1)=ceil(xriv/dx-1);
           b2(ncell,2)=q;
           ncell=ncell+1;
           if active(b2(ncell-1,1),q-1)==0
              b2(ncell,1)=ceil(xriv/dx-2);
              b2(ncell,2)=q;
              ncell=ncell+1;
           end
        end
     end
  end

  active(1:ceil(xriv/dx),q)=1;

end
r=r.*active;
depth=getdepth(b1,b2,m,n,active,dx);

%aquifer parameters
Kref=ones(m,n)*.027;

Kref(:,(n-2):n)=Klow;
depth(:,(n-2):n)=5;
for q=16:m
   yline=(1270-(n-2+.5)*dx)/(m-16)*(q-16)+(n-2+.5)*dx;
   edge=floor(yline/dx);
   depth(q,edge:n)=5;
   Kref(q,edge:n)=Klow;
end
depth=depth.*active
xi=(1:m)*dx-dx/2;
yi=(1:n)'*dx-dx/2;

KKref=Kref.*active.*depth;

%T-dependent viscosity
Ttable=[0,5,10,15,20,25,30];
mu=[1,.85,.73,.64,.56,.50,.45];
viscfit=polyfit(Ttable,mu,2);
Tref=10;
muref=polyval(viscfit,Tref);

[m,n]=size(Kref);
rhof=1000;
Cf=4216;
```

```
rhoCavg=3.2e6;
Rf=rhof*Cf/rhoCavg;
k=2.0;
D=k/rhoCavg;
S=0.1;

%initial values
[hnew,Tnew]=initmodel(Kref);


%make particles
[px,py,pT,np]=particleinit(Tnew,81,dx,active,time,b1,b2);
pii=ceil(px./dx);
pjj=ceil(py./dx);
nempty=0;

%numerical parameters
alpha=0.5;
tol=0.01;

hold=hnew;

%iterate through time
for nt=1:ntend;
   nt
   numit=0;
   time=time+dt;
   amax=1;

   %calculate K as a function of T
   mu=polyval(viscfit,Tnew);
   K=Kref*muref./mu;
   KK=KKref*muref./mu;


   Kn=sqrt(KK(1:(m-2),2:(n-1)).*KK(2:(m-1),2:(n-1)));
   Ks=sqrt(KK(3:(m),2:(n-1)).*KK(2:(m-1),2:(n-1)));
   Ke=sqrt(KK(2:(m-1),3:(n)).*KK(2:(m-1),2:(n-1)));
   Kw=sqrt(KK(2:(m-1),1:(n-2)).*KK(2:(m-1),2:(n-1)));

%correct stage for navigation or non-navigation season
   dayofyear=time/3600/24-floor(time/3600/24/365)*365;
   if and(dayofyear>=124,dayofyear<=319)
      lockstage=68.9;
      rivstage=64.6;
   else
```

```
    lockstage=64.9;
    rivstage=64.6;
end
if and(dayofyear>=15,dayofyear<124)
    rivstage=64.0;
end
for q=1:length(b1)
    mu=polyval(viscfit,Tnew(b1(q,1),b1(q,2)));
    r(b1(q,1),b1(q,2))=(lockstage-hnew(b1(q,1),b1(q,2)))*...
        conductance*100/dx*muref/mu;
    %r(b1(q,1),b1(q,2))=0;
    Qriv=Qriv+r(b1(q,1),b1(q,2))*dx*dx*dt;
end
for q=1:(length(b2)-5)
    if and(q>25,q<30)
    mu=polyval(viscfit,Tnew(b2(q,1),b2(q,2)));
    r(b2(q,1),b2(q,2))=(rivstage-hnew(b2(q,1),b2(q,2)))*.1*...
        conductance*100/dx*muref/mu;
    else
                mu=polyval(viscfit,Tnew(b2(q,1),b2(q,2)));
                r(b2(q,1),b2(q,2))=(rivstage-hnew(b2(q,1),b2(q,2)))*.1*...
                    conductance*100/dx*muref/mu;
    end
            Qriv=Qriv+r(b2(q,1),b2(q,2))*dx*dx*dt;
    %r(b2(q,1),b2(q,2))=2.1e-5;
end

while amax>tol;
    numit=numit+1;
    oldval=hnew;
    h1=(Kw.*hold(2:(m-1),1:(n-2))+Ke.*hold(2:(m-1),3:n)+Kn.*...
        hold(1:(m-2),2:(n-1))+Ks.*hold(3:m,2:(n-1)))./4;
    h2=alpha*(Kw.*hnew(2:(m-1),1:(n-2))+Ke.*hnew(2:(m-1),3:n)+...
        Kn.*hnew(1:(m-2),2:(n-1))+Ks.*hnew(3:m,2:(n-1)))./4;
    f1=dx^2*S/4/dt;
    f2=1./(f1+alpha*(Kn+Ks+Ke+Kw)./4);
    f3=r(2:(m-1),2:(n-1))*dx*dx/4;
    hnew(2:(m-1),2:(n-1))=(f1.*hold(2:(m-1),2:(n-1))+(1-alpha)*...
        (h1-(Kn+Ks+Ke+Kw)./4.*hold(2:(m-1),2:(n-1)))+h2+f3).*f2;
    amax=max(max(abs(hnew-oldval)));
    %calculate boundary conditions

    hnew(:,n)=66.5;
    hnew(1,:)=hnew(2,:);

end
```

```
   hold=hnew;

   %JURY RIG PORTION- REMOVE WHEN T IS RUNNING
%         Triver=14.7*sin(2*pi/365/3600/24*(time-111.45*3600*24))+7.65;
%      if Triver<0
%         Triver=0;
%     end
% %     %Triver=20;
%     for q=1:length(b1)
%        Tnew(b1(q,1),b1(q,2))=Triver;
%     end
%     for q=1:length(b2)
%        Tnew(b2(q,1),b2(q,2))=Triver;
%     end


   %regenerate particles if more than 2% are empty
   if nempty-nwells>.02*sum(sum(active))
      [px,py,pT,np]=particleinit(Tnew,81,dx,active,time,b1,b2);
      disp('regenerating particles')
      pii=ceil(px./dx);
      pjj=ceil(py./dx);
   end
   %calculate velocities- specific to this aquifer
   velx=zeros(size(hnew));
   vely=zeros(size(hnew));
   velx(2:(m-1),1:n)=Rf*K(2:(m-1),1:n).*(hnew(1:(m-2),1:n)-hnew(3:m,1:n))./(2*dx);
   velx(1,:)=Rf*K(1,:).*(hnew(1,:)-hnew(2,:));
   velx(m,:)=Rf*K(m,:).*(hnew((m-1),:)-hnew(m,:))./dx;
   vely(:,2:(n-1))=Rf*K(:,2:(n-1)).*(hnew(:,1:(n-2))-hnew(:,3:n))./(2*dx);
   vely(:,1)=Rf*K(:,1).*(hnew(:,1)-hnew(:,2))./dx;
   vely(:,n)=Rf*K(:,n).*(hnew(:,(n-1))-hnew(:,n))./dx;

   for q=1:length(b1)

      if b1(q,1)==1
         velx(b1(q,1),b1(q,2))=0;

      else
         velx(b1(q,1),b1(q,2))=Rf*K(b1(q,1),b1(q,2))*...
            (hnew(b1(q,1)-1,b1(q,2))-hnew(b1(q,1),b1(q,2)))/dx;
      end
      vely(b1(q,1),b1(q,2))=Rf*K(b1(q,1),b1(q,2))*...
         (hnew(b1(q,1),b1(q,2))-hnew(b1(q,1),b1(q,2)+1))/dx;
```

```
end
for q=1:length(b2)
   velx(b2(q,1),b2(q,2))=Rf*K(b2(q,1),b2(q,2))*...
      (hnew(b2(q,1)-1,b2(q,2))-hnew(b2(q,1),b2(q,2)))/dx;
   if b2(q,2)==n
      vely(b2(q,1),b2(q,2))=vely(b2(q,1)-1,b2(q,2));
   else
      vely(b2(q,1),b2(q,2))=Rf*K(b2(q,1),b2(q,2))*...
         (hnew(b2(q,1),b2(q,2))-hnew(b2(q,1),b2(q,2)+1))/dx;
   end
end


%calculate particle velocities
velxvec=reshape(velx,m*n,1);
velyvec=reshape(vely,m*n,1);

pvelx=zeros(size(px));
pvely=zeros(size(py));
%calculate pvelx
%case 1- left and right edges
aa=find(or(px<=.5*dx,px>=(m-.5)*dx));
if not(isempty(aa))
   nvecij=(pjj(aa)-1)*m+pii(aa);
   pvelx(aa)=velxvec(nvecij);
end
%case 2- top and bottom
%case2a- left of center
aa=find(and(and(not(or(px<.5*dx,px>(m-.5)*dx)),...
   or(py<.5*dx,py>(n-.5)*dx)),px<(pii-.5)*dx));

if not(isempty(aa))
   nvecij=(pjj(aa)-1)*m+pii(aa);
   nvecimj=(pjj(aa)-1)*m+(pii(aa)-1);
   pvelx(aa)=(velxvec(nvecij)-velxvec(nvecimj))./dx.*...
      (px(aa)-(pii(aa)-1.5)*dx)+velxvec(nvecimj);
end
%case2b- right of center
aa=find(and(and(not(or(px<.5*dx,px>(m-.5)*dx)),...
   or(py<.5*dx,py>(n-.5)*dx)),px>(pii-.5)*dx));

if not(isempty(aa))
   nvecij=(pjj(aa)-1)*m+pii(aa);
   nvecipj=(pjj(aa)-1)*m+(pii(aa)+1);
   pvelx(aa)=(velxvec(nvecipj)-velxvec(nvecij))./dx.*...
      (px(aa)-(pii(aa)-.5)*dx)+velxvec(nvecij);
```

```
end
%case 3, la deluge
aa=find(and(and(px>=.5*dx,px<=(m-.5)*dx),and(py>=.5*dx,py<=(n-.5)*dx)));

pvelx(aa)=interp2(([1:m]-.5)*dx,([1:n]-.5)*dx,velx',px(aa),py(aa));


%calculate pvely
%case 1- top and bottom edges
aa=find(or(py<=.5*dx,py>=(n-.5)*dx));
if not(isempty(aa))
   nvecij=(pjj(aa)-1)*m+pii(aa);
   pvely(aa)=velyvec(nvecij);
end
%case 2- left and right edges
%case2a- below the center
aa=find(and(and(not(or(py<.5*dx,py>(n-.5)*dx)),...
   or(px<.5*dx,px>(m-.5)*dx)),py<(pjj-.5)*dx));
if not(isempty(aa))
   nvecij=(pjj(aa)-1)*m+pii(aa);
   nvecijm=(pjj(aa)-2)*m+(pii(aa));
   pvely(aa)=(velyvec(nvecij)-velyvec(nvecijm))./dx.*...
      (py(aa)-(pjj(aa)-1.5)*dx)+velyvec(nvecijm);
end
%case2b- above center
aa=find(and(and(not(or(py<.5*dx,py>(n-.5)*dx)),...
   or(px<.5*dx,px>(m-.5)*dx)),py>(pjj-.5)*dx));

if not(isempty(aa))
   nvecij=(pjj(aa)-1)*m+pii(aa);
   nvecijp=(pjj(aa))*m+(pii(aa));
   pvely(aa)=(velyvec(nvecijp)-velyvec(nvecij))./dx.*...
      (py(aa)-(pjj(aa)-.5)*dx)+velyvec(nvecij);
end
%case 3, la deluge
aa=find(and(and(px>=.5*dx,px<=(m-.5)*dx),and(py>=.5*dx,py<=(n-.5)*dx)));

pvely(aa)=interp2(([1:m]-.5)*dx,([1:n]-.5)*dx,vely',px(aa),py(aa));


%special case at b1 and b2
   for q=1:length(b1)
   aa=find(and(pii==b1(q,1),pjj==b1(q,2)));
   if not(isempty(aa))
      pvelx(aa)=velx(b1(q,1),b1(q,2));
      pvely(aa)=vely(b1(q,1),b1(q,2));
```

```
        end
        end
        for q=1:length(b2)
        aa=find(and(pii==b2(q,1),pjj==b2(q,2)));
        if not(isempty(aa))
           pvelx(aa)=velx(b2(q,1),b2(q,2));
           pvely(aa)=vely(b2(q,1),b2(q,2));
        end
        end
%special case near wells
   for q=1:length(wellsi);
      aa=find(and(and(pii==wellsi(q)+1,pjj==wellsj(q)),px<=(wellsi(q)+.5)*dx));
      if not(isempty(aa))
         pvelx(aa)=Rf*(K(wellsi(q)+1,wellsj(q))+K(wellsi(q),wellsj(q)))/2...
         *(hnew(wellsi(q),wellsj(q))-hnew(wellsi(q)+1,wellsj(q)))./dx;
      end
      aa=find(and(and(pii==wellsi(q)-1,pjj==wellsj(q)),px>=(wellsi(q)-1.5)*dx));
      if not(isempty(aa))
         pvelx(aa)=Rf*(K(wellsi(q)-1,wellsj(q))+K(wellsi(q),wellsj(q)))/2...
         *(hnew(wellsi(q)-1,wellsj(q))-hnew(wellsi(q),wellsj(q)))./dx;
      end
      aa=find(and(and(pii==wellsi(q),pjj==wellsj(q)+1),py<=(wellsj(q)+.5)*dx));
      if not(isempty(aa))
         pvely(aa)=Rf*(K(wellsi(q),wellsj(q)+1)+K(wellsi(q),wellsj(q)))/2...
         *(hnew(wellsi(q),wellsj(q))-hnew(wellsi(q),wellsj(q)+1))./dx;
      end
      aa=find(and(and(pii==wellsi(q),pjj==wellsj(q)-1),py>=(wellsj(q)-1.5)*dx));
      if not(isempty(aa))
         pvely(aa)=Rf*(K(wellsi(q),wellsj(q)-1)+K(wellsi(q),wellsj(q)))/2...
         *(hnew(wellsi(q),wellsj(q)-1)-hnew(wellsi(q),wellsj(q)))./dx;
      end
   end

   %move particles


   px=px+pvelx*dt;
   py=py+pvely*dt;


   %reflect across no flow boundaries
   aa=find(px<0);
   if not(isempty(aa))
      px(aa)=0-px(aa);
   end
```

```
pinew=ceil(px./dx);
pjnew=ceil(py./dx);



%now generate new particles at b1
for q=1:length(b1)
   aa=find(and(and(pjj==b1(q,2),pii==b1(q,1)),or(pjnew~=b1(q,2),pinew~=b1(q,1))));

   if not(isempty(aa))
      newpy=py(aa)-dx;
      newpx=px(aa);
      Tnewvec=reshape(Tnew,m*n,1);
      nvecij=(pjj(aa)-1)*m+pii(aa);
      newpT=Tnewvec(nvecij);
      px=[px;newpx];
      py=[py;newpy];
      pT=[pT;newpT];
   end

end
%now generate new particles at b2
for q=1:length(b2)
   aa=find(and(and(pjj==b2(q,2),pii==b2(q,1)),or(pjnew~=b2(q,2),pinew~=b2(q,1))));


   if not(isempty(aa))

      newpy=py(aa)-dx;
      newpx=px(aa);
      Tnewvec=reshape(Tnew,m*n,1);
      nvecij=(pjj(aa)-1)*m+pii(aa);
      newpT=Tnewvec(nvecij);
      px=[px;newpx];
      py=[py;newpy];
      pT=[pT;newpT];

   end

end

%now generate new particles at the bottom edge
aa=find(and(pjj==n,pjnew<n));
if not(isempty(aa))
   newpy=py(aa)-dx;
```

```
        newpx=px(aa);

        px=[px;newpx];
        py=[py;newpy];
        pT=[pT;ones(size(newpx))*10];
    end
    pii=ceil(px./dx);
    pjj=ceil(py./dx);
    nempty=0;
    Told=Tnew;
    %variable T at b1
     Triver=14.7*sin(2*pi/365/3600/24*(time-111.45*3600*24))+7.65;
     if Triver<0.1
         Triver=0.1;
    end
     %Triver=20;
    for q=1:length(b1)
        aa=find(and(pii==b1(q,1),pjj==b1(q,2)));
        pT(aa)=Triver;
    end
    for q=1:length(b2)
        aa=find(and(pii==b2(q,1),pjj==b2(q,2)));
        pT(aa)=Triver;
    end
    for p=2:m
        for q=1:n
            if active(p,q)==1
                aa=find(and(pii==p,pjj==q));
                if isempty(aa)
                    nempty=nempty+1;
                else
                    Tnew(p,q)=mean(pT(aa));

                end

            end
        end
    end
%eliminate conductive loss across valley wall boundary

Tnew(1,:)=Tnew(2,:);

    %now erase particles that have left the grid;
    aa=find(and(and(py>=0,py<=n*dx),and(px>=0,px<=m*dx)));
    px=px(aa);
    py=py(aa);
```

```
pT=pT(aa);

pii=ceil(px./dx);
pjj=ceil(py./dx);

ok=ones(length(px),1);

for z=1:length(wellsi)

   welli=wellsi(z);
   wellj=wellsj(z);

   for q=1:length(px)
      if and(pii(q)==welli,pjj(q)==wellj)

         ok(q)=0;
      elseif active(pii(q),pjj(q))==0
         ok(q)=0;
      end
   end

end

aa=find(ok);
px=px(aa);
py=py(aa);
pT=pT(aa);

pii=ceil(px./dx);
pjj=ceil(py./dx);



%calculate dispersion
grad2x=zeros(size(hnew));
grad2y=zeros(size(hnew));
grad2x(2:(m-1),:)=(Tnew(1:(m-2),:)+Tnew(3:m,:)-2*Tnew(2:(m-1),:))/(dx^2);
grad2x(1,:)=(Tnew(2,:)-Tnew(1,:))/(dx^2);
grad2x(m,:)=grad2x((m-1),:);
grad2y(:,2:(n-1))=(Tnew(:,1:(n-2))+Tnew(:,3:n)-2*Tnew(:,2:(n-1)))/(dx^2);
grad2y(:,1)=(Tnew(:,2)-Tnew(:,1))/(dx^2);
grad2y(:,n)=grad2y(:,(n-1));
for q=2:length(b1)
   ii=b1(q,1);
   jj=b1(q,2);
   grad2x(ii,jj)=(Tnew(ii-1,jj)-Tnew(ii,jj))/(dx^2);
```

```
        grad2y(ii,jj)=(Tnew(ii,jj+1)-Tnew(ii,jj))/(dx^2);
    end
    for q=1:(length(b2)-1)
        ii=b2(q,1);
        jj=b2(q,2);
        grad2x(ii,jj)=(Tnew(ii-1,jj)-Tnew(ii,jj))/(dx^2);
        grad2y(ii,jj)=(Tnew(ii,jj+1)-Tnew(ii,jj))/(dx^2);
    end
    deltaTnew=dt*D*(grad2x+grad2y);
    grad2x(2:(m-1),:)=(Told(1:(m-2),:)+Told(3:m,:)-2*Told(2:(m-1),:))/(dx^2);
    grad2x(1,:)=(Told(2,:)-Told(1,:))/(dx^2);
    grad2x(m,:)=grad2x((m-1),:);
    grad2y(:,2:(n-1))=(Told(:,1:(n-2))+Told(:,3:n)-2*Told(:,2:(n-1)))/(dx^2);
    grad2y(:,1)=(Told(:,2)-Told(:,1))/(dx^2);
    grad2y(:,n)=grad2y(:,(n-1));
    for q=2:length(b1)
        ii=b1(q,1);
        jj=b1(q,2);
        grad2x(ii,jj)=(Told(ii-1,jj)-Told(ii,jj))/(dx^2);
        grad2y(ii,jj)=(Told(ii,jj+1)-Told(ii,jj))/(dx^2);
    end
    for q=1:(length(b2)-1)
        ii=b2(q,1);
        jj=b2(q,2);
        grad2x(ii,jj)=(Told(ii-1,jj)-Told(ii,jj))/(dx^2);
        grad2y(ii,jj)=(Told(ii,jj+1)-Told(ii,jj))/(dx^2);
    end
    deltaTold=dt*D*(grad2x+grad2y);
    %deltaT(welli,wellj)=(deltaC(welli,wellj)+W*(T(welli,wellj)-
Tprime(nt))/thickness(welli,wellj))*dt;
    deltaT=.5*deltaTold+.5*deltaTnew;


    deltaT2=Rf*dt./depth.*rnowells.*(Trecharge-(.5*Tnew+.5*Told)).*active;
    deltaT=deltaT+deltaT2;


    %give all particles in same cell the same T
    for q=1:length(pT)
        if deltaT(pii(q),pjj(q))>=0
            pT(q)=pT(q)+deltaT(pii(q),pjj(q));
        else
            pT(q)=pT(q)*(Tnew(pii(q),pjj(q))+deltaT(pii(q),pjj(q)))/Tnew(pii(q),pjj(q));
        end
    end
    if time==recordtimes(recordflag+1)
```

```
        recordflag=recordflag+1;
        Trecord(:,:,recordflag)=Tnew;
        hrecord(:,:,recordflag)=hnew;
    end

end
Qriv
percent=Qriv/(.8*3600*24*365)
% figure
% imagesc(hnew')
% axis ij
% axis equal
% colorbar
% title('head')
% figure
% imagesc(Tnew')
% axis ij
% axis equal
% colorbar
% title('Temperature')
% haug=reshape(hrecord(:,:,215),45,52);
% figure
% [cc,hh]=contour((1:m)*dx-dx/2,(1:n)*dx-dx/2,haug');
% clabel(cc,hh)
% axis ij
% axis equal
% colorbar
% title('August 3rd Head')
%
Tswing=max(Trecord,[],3)-min(Trecord,[],3);
figure
imagesc(Tswing')

axis ij
axis equal
colorbar
title('Temperature Swing')
%
% hwell=reshape(hrecord(16,41,:),1,365);
% figure
% plot(hwell)



%%%%%%%%%%%%%%%%%%%%%%%%%%%%SUBFUNCTIONS%%%%%%%
%%%%%%%%%%%%%
```

```
function [h,T]=initmodel(K);
[m,n]=size(K);
T=zeros(m,n);
h=zeros(m,n);
for p=1:n
   %h(:,p)=(58-60)/(n-1)*(p-1)+60;
   h(:,p)=63;
   T(:,p)=10;
end

function [px,py,pT,np]=particleinit(T,npercell,dx,active,time,b1,b2);
np=0;
[m,n]=size(T);
if npercell==4
   xx=[.25,.75,.25,.75]'*dx;
   yy=[.25,.25,.75,.75]'*dx;
elseif npercell==5
   xx=[.25,.75,.25,.75,.5]'*dx;
   yy=[.25,.25,.75,.75,.5]'*dx;
elseif npercell==9
   xx=[.25,.75,.25,.75,.5,.5,.5,.75,.25]'*dx;
   yy=[.25,.25,.75,.75,.5,.75,.25,.5,.5]'*dx;
   elseif npercell==81
   xx1=[.1:.1:.9];
   xx2=[xx1,xx1,xx1];
   xx=[xx2,xx2,xx2]'*dx;
   yy=[ones(1,9)*.1,ones(1,9)*.2,ones(1,9)*.3,ones(1,9)*.4,ones(1,9)*.5,...
      ones(1,9)*.6,ones(1,9)*.7,ones(1,9)*.8,ones(1,9)*.9]'*dx;
else
   disp('Only 4, 5, 9, or 81 have been set up properly')
end
px=zeros(0);
py=zeros(0);
pT=zeros(0);
np=0;
if time==0
   for q=1:m
      for r=1:n
         if active(q,r)==1
            px=[px;xx+dx*(q-1)];
            py=[py;yy+dx*(r-1)];
            pT=[pT;ones(npercell,1)*T(q,r)];
            np=np+npercell;
         end
      end
```

```
   end
else


   np=np+npercell;
   for q=1:m
      for r=1:n
         if active(q,r)==1
            px=[px;xx+dx*(q-1)];
            py=[py;yy+dx*(r-1)];
            aa=find(or(and(b1(:,1)==q,b1(:,2)==r),and(b1(:,1)==q,b1(:,2)==r)));

            TT=ones(npercell,1)*T(q,r);

            pT=[pT;TT];

         end
      end
   end
end

function depth=getdepth(b1,b2,m,n,active,dx)
data=[156.744 184.128        3.048
161.544       414.528        1.524
262.344       448.128        6.7056
305.544       625.728        4.572
334.344       755.328        1.524
478.344       832.128        11.5824
555.144       846.528        18.5928
617.544       908.928        19.812
507.144       918.528        10.668
540.744       932.928        13.716
579.144       956.928        18.8976
228.744       913.728        1.524
343.944       1024.128       3.048
684.744       980.928        15.24
646.344       1024.128       15.5448
372.744       1076.928       4.572
550.344       1105.728       9.144
766.344       1057.728       10.668
310.344       1115.328       3.048
238.344       1192.128       1.524
343.944       1139.328       4.572
319.944       1192.128       3.6576
483.144       1168.128       8.5344
406.344       1148.928       6.7056
```

```
415.944         1168.128        7.0104
420.744         1187.328        7.62
483.144         1211.328        7.3152
439.944         1105.728        8.5344
439.944         1225.728        7.0104
516.744         1240.128        6.4008
588.744         1244.928        3.048
828.744         1235.328        3.6576
454.344         1249.728        7.0104
459.144         1264.128        6.7056
497.544         1278.528        6.4008
430.344         1273.728        6.4008
377.544         1249.728        5.1816
319.944         1283.328        3.6576
281.544         1307.328        2.4384
415.944         1326.528        3.048
487.944         1307.328        6.096
497.544         1331.328        4.8768
559.944         1321.728        3.048
396.744         1388.928        1.8288
511.944         1388.928        3.3528
972.7,1160,8.23
650.144         870.928         20];
data=[data;[zeros(16,1),[100:100:1600]',zeros(16,1)]];
xi=(1:m)*dx-dx/2;
yi=(1:n)'*dx-dx/2;
depth=griddata(data(:,2),data(:,1),data(:,3),yi,xi);

ii=isnan(depth);
depth(ii)=4;
for q=1:m
   for qq=1:n
      if depth(q,qq)<2;
         depth(q,qq)=2;
      end
   end
end

depth=depth.*active;
```

Appendix C

Geochemical Data

We collected ground-water and surface-water samples from the Mohawk River site between June 28th and June 30th, 2005 (Table C.1). While samples were collected in several monitoring wells, the depth of silt in the wells and the results of the chemical analyses on the samples suggest that they were not representative of the water in the aquifer, so they are not listed here. We were not able to gain access to the Schenectady pumping wells, so we used a sample of tap water from a motel to the south of the site. We were not able to sample Rotterdam Well 3 because of the attached fluoridation equipment.

Total dissolved solids (TDS) were measured immediately after sampling using a temperature-corrected TDS probe, and are reported in units of ppm. Alkalinity was measured within 24 hours of sampling using the titration method outlined in Standard Methods (20th Edition) , and is reported in mg of $CaCO_3$ per liter required to bring the sample to a pH of 4.5. The results of these tests are reported in Table C.2.

Samples analyzed for anions were filtered in the field and then refrigerated. The analysis was performed using an ion chromatograph (IC), specifically a Dionex 100. The results are reported in μM in Table C.3.

Samples analyzed for cations were filtered in the field, acidified, and then refrigerated. The analysis was performed using an inductively coupled plasma atomic emissions spectrometer (ICP-AES), specifically a Leeman Labs PS3000UV. The results are reported in ppm in Table C.4.

Sample Name	Abbreviation	Date Collected	Collection Location
Rotterdam Well 1	R.W.1	June 29 2005	access tap on well
Rotterdam Well 2	R.W.2	June 29 2005	access tap on well
Rotterdam Well 4	R.W.4	June 29 2005	access tap on well
Schenectady Tap Water	S.T.W.	June 30 2005	motel south of site
Mohawk River 1	M.R. 1	June 28 2005	west bank ~100 m below lock
Mohawk River 2	M.R. 2	June 29 2005	west bank ~100 m below lock
Mohawk River 3	M.R. 3	June 29 2005	west bank ~100 m below lock
Mohawk River 4	M.R. 4	June 30 2005	west bank ~100 m below lock
Mohawk River 5	M.R. 5	June 30 2005	west bank ~100 m below lock

Table C.1. List of water samples.

Sample	Alkalinity (ppm $CaCO_3$)	TDS (ppm)
R.W.1	150	279
R.W.2	161	308
R.W.4	199	395
S.T.W.	165	-
M.R.1	70	160
M.R.2	81	154
M.R.3	67	156
M.R.4	70	150
M.R.5	70	151

Table C.2. Chemical parameters measured in the field.

Sample	F^-	Cl^-	$SO4^{2-}$	NO_3^-
R.W.1	35	787	212	132
R.W.2	37	988	248	140
R.W.4	6	1196	264	184
S.T.W.	51	1026	223	124
M.R.1	7	515	158	121
M.R.2	-	-	-	-
M.R.3	28	498	149	128
M.R.4	5	496	149	45
M.R.5	7	498	148	75

Table C.3. Chemical constituents measured using IC.

Sample	Ba	Ca	Fe	K	Mg	Mn	Na	P	Si	Sr
R.W.1	0.04	51	0.14	1.6	9.4	0.25	20	0.62	3	0.16
R.W.2	0.04	59	nd	1.3	10	0.12	23	0.14	3.3	0.17
R.W.4	0.04	75	nd	1.4	14	0.08	32	1.3	3.8	0.18
S.T.W.	0.02	62	nd	1.4	10	nd	23	0.32	3.3	0.18
M.R.1	0.02	31	nd	1	4.9	nd	15	0.04	1.8	0.15
M.R.2	-	-	-	-	-	-	-	-	-	-
M.R.3	-	-	-	-	-	-	-	-	-	-
M.R.4	0.01	28	nd	1	4.5	nd	13	0.02	1.7	0.13
M.R.5	0.01	28	nd	0.8	4.4	nd	13	0.09	1.7	0.13

Table C.4. Chemical constituents measured using ICP-AES.

Appendix D

Modeling Annual Ground-water Temperature Variations at the Hierakonpolos Temple Site

D.1 Introduction

A multidisciplinary geosciences investigation is being carried out to investigate the rising water-table at the Hierakonpolos Temple site north of Idfu, Egypt (for background on the project and the results of early surveys, see Alexander et al.(2000) and Montandon (2004)). As part of this investigation, shallow ground-water temperatures were measured in piezometers on a roughly bimonthly basis. The purpose of this appendix is to briefly report the results of a modeling study testing the hypothesis that the observed temperature variations in the piezometers reflect the annual variation in the temperature of the water that seeps into the aquifer from the unlined irrigation canals on the site.

D.2 Ground-water Temperature Data

In January of 1999, 145 piezometers were installed at the Hierokonpolos site (Figure D.1). Piezometers could not be placed in the village or the cultivated fields, so most of them are located in the archeological site. The piezometers were monitored on a roughly bimonthly basis between January 2001 and March 2003, with depth to water, temperature, electrical conductivity, and salinity recorded. The changing water levels in these piezometers have been used to estimate the rate of water-table rise (Montandon, 2004). The temperatures measured on 13 occasions between January 2001 and March 2003 (Figure D.2) are used in this study.

We fit the temperature time series in each piezometer with a sinusoidal signal. Montandon (2004) found that the water-table rose by ~1 cm per month between 1999 and 2000, so non-sinusoidal temperature variations are expected. By fitting the temperature signal in each piezometer with a sine wave, however, the spatial variations in the first order attributes of the signals can be readily interpreted.

The best fit sine wave for each of the temperature signals was chosen using a grid search algorithm. Temperatures measured above the water-table or in pooled surface-water were omitted from the inversion. The mean RMS misfit was 0.8 °C, while the highest was 2.0 °C. Figure D.3 maps the magnitude of the best fit sine wave for each of the piezometers. The majority of borings have magnitudes between 2 and 5 °C, while some of the piezometers near the diggings have magnitudes as high as 7.5 °C. Figure D.4 maps the lag of the best fit sine waves. While most of the borings have lags of 130 to 160 days, a few near the diggings have lags as low as 80 days.

D.3 Canal Infiltration Model

One possible source for the observed temperature oscillations could be the infiltration of surface-water from the unlined irrigation canal. I constructed a 1-D ground-water model of the site to assess the expected magnitude of the temperature oscillation due to infiltrated canal water. The model uses a 2-D coupled ground-water flow and heat transport finite element code (Appendix A). This model simultaneously solves the governing differential equations for ground-water flow and heat transport and accounts for the couplings between them.

The model domain for this simulation is a map-view slice of the aquifer extending from an irrigation canal boundary to a constant head boundary 0.25 lower than the mean canal

level 50 m away. The simulation is intended to represent a 1-D model, so a 3 m wide swath of aquifer was simulated with no-flow boundaries on each side.

The aquifer at the site consists of a ~30 m deep silt layer (Alexander et al. 2000). Several drill holes, however, have encountered a yellow clay at 3-4 m depth that would act as an aquitard. The extent of this clay layer is unclear, and to fully model its effect a three dimensional model would be required. The purpose of this study, however, is to determine whether the temperature signal from the infiltrating canal water could propagate to the locations of the piezometers. As the ground-water flux per cross-sectional area increase with decreasing aquifer thickness, modeling the entire aquifer as 3 m thick enhances the propagation of the temperature signal, and is the conservative assumption in this case.

The model uses a hydraulic conductivity of 5×10^{-6} m/s, near the upper limit of the range of typical values for silts reported by Freeze and Cherry (1979). The thermal conductivity and heat capacity of the saturated aquifer, chosen from values compiled by Stonestrom and Blasch (2003) were 1.8 W m^{-1} $°C^{-1}$ and 3.2×10^{6} J m^{-3} $°C^{-1}$ respectively. The specific yield of 0.18 was the average value for silt given by Fetter (1988).

The purpose of the model is to investigate whether infiltration from the irrigation canals could be the cause of the temperature variations measured in the piezometers. Thus, the irrigation canal boundary conditions were chosen to maximize the propagation of the temperature signal into the aquifer. The water level in the irrigation canals varies on a weekly cycle, with high water for two days and low water for five days (the difference between the two levels is 1 m, and the low water level is 1.5 m above the water level in the drainage canal). While surface-water infiltration is typically modeled as a head-

dependent flux, the irrigation canals at the site are unlined, so they are treated as variable head boundaries. This method assumes complete hydraulic connection between the canal and the aquifer, and thus represents the maximum amount of infiltration. The water in the canal cannot have a temperature variation greater than the atmospheric temperature. Therefore, the model uses a sinusoidal temperature signal based on the air temperature recorded at the Luxor airport further down the Nile to represent the aquifer temperature at the irrigation canal boundaries.

The annual precipitation at Hierakonpolos totals less than 25 mm per year, so it is not a significant source of recharge. The cultivated portions of the modeled area, however, receive a significant amount of irrigation. The application rate and proportion lost to evapotranspiration are unknown. The site also receives recharge from below, which Montandon (2004) attributed to the recent irrigation of in a wadi to the south. The ground-water rise at Hierokonpolos due to this irrigation is roughly 0.12 m/year. As the flux need only fill the pore space in the sediment, the minimum flux is less than the water-table rise. The net effect of these areal fluxes, however, is to reduce the impact of the canal leakage temperature signal on the aquifer temperature signal, so they are not included in this simulation.

Figure D.5 shows the aquifer temperature profile 10 years after the beginning the simulation. The temperature signal does not oscillate significantly more than 15 m from the canal.

D.4. Discussion and Conclusions

If the annual variation in the temperature of the water infiltrating from the irrigation canals was a significant component of the temperature signals observed in the

piezometers, then we would expect to see the magnitude and phase of those signals vary systematically with distance from the canals. In fact, the magnitude and phase of the best fit sinusoids stay relatively constant across the site except near the diggings, a behavior more consistent with temperature signals caused by the annual variation in surface temperature.

Our 1-D model suggests that the temperature oscillations due to canal infiltration will not be detectable more than a few meters from the canal. Given the negative result of this simulation, a 2-D simulation of the aquifer does not seem to be required.

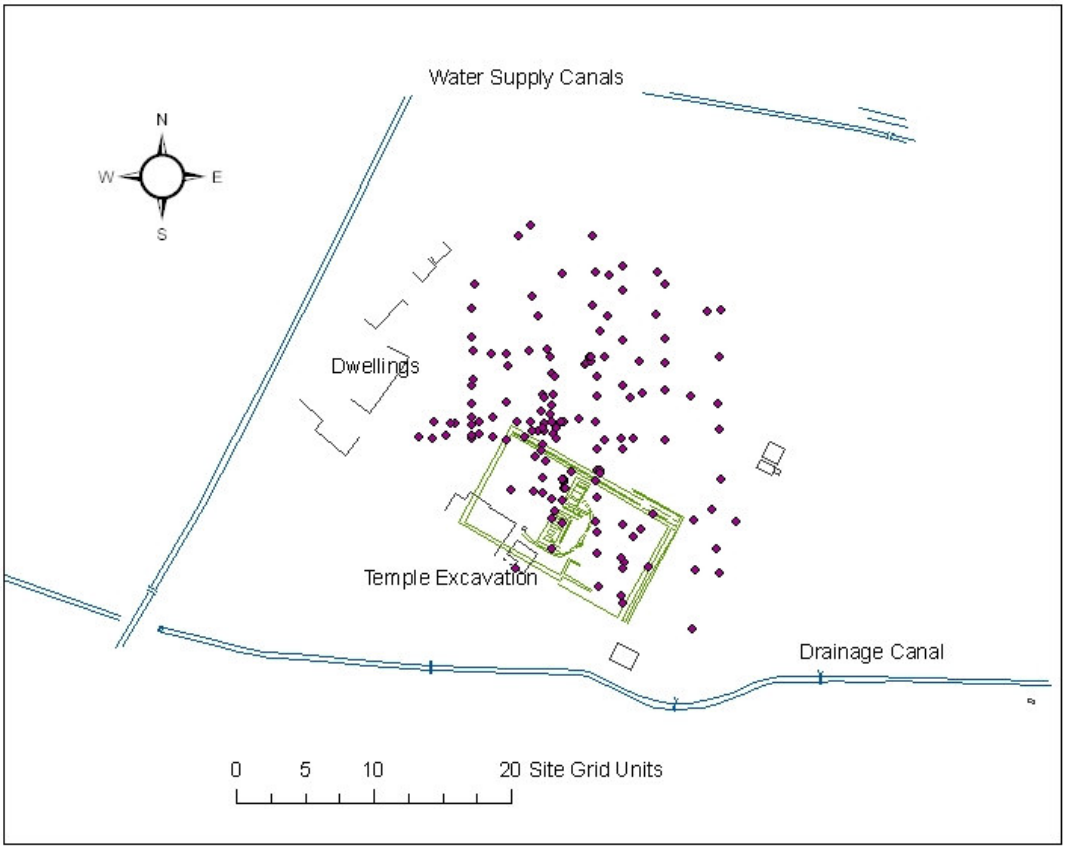

Figure D.1. Map of the Hierakonpolos temple site showing the piezometers used in this study. Each site grid unit is 10 m. Map data is taken from data compiled by Montandon (2004).

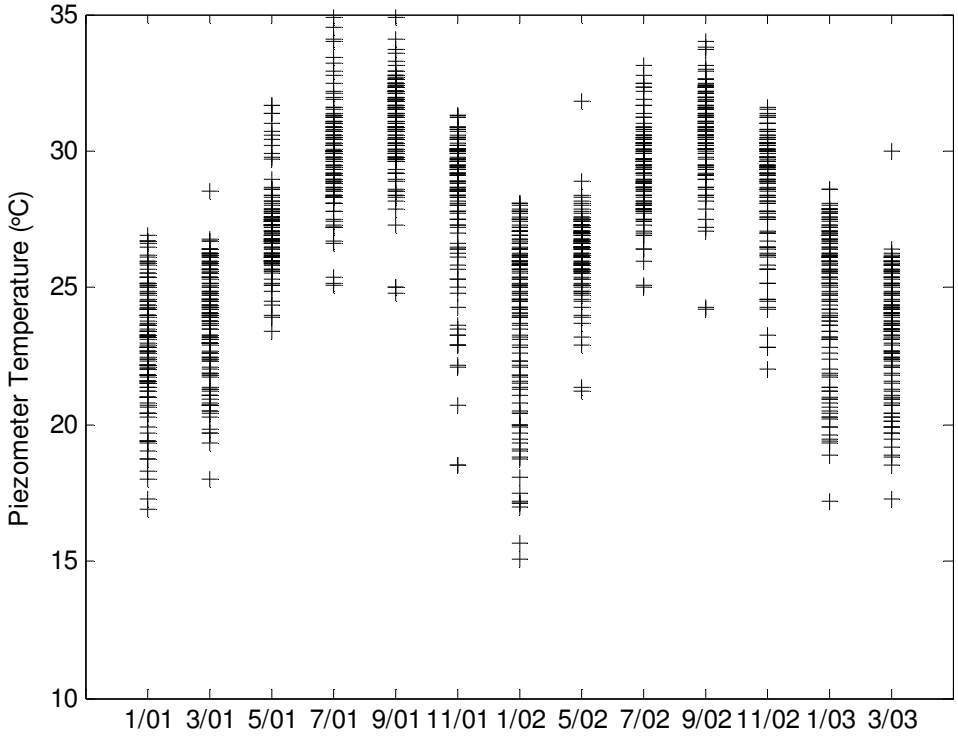

Figure D.2. Temperatures measured in the piezometers at the Hierakonpolos site. While the water-table is rising, the temperature signal over this period is broadly sinusoidal.

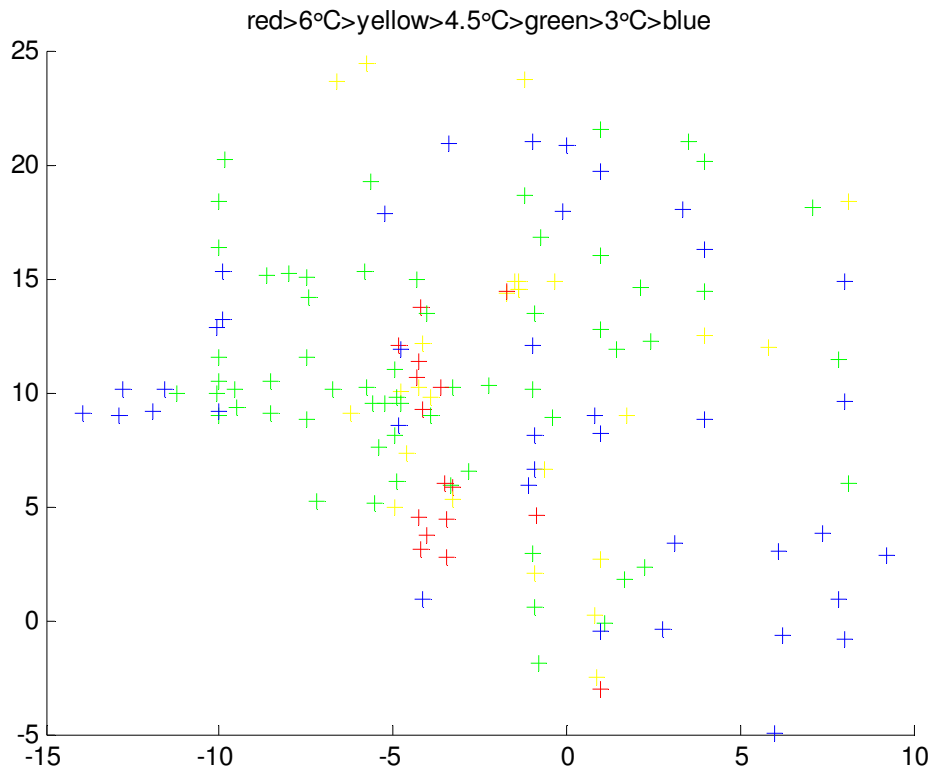

Figure D.3. Map of the amplitudes of the best fit sinusoids for each piezometer. The anomalously high amplitudes (>5 ºC) are in the vicinity of archeological excavations. The axes are in site grid units.

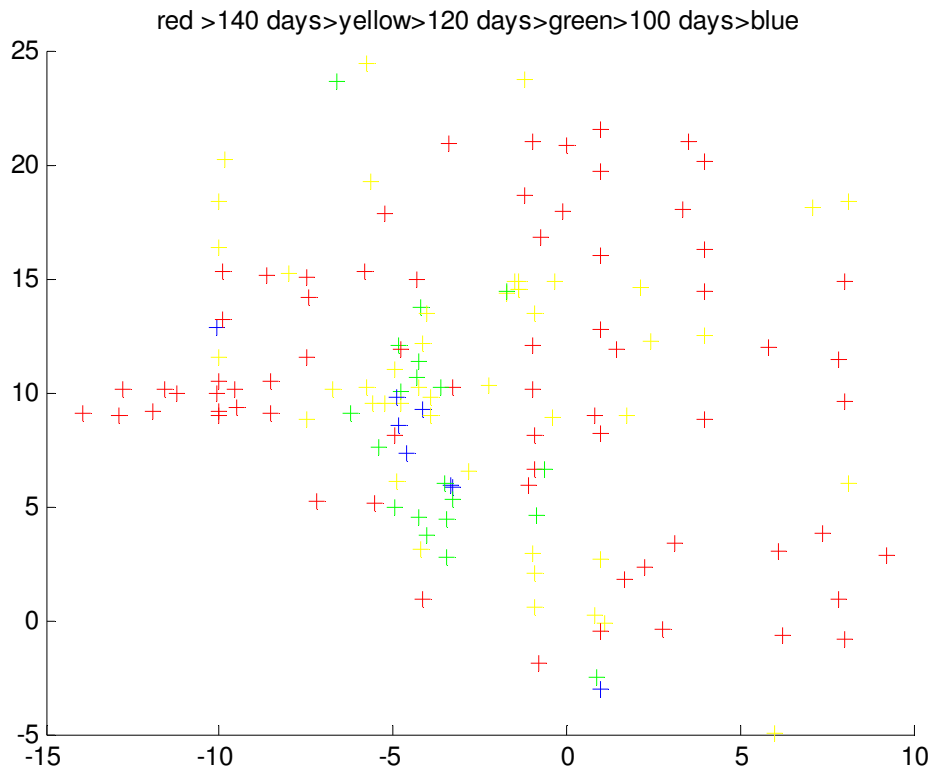

Figure D.4. Map of the phase lags of the best fit sinusoids for each piezometer. The anomalously low lags (<100 days) are in the vicinity of archeological excavations. The axes are in site grid units.

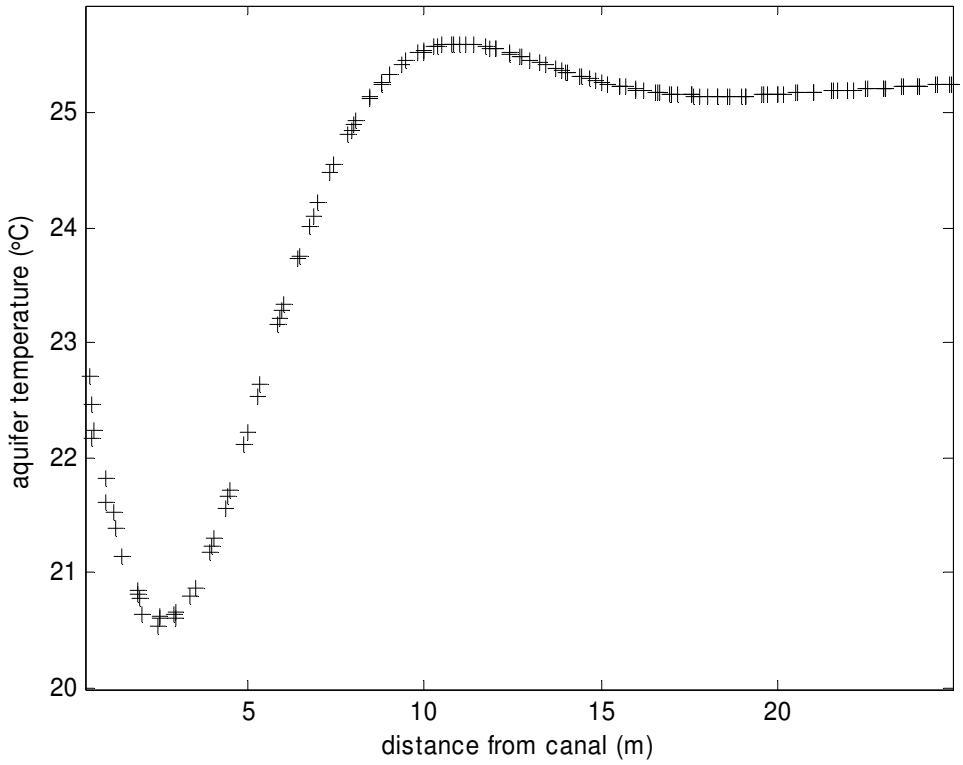

Figure D.5. Simulated aquifer temperature as a function of distance from the irrigation canal. The temperature oscillations are insignificant more than 15 m from the canal.

BIBLIOGRAPHY

Alexander, S.S., S.M. Brown, R.R. Parizek, D.P. Gold, 2000, Combined shallow seismic and hydrological investigation of the ancient Hierakonpolis site in Southern Egypt. SAGEEP 2000, 389-398,

Anderson, M.P. 2005. Heat as a ground water tracer. *Ground Water* **43**, 951-968.

Bair, E S, and Parizek, R R. 1978. Detection of permeability variations by a shallow geothermal technique. *Ground Water* **16**, 254-263.

Barroll, P. 2001. Documentation of the administrative groundwater model for the Middle Rio Grande Basin: Santa Fe, New Mexico Office of the State Engineer. Hydrology Bureau Report 99-3, 22 p., 8 figs., 2 app.

Bartolino, J.R., 2002. How we have examined ground-water/ surface-water interaction of the Rio Grande. In *Ground-water resources of the Middle Rio Grande Basin, New Mexico: U.S. Geological Survey Circular 1222*, ed. J. R. Bartolino and J.C. Cole, 78-79.

Bartolino, J.R. 2003. The Rio Grande—Competing demands for a desert river. In *Heat as a Tool for Studying the Movement of Ground Water Near Streams*, ed. D.A. Stonestrom and J. Constantz, 8–16. USGS Circular 1260. Reston, Virginia: USGS.

Bartolino, J.R., and J.C. Cole, ed. 2002. Ground-water resources of the Middle Rio Grande Basin, New Mexico. USGS Circular 1222. Albuquerque, New Mexico: USGS.

Bartolino, J.R., and R.G. Niswonger. 1999. Numerical simulation of vertical ground-water flux of the Rio Grande from ground-water temperature profiles, central New Mexico. Water Resources Investigation Report 99-4212. Albuquerque, New Mexico: USGS.

Becker, M.W., T. Georgian, H. Ambrose, J. Siniscalchi, and K. Fredrick. 2004. Estimating flow and flux of groundwater discharge using water temperature and velocity. *Journal of Hydrology* 296, no. 1–4: 221–233.

Birman, J.H. 1969. Geothermal exploration for ground water, *Geological Society of America Bulletin* **80**, 617-630.

Bravo, H. R., J. Feng, and R. J. Hunt. 2002. Using groundwater temperature data to constrain parameter estimation in a groundwater flow model of a wetland system. *Water Resources Research* 38, no. 8: 10.1029/2000WR000172.

Bredehoeft, J.D., and I.S. Papadopulos. 1965. Rates of vertical ground-water movement estimated from the Earth's thermal profile. Water Resources Research 1, no. 2: 325–328.

Burow, K.R., J. Constantz, and R. Fujii. 2005. Using heat as a tracer to estimate dissolved organic carbon flux beneath a restored wetland. *Ground Water* 43, no. 4: 545–556.

Carslaw, H.S., and J.C. Jaeger. 1959. Conduction of Heat in Solids, 2nd ed. New York: Oxford University Press.

Cartwright, K. 1968. Thermal prospecting for ground water. *Water Resources Research* **4**, 395-401.

Cartwright, K. 1974. Tracing shallow groundwater systems by soil temperature. *Water Resources Research* **10**, no. 4: 847-855.

Conant, B.J. 2004. Delineating and quantifying ground water discharge zones using streambed temperature. *Ground Water* 42, no. 2: 243-257.

Constantz, J., A.E. Stewart, R. Niswonger, and L. Sarma. 2002. Analysis of temperature profiles for investigating stream losses beneath ephemeral channels. *Water Resources Research* **38**, no. 12: 52-1-52-13.

Constantz, J., C.L. Thomas, and G. Zellweger. 1994. Influence of diurnal variations in stream temperature on streamflow loss and groundwater recharge. *Water Resources Research* 30, no. 12: 3253–3264.

deMarsily, G. 1986. *Quantitative hydrogeology.* San Diego, California: Academic Press.

Ebaugh, W. F., R. R. Parizek, and R. Greenfield. 1976. Channel detection by geothermal methods. In: *Karst Hydrology and Water Resources, Proceedings of the U.S.-Yugoslavian Symposium, Dubrovnik, June 2-7, 1975*, V. Yevjevich, ed., Water Resources Publications, Fort Collins, CO, v. 2, 648-658.

Fetter, C.W. 1994. Applied Hydrogeology 3rd Edition. Upper Saddle River, NJ: Prentice Hall, Inc.

Freeze, A.R. and J.A. Cherry. 1979. Groundwater. Upper Saddle River, NJ: Prentice Hall, Inc.

Fryar, A.E., E.J. Wallin, and D.L. Brown. 2000. Spatial and temporal variability in seepage between a contaminated aquifer and tributaries to the Ohio River. *Ground Water Monitoring and Remediation* 20, no. 3: 129–146.

Gould, J. 1994. Middle Rio Grande channel permeameter investigations: Bureau of Reclamation Albuquerque Area Office, Middle Rio Grande Water Assessment Supporting Document No. 11, variously paged.

Hatch, C.E., A.T. Fisher, J.S. Revenaugh, J. Constantz, and C Ruehl. 2006. Quantifying surface water–groundwater interactions using time series analysis of streambed thermal records: method development. *Water Resources Research* 42, 1029/2005WR004787.

Johnson, A. N., B. R. Boer, W. W. Woessner, J. A. Stanford, G. C. Poole, S. A. Thomas, and S. J. O'Daniel. 2005. Evaluation of an inexpensive small diameter temperature logger for documenting ground water –river interactions. *Ground Water Monitoring and Remediation*, **25**, 68-74.

Kernodle, J.M., D.P. McAda, and C.R. Thorn. 1995. Simulation of ground-water flow in the Albuquerque Basin, central New Mexico, 1901-1994, with projections to 2020. Water-Resources Investigations Report 94-4251. Albuquerque, New Mexico: USGS.

Kintzinger, P.R. 1956. Geothermal survey of hot ground near Lordsburg, New Mexico. *Science*, **124**, 629-630.

Koltermann, C.E., and S.M. Gorelick. 1995. Fractional packing model for hydraulic conductivity derived from sediment mixtures. *Water Resources Research* 31, no. 12: 3283-3297.

Lapham, W.W. 1989. Use of temperature profiles beneath streams to determine rates of vertical ground-water flow and vertical hydraulic conductivity. Water Supply Paper 2337. Denver, Colorado:USGS.

Larson, T.H., and A.T. Hsui. 1992. An analytical study of a two-layer transient thermal conduction problem as applied to soil temperature surveys. *Geophysics* 57, no. 2: 306-312.

LeSchack, L.A., and J.E. Lewis. 1983. Geothermal prospecting with Shallo-Temp surveys. *Geophysics* **48**, 975-996.

Lewis, T.J, and Wang, K. 1998. Geothermal evidence for deforestation-induced warming: implications for the climatic impact of land development. *Geophysical Research Letters* **25**, 535-538.

Lunardini, V.J., 1992. On: "An analytical study of a two-layer transient thermal conduction problem as applied to soil temperature surveys" by T. H. Larson and A. T. Hsui (February 1992 GEOPHYSICS, p. 306-312). Geophysics, 57, no. 12, 1544.

Markle, J.M., R.A. Schincariol, J.H. Sass, and J.W. Molson. 2006. Characterizing the Two-Dimensional Thermal Conductivity Distribution in a Sand and Gravel Aquifer. *Soil Science Society of America Journal* 70, 1281-1294.

Mazor, E. 2004. *Chemical and Isotopic Groundwater Hydrology*, *3rd Edition*. New York: CRC.

Montandon, L.M.. 2004. Use of Remote Sensing with Ground Truth and GIS to Study the Hydrological Setting of the Hierakonopolis Archeological Site in Egypt: M.S. Thesis, Pennsylvania State University.

Niswonger, R.G., and D.E. Prudic. 2003. Modeling heat as a tracer to estimate streambed seepage and hydraulic conductivity. In *Heat as a Tool for Studying the Movement of Ground Water Near Streams*, ed. D.A. Stonestrom and J. Constantz, 81-89. USGS Circular 1260. Reston, Virginia: USGS.

O'Brien, P. J., 1970, Aquifer transmissivity distribution as reflected by overlying soil temperature patterns: Ph.D. Thesis, Pennsylvania State University.

Olmsted, F.H., 1977, Use of temperature surveys at a depth of 1 m in geothermal exploration in Nevada, USGS Prof. Paper 1044-B. Reston, Virginia: USGS.

Parizek, R. R., and E. S. Bair, 1990, Ground-water exploration using shallow geothermal techniques: in Water Resources in Pennsylvania: Availability, Quality, and Management, S. K. Majunder, E. W. Miller, and R. R. Parizek, ed.s, The Pennsylvania Academy of Science, Easton, PA, 80-95.

Pruitt, T., and Bowser, S., 1994, Flood wave test and transient groundwater analysis: Bureau of Reclamation Albuquerque Area Office, Middle Rio Grande Water Assessment Supporting Document No. 10, variously paged.

Roark, D.M., 1998, Use of surface-water pulses to estimate hydraulic characteristics of the Rio Grande alluvium, Albuquerque area, New Mexico, in Slate, J.L., ed., U.S. Geological Survey Middle Rio Grande Basin Study--Proceedings of the Second Annual Workshop, Albuquerque, New Mexico, February 10-11, 1998: U.S. Geological Survey Open-File Report 98-337, p. 53-54.

Ronan, A.D., D.E. Prudic, C.E. Thodal, and J. Constantz. 1998. Field study and simulation of diurnal temperature effects on infiltration and variably saturated flow beneath an ephemeral stream. *Water Resources Research*, 34, no. 9,: 2137-2153.

Schneider, R. 1962. Use of thermometry in hydrogeologic studies of glacial deposits at Worthington, Minnesota. *GSA Bulletin*, 73, 1305-1308.

Silliman, S.E., and D.F. Booth. 1993. Analysis of time-series measurements of sediment temperature for identification of gaining vs. losing portions of Juday Creek, Indiana. *Journal of Hydrology* 146, 131–148.

Silliman, S.E., J. Ramirez, and R.L. McCabe. 1995. Quantifying downflow through creek sediments using temperature time series: One-dimensional solution incorporating measured surface temperature. *Journal of Hydrology* 167, no. 1-4: 99-119.

Smerdon, J. E., H. N. Pollack, V. Cermak, J. W. Enz, M. Kresl, J. Safanda and J. F. Wehmiller. 2004. Air-ground temperature coupling and subsurface propagation of annual temperature signals. *Journal of Geophysical Research-Atmospheres*, 109(D21).

Spectra Environmental Group Inc., 2001, Great Flats Aquifer evaluation: Report to Schenectady County Intermunicipal Watershed Rules and Regulations Board, Schenectady, NY.

Stallman, R.W. 1965. Steady one-dimensional fluid flow in a semi-infinite porous medium with sinusoidal surface temperature. *Journal of Geophysical Research* 70, no. 12: 2821–2827.

Stonestrom, D.A., and K.W. Blasch. 2003. Determining temperature and thermal properties for heat-based studies of surface-water ground-water interactions. In *Heat as a Tool for Studying the Movement of Ground Water Near Streams*, ed. D.A. Stonestrom and J. Constantz, 73–80. USGS Circular 1260. Reston, Virginia: USGS.

Su, G. W., J. Jasperse, D. Seymour, and J. Constantz. 2004. Estimation of hydraulic conductivity in an alluvial system using temperatures. *Groundwater* 42, 890-901.

Suzuki, S. 1960. Percolation measurements based on heat flow through soil with special reference to paddy fields. *Journal of Geophysical Research* 65, no. 9: 2883–2885.

Theis, C.V., and C.S. Conover. 1963. Chart for the computation of drawdown in the vicinity of a discharging well, In Shortcuts and Special Problems in Aquifer Tests, ed. R. Bentall, C10-C15: USGS Water-Supply Paper 1545-C. Reston, Virginia: USGS.

Tiedeman, C.R., J.M. Kernodle, and D.P. McAda. 1998. Application of nonlinear-regression methods to a ground-water flow model of the Albuquerque Basin, New Mexico: USGS Water-Resources Investigation Report 98-4172, 90 p.

Wall, G.R., 1995, Postglacial drainage in the Mohawk River Valley with emphasis on paleodischarge and paleochannel development. Ph.D. Thesis, Rensselaer Polytechnic Institute, 352 pp.

Wall, G. R., and R. G. LaFleur. 1994. Post-glacial paleochannel development in the Hudson/Mohawk lowlands, New York. *Northeastern Geology* 16, 116-122.

Winslow, J. D., H. G. Stewart Jr., R. H. Johnston, and L. J. Crain. 1965. Ground-water Resources of Eastern Schenectady County, New York, with Emphasis on Infiltration from the Mohawk River: State of New York Conservation Department Water Resources Commission, Bulletin 57.

Woodbury, A. D., and L. Smith. 1988. Simultaneous inversion of hydrogeologic and thermal data, 2, incorporation of thermal data. *Water Resources Research* 24, 1586-1606.

Yeh, G.-T., and R.J. Luxmoore. 1983. Modeling moisture and thermal transport in unsaturated porous media. *Journal of Hydrology* 64, no.1-4, pp.299-309.

Vita

Geoffrey J.M. Moret

Education

- Ph.D. Geosciences, 2007, Pennsylvania State University, *Annual Variations in Ground-Water Temperature as a Tracer of River-Aquifer Interactions*. Advisor: R.R. Parizek

  M.S. Geophysics, 2003, Boise State University, *P-wave Velocity Characterization of the Boise Hydrogeophysical Research Site*. Advisor: M.D. Knoll

- B.Sc. Geophysics, 2001, University of British Columbia

Experience

- *2006-2007*- Graduate Research Assistant: Living Filter Project, Pennsylvania State University
- *2005-2006*- Visiting Assistant Professor: Geology Department, Bucknell University
- *2004-2005*- Lead Instructor: World Campus Certificate Program in GIS, Pennsylvania State University
- *2003*- Graduate Teaching Assistant: Department of Geosciences, Pennsylvania State University
- *2001-2002*- Graduate Research Assistant: Center for the Geophysical Investigation of the Shallow Subsurface, Boise State University
- *1998-2000*- Undergraduate Research Assistant: Rock Physics Group, Department of Earth and Ocean Sciences, University of British Columbia

Selected Publications

Moret, G.J.M., and Rose, A.W., 2007, Resistivity Level Runs to Locate Water-Filled Mine Voids between Drill Holes: Mine Water and the Environment (Journal of the International Mine Water Association), **26**, 23-28.

Moret, G.J.M., Gold, D.P., and Rose, A.W., 2006, Detecting and Characterizing Hydrothermal Pyritic Zones along Bald Eagle Ridge Using Induced Polarization: Environmental and Engineering Geoscience, **12**, 377-384.

Moret, G.J.M., Knoll, M.D., Barrash, W. and Clement, W.P., 2006, Investigating the Stratigraphy of an Alluvial Aquifer Using Crosswell Seismic Traveltime Tomography: Geophysics, **71**, doi 10.1190/1.2195487.

Moret, G.J.M., Clement, W.P., Barrash, W. and Knoll, M.D., 2004, Curved-Ray VSP Inversion: Near Surface Issues: Geophysics, **69**, 345-351.